Lappeenranta
University of Technology

Alexander Maximov

THEORETICAL ANALYSIS AND NUMERICAL SIMULATION OF SPECTRAL RADIATIVE PROPERTIES OF COMBUSTION GASES IN OXY/AIR-FIRED COMBUSTION SYSTEMS

Thesis for the degree of Doctor of Science (Technology) to be presented with due permission for public examination and criticism in the Auditorium 1383 at Lappeenranta University of Technology, Lappeenranta, Finland on the 11th of December, 2012, at noon.

Acta Universitatis
Lappeenrantaensis 501

Supervisors Professor Timo Hyppänen
Department of Energy Technology
Faculty of Technology
Lappeenranta University of Technology
Finland

Doctor Mohammad Hadi Bordbar
Department of Energy Technology
Faculty of Technology
Lappeenranta University of Technology
Finland

Reviewers Professor Bo Leckner
Department of Energy and Environment
Chalmers University of Technology, Göteborg
Sweden

Professor Gabriel Węcel
Institute of Thermal Technology
Silesian University of Technology, Gliwice
Poland

Opponents Professor Gabriel Węcel
Institute of Thermal Technology
Silesian University of Technology, Gliwice
Poland

Professor Reijo Karvinen
Department of Energy and Process Engineering
Faculty of Science and Environmental Engineering
Tampere University of Technology
Finland

ISBN 978-952-265-346-8
ISBN 978-952-265-347-5 (PDF)
ISSN 1456-4491
Lappeenrannan teknillinen yliopisto
Digipaino 2012

Abstract

Alexander Maximov
Theoretical Analysis and Numerical Simulation of Spectral Radiative Properties of Combustion Gases in Oxy/Air-Fired Combustion Systems
Lappeenranta 2012
127 pages
Acta Universitatis Lappeenrantaensis 501
Diss. Lappeenranta University of Technology
ISBN 978-952-265-346-8, ISBN 978-952-265-347-5 (PDF), ISSN 1456-4491

Energy efficiency is one of the major objectives which should be achieved in order to implement the limited energy resources of the world in a sustainable way. Since radiative heat transfer is the dominant heat transfer mechanism in most of fossil fuel combustion systems, more accurate insight and models may cause improvement in the energy efficiency of the new designed combustion systems. The radiative properties of combustion gases are highly wavelength dependent. Better models for calculating the radiative properties of combustion gases are highly required in the modeling of large scale industrial combustion systems. With detailed knowledge of spectral radiative properties of gases, the modeling of combustion processes in the different applications can be more accurate.

In order to propose a new method for effective non gray modeling of radiative heat transfer in combustion systems, different models for the spectral properties of gases including SNBM, EWBM, and WSGGM have been studied in this research. Using this detailed analysis of different approaches, the thesis presents new methods for gray and non gray radiative heat transfer modeling in homogeneous and inhomogeneous H_2O–CO_2 mixtures at atmospheric pressure. The proposed method is able to support the modeling of a wide range of combustion systems including the oxy-fired combustion scenario. The new methods are based on implementing some pre-obtained correlations for the total emissivity and band absorption coefficient of H_2O–CO_2 mixtures in different temperatures, gas compositions, and optical path lengths. They can be easily used within any commercial CFD software for radiative heat transfer modeling resulting in more accurate, simple, and fast calculations.

The new methods were successfully used in CFD modeling by applying them to industrial scale backpass channel under oxy-fired conditions. The developed approaches are more accurate compared with other methods; moreover, they can provide complete explanation and detailed analysis of the radiation heat transfer in different systems under different combustion conditions. The methods were verified by applying them to some benchmarks, and they showed a good level of accuracy and computational speed compared to other methods. Furthermore, the implementation of the suggested banded approach in CFD software is very easy and straightforward.

Keywords:

radiation heat transfer, numerical modeling, gray and non gray modeling, gas spectral radiation, emissivity, exponential wide band model, statistical narrow band model, H_2O–CO_2 mixture

UDC 662.612:536.24:004.942

Acknowledgments

This study was carried out at the Department of Energy Technology of Lappeenranta University of Technology (LUT) during 2009-2012, funded by the Academy of Finland under grant No. 124368 and the Graduate School in Computational Fluid Dynamics (CFD).

I express my deepest gratitude to my supervisors, Professor Timo Hyppänen and Doctor Mohammad Hadi Bordbar, for their valuable guidance and giving me the possibility to obtain my research work and the freedom to be a student. I am also thankful for the scientific discussions and friendly advice.

I am grateful to Professors Bo Leckner and Gabriel Węcel for their fruitful comments and suggestions which certainly enhanced the quality of the present thesis.

I thank Doctor Jouni Ritvanen for a teamwork rhythm, for providing morning coffee breaks every Tuesday and the Christmas cards which I have been receiving each year.

I would like to express my appreciation towards the following professionals of their fields for the bright classes and interesting moments: Esa Vakkilainen, Payman Jalali, Jari Backman, Julia Vauterin-Pyrhönen, Peter Jones, Barbara Miraftabi, and Sari Silventoinen.

I would like also to thank all the LUT colleagues who have helped me a lot in making this research a success. Firstly, I would like to thank Srujal Shah and Heikki Suikkanen whose energetic efforts helped me during all the years in Lappeenranta. Secondly, I would like to thank Petri Rousku for helpful discussions and uncontentious support. I would also like to thank Ari Vepsäläinen, Petteri Peltola, Markku Nikku, Matti Koski, Yury Avramenko, Maxim Mikhnevich, Egor Nikolaev, Denis Semeyonov, and Mahsa Dabaghmeshin.

The friendship of many persons is highly appreciated, and I would like to mention some of them personally: A. Ivanov, N. Khodyreva, S. Groshev, D. Kuleshov, K. Kamiev, Y. Alexandrova, C. Ani, V. Panapanaan, M. Mannila, M. Hamaguchi, S. Segovia, W. Ratchananusorn, I. Panorel, W. Srithammavut, H. Lintu, P. Belova, S. Voronin, M. Garcia, P. Ponomarev, T. Minav, V. Tyyster, and S. Porohov.

My special thanks go to a colleague, friend, flatmate, and language teacher Teemu Puhakka.

Of course, the biggest honor of great attitude is fully given to my family. Without you, without your love and support, I could not have managed to pass this way even to the half, even to the start... .

Alexander Maximov
November 2012
Lappeenranta, Finland

Dedicated

to the memory of my father

Contents

List of publications supporting present monograph

The present work is presented in form of monograph which is supported by accepted, submitted and to be submitted articles. The present monograph is related to the following list of journal and conference papers.

Publication I
Maximov A., Bordbar M. H., and Hyppänen T. Spectral calculation of radiative properties of gas mixtures. The 7-th International Conference on Heat Transfer, Fluid Mechanics and Thermodynamics, Antalya, Turkey, 2010.

The author of this thesis is the corresponding author of this conference paper. The correlations were obtained for partial absorption coefficients of separate absorption bands in the specified gas mixture by applying a non gray gas assumption based on the EWBM. The author also gave an oral presentation in the conference.

The content of the conference article is presented in Chapter 3 starting from page 55. Proceedings of the 7th International Conference on Heat Transfer, Fluid Mechanics and Thermodynamics (HEFAT 2010), pp. 1041–1045, Antalya, Turkey. Editor J.P. Meyer. Publisher: HEFAT. ISBN: 978-1-86854-818-7

Publication II
Maximov A., Bordbar M. H., and Hyppänen T. Spectral Calculations of the Flame Radiation in H_2O–CO_2 Gas Mixtures, Indian Journal of Chemical Technology.

The author is the corresponding author of this journal article. A comprehensive spectral analysis of the EWBM and the WSGGM for different gas compositions involving H_2O–CO_2 mixtures for practical applications was performed and the absorption bands that cause the largest differences in the predictions of two methods for total properties were reported.

The content of the journal article is presented in Chapters 2 and 3 starting from pages 23 and 55, respectively. The current status of the paper is under peer review in Indian Journal of Chemical Technology (has been since March 2011; status updated on 2 July 2012 by the editor of the journal via e-mail communication).

Publication III
Maximov A., Bordbar M. H., and Hyppänen T. From gray to non gray radiation heat transfer modeling of combustion products using banded approach. To be submitted.

The author is the first author of this journal article. Based on the SNBM, some correlations for the total and band emissivities of H_2O–CO_2 mixtures under oxy/air-fired scenarios are presented which are in use for gray and non gray radiative heat transfer modeling of combustion systems. Mohammad Hadi Bordbar is the corresponding author.

The corresponding author provides a databases of the emissivity properties based on the SNBM results for obtaining the total and band emissivity correlations.

The content of the journal article is presented in Chapters 4 and 5 starting from pages 69 and 87, respectively. The current status of the paper is under process, to be submitted.

Publication IV
Maximov A., Bordbar M. H., and Hyppänen T. Spectral analysis of the various implementations of the exponential wide band model (EWBM) for H_2O–CO_2 mixtures, International Review of Mechanical Engineering, 2012, available on-line (Vol. 6 N. 3) - Papers Part A.

The author is the corresponding author of this journal article. Two implementations of the EWBM – EWBM-4RE and EWBM-IM – were analyzed. A comparison of these methods with SNBM as the benchmark showed the EWBM-4RE with its originally developed parameters to be a more accurate model for obtaining total properties calculations. Therefore, the accuracy of the EWBM-IM of the total property calculations can be improved by obtaining the new spectral parameters for EWBM-IM instead of using those which were originally developed to be used in the EWBM-4RE.

The content of the journal article is presented in Chapter 3 starting from page 55. Current status of the paper is published in International Review of Mechanical Engineering Journal in Vol. 6 n. 3, pp. 411–419.

Nomenclature

Latin alphabet

$\boldsymbol{s}$	unit vector of certain direction	–
$\boldsymbol{r}$	position vector	–
$\hat{\boldsymbol{s}}_{\mathrm{m}}$	different directions	–
A	absorption	–
a	fitting coefficient	–
B	rotational constant that fixes the band location	–
b	fitting coefficient	–
B_i	pressure self-broadening coefficient	–
C_2	Planck second radiation constant	mK
C	concentration	$\mathrm{mole/m^3}$
c	speed of light in vacuum ($\mathrm{c} = 2.9979 \times 10^8$)	m/s
E	blackbody monochromatic emissive power (Plank function)	$\mathrm{W/m^2}\mu\mathrm{m}$
$\mathrm{f_v}$	volume fraction ($\mathrm{f_v} = \mathrm{C_m}\rho$)	–
G	incident radiation (irradiance)	$\mathrm{W/m^2}$
$\mathrm{I_m}$	total radiation intensity	$\mathrm{W/m^2\ cm^{-1}\ sr}$
I	intensity	$\mathrm{W/m^2\ cm^{-1}\ sr}$
J	rotational quantum number	–
k^*	pseudo-absorption coefficient in the SNBM	$\mathrm{cm^{-1}\ bar^{-1}}$
K	absorption coefficient	$\mathrm{m^{-1}}$
k	Boltzmann's constant ($\mathrm{k} = 1.3807 \times 10^{-23}$)	J/K
L	path length, characterizing dimension	m
MG	molar mass	kg/mole
p(S)	probability density function	–
$\mathrm{P_{w+c}}$	sum of $\mathrm{H_2O}$ and $\mathrm{CO_2}$ mole species ($\mathrm{P_{w+c}} = \mathrm{p_{H_2O}} + \mathrm{p_{CO_2}}$)	bar
Pr	$\mathrm{H_2O}$ to $\mathrm{CO_2}$ molar fractions ratio ($\mathrm{Pr} = \mathrm{p_{H_2O}/p_{CO_2}}$)	–
P	total pressure	bar
q	total radiative heat flux	$\mathrm{W/cm^2}$
R	gas constant $\mathrm{R} = 8.205 \times 10^{-5}$	$\mathrm{m^3\ bar\ K^{-1}\ mole^{-1}}$
T	temperature	K
X	absorber density path length product	bar m
x	molar fraction	–

Greek alphabet

α	integrated band intensity	$\mathrm{cm^{-1}gm\ m^{-2}}$
β	mean line-width-to-spacing parameter	–
δ	transmissivity over $\Delta\eta$ in the SNBM	$\mathrm{cm^{-1}}$
ϵ	emissivity	–
$\eta_{\mathrm{b,b}}$	beginning of the wavenumber block	$\mathrm{cm^{-1}}$
$\eta_{\mathrm{e,b}}$	end of the wavenumber block	$\mathrm{cm^{-1}}$

η	wavenumber	cm^{-1}
γ	line width parameter	–
λ	wavelength	$\mu\mathrm{m}$
μ_m	direction cosines of an ordinate direction m	–
ω_m	angular weight in a direction m	m^2
ω	band width parameter	cm^{-1}
ρ	density of particle	$\mathrm{g/cm}^3$
σ	Stefan-Boltzmann constant ($\sigma = 5.670 \times 10^{-8}$)	$\mathrm{W/m}^2\,\mathrm{K}^4$
τ	transmittance	–
ς_m	direction cosines of an ordinate direction m	–
ϑ	vibrational quantum number	–
ζ_M	lines collisional half-width in the SNBM	cm^{-1}
ζ_m	direction cosines of an ordinate direction m	–
ζ	line-width-to-spacing ratio $\zeta = \beta \mathrm{P_e}$	–

Superscripts

$'$	incoming direction
$''$	outgoing direction
$\bar{}$	average value
*	dimensionless properties

Subscripts

0	reference value
η	spectral, function of wavenumber
b	blackbody
c	center
g	gas
k	band of a gas component
l	lower
m	mass
s	surface
t	total
u	upper
i	particular gas band
j	participating species

Abbreviations

2D	two dimensional
3D	three dimensional
BBEF	blackbody emissivity function
BM	band model

CFD	computational fluid dynamics
CPU	central processing unit
DOM	discrete ordinates method
EWBM	exponential wide band model
FSKM	full spectrum k - distribution model
FVM	finite volume method
NBM	narrow band model
P_1	spherical harmonics method (approximate method)
RTE	radiative heat transfer equation
SBM	spectral band model
SLBLM	spectral line-by-line model
SLWM	spectral line-based weighted sum of gray gases model
SNBM	statistical narrow band model
WBM	wide band model
WSGGM	weighted sum of gray gases model

1 Introduction

The modern need of producing less CO_2 emissions by improving the overall efficiency of combustion processes has become significantly important in last decades. It has raised the greatest interest in the proper calculations of radiative heat transfer within the industrial applications. Because of the complexity of the radiative heat transfer problem, it is always challenging to balance the accuracy and the computational costs of the radiative property models in this field. There are some radiative property models of participating gases that provide a high level of accuracy, but their high computational costs limit their use in real applications. Other proposed methods are simpler but less accurate. More effective numerical models for spectral radiative properties of gases which could provide fast and accurate enough predictions and could be easily applied in modern computational fluid dynamics (CFD) calculations are still needed to simulate radiative heat transfer in industrial applications.

In this thesis, the objective was to propose the new methods for the radiative property of combustion products and also to improve the performance of the existing methods in this field. This results in improving the capability of the CFD methods to model the gray and non gray radiation heat transfer in industrial large scale combustion systems in more accurate and computationally efficient way. Radiative heat transfer in gas mixtures is a physical phenomenon which due to its complex behavior requires much effort to be accurately modeled in industrial applications. In addition, the radiative heat transfer phenomenon is difficult, expensive, and sometimes impossible to be measured with adequate accuracy even in the modern experimental devices, especially with high temperatures, and variable gas compositions.

The comprehensive analyses of the two different formulations of the exponential wide band model (EWBM) were carried out using the total and spectral property calculations of H_2O–CO_2 gas mixtures under the air-fired combustion conditions. The first one is the original exponential wide band method with the four region equation (EWBM-4RE), and the second one is the numerical integration method (EWBM-IM). Using the statistical narrow band model (SNBM) as a benchmark as well as available experimental data, the spectral analysis of two implementations of the EWBM have been performed to obtain the most important absorption bands of H_2O and CO_2. The knowledge of these absorption bands is used in the later steps of this study to develop new approaches for the gray and non gray radiative heat transfer calculation of H_2O–CO_2 mixtures.

A significant part of the research is carried out by using the statistical narrow band model (SNBM), which is one of the most accurate models for spectral radiative properties of gases, to obtain the correlations for the gray mean and band absorption coefficients of H_2O–CO_2 mixtures found in air/oxy-fired combustion systems. The obtained correlations are compared with the weighted sum of the gray gases model (WSGGM) which is widely used in the CFD simulations of industrial combustions systems to calculate the radiative properties of H_2O–CO_2 gas mixtures. In order to include the gas spectral radia-

tive feature in the radiation heat transfer calculations of combustion systems in a fast and accurate manner, the spectral emissivity/absorptivity predicted by different approaches was compared with available experimental data. The proposed approach supports inhomogeneous media by the changes in the gas compositions of the H_2O–CO_2 mixtures in gray and non gray modeling. The new approach of the radiative heat transfer modeling provides more efficient, accurate, and simple calculations in a wide range of industrial applications, and it can simply be used in different commercial CFD software.

1.1 Modeling of combustion systems

Even with the modern availability of high computational resources, the high fidelity models for spectral radiative properties of gas mixtures such as the line-by-line calculations and the statistical narrow band model can be only used in small scale combustion systems. The high computational cost of the modeling of large industrial applications causes demands for more computationally effective methods. Moreover, the obtained methods should provide sufficient accuracy in addition to computational time.

There are many research groups who have created a number of radiative property models for gas mixtures with a different level of accuracy and complexity. These methods have been created and tested for air-fired combustion conditions by Hottel and Sarofim (1967), Smith et al. (1982), Denison and Webb (1993), Soufiani and Djavdan (1994), Lallemant and Weber (1996), Liu et al. (1998), Pierrot et al. (1999), Goutiere et al. (2000), Coelho (2002), Ströhle and Coelho (2002), and Cumber and Fairweather (2005). The modern struggle with green house gas emissions has created an interest towards accurate numerical modeling of the oxy-fired combustion systems. Today researchers work with the new methods for oxy-fired combustion which is characterized by significantly smaller H_2O to CO_2 ratio affecting the radiative properties. For oxy-fired combustion the H_2O to CO_2 ratio can be as small as $1/8$ compared with a ratio of one or two which are quite usual in the air-fired combustion scenario.

Large scale industrial combustion systems contain some devices which are free of soot and fuel particles, and mainly contain gases which, in turn, can be simplified to be a H_2O–CO_2 mixture. Some of the high accurate spectral methods, like the EWBM or even the more accurate SNBM with a narrow band resolution of $25\ \mathrm{cm}^{-1}$ can be directly applied into small scale CFD modeling to produce the high-precision simulations. However, both the EWBM and the SNBM are still too costly in terms of computation for large scale industrial applications. The ratio of computational power to accuracy has created a room for different methods of radiative properties specified by scientific and industrial needs. The new approaches are highly required to reduce the computational cost of these methods and to improve the accuracy of combustion modeling of large scale industrial applications.

The radiative properties of combustion products are strongly affected by the presence of soot and fuel particles in gas mixture. However, in some parts of the combustion equip-

ments, the present of particles are quite small and their radiation effect can be ignored. In such devices as backpass channel, the role of gas mixture is larger or even dominant source of radiation. In this work, only radiation by gases has been treated.

The difficulties related to more complex methods can be solved by increasing computational resources and by optimizing the modeling methods for specific applications. During the development process of the method, a significant attention should be paid to the validation of the developed approach with widely used radiative methods and the available experimental data. The complexity of spectral radiative properties under different combustion conditions and different effective parameters creates some difficulties for obtaining such an effective model.

1.2 Scientific contribution

The spectral analysis of two implementations of the EWBM has been performed to provide a better understanding of how the spectral radiative properties change with effective parameters, that is temperature, pressure, and optical path length. The effective parameters represent the certain ranges that meet the conditions of industrial combustion applications for air-fired scenarios. Using the SNBM (Soufiani and Taine, 1997) as a benchmark method, the changes of the band absorptivity/emissivity in the certain ranges of effective parameters are obtained to investigate the spectral behavior of absorption bands. Through the spectral comparison it has been found out that the differences concentrate mainly in the $4.3-\mu$m CO_2 (band with upper limit) and in the $6.3-\mu$m H_2O and $9.4-\mu$m CO_2 (symmetrical overlapping bands) absorption bands. For the predictions of the radiative properties, the listed absorption bands can be modified to improve the accuracy of the two formulations of the EWBM (Edwards and Balakrishnan, 1973) in the further steps of research. The accuracy analysis of the two formulations of the EWBM is obtained through a benchmark which introduces the exact solution of radiative heat transfer in real participating gas in 2D rectangular enclosure. Moreover, it will be discussed that in order to improve the accuracy of the integrated approach of the EWBM for spectral radiation predictions, the model parameters should be modified instead of using those which were originally developed to be used in the original EWBM (Edwards and Balakrishnan, 1973) as a further research in this field.

Because of the industry requirements for creating simple, fast, and sufficiently accurate models to obtain the radiative properties of combustion products, the correlations of the total emissivity of H_2O–CO_2 mixture for gray gas modeling are obtained. Some correlations that support air-fired scenarios are related to homogeneous media while others that support oxy/air-fired scenarios are related to inhomogeneous media, respectively. Moreover, a new approach towards the non gray radiative heat transfer modeling of H_2O–CO_2 mixtures is presented. The new approach is based on dividing the wavenumber spectrum into some limited wavenumber intervals. The suitable number of wavenumber intervals and their limits are found by the spectral analysis of the absorption spectrum and the

results of some benchmark analyses. Considering the temperature, pressure path length product, and the ratio of the molar fractions of H_2O and CO_2, the correlations are obtained for the band absorption coefficient of each wavenumber interval. The range of effective parameters is selected according to the industrial needs of the oxy-fired combustion scenario.

The new correlation (Eq. 4.8) of the total properties (Tables 4.6–4.8) provides more accurate, simple, and faster calculations compared with the EWBM, various formulations of the WSGGM, the Leckner method, and the empirical correlation obtained by Green and Perry. Furthermore, both correlations of total and band properties show significant improvement of radiative heat transfer calculations when they have been applied to CFD modeling of oxy-fired combustion in 3D rectangular enclosure.

One of the main aims of the presented research is to provide more accurate insight into the spectral behavior of the absorption bands of homogeneous and inhomogeneous H_2O–CO_2 mixtures and by means of spectral analysis, to create a more efficient, faster, and accurate enough method suitable for both gray and non gray radiative heat transfer modeling. Additionally, the current research demonstrates the inconsistency of the widely used standard WSGGM with the coefficients proposed by Smith et al. (1982) for the modeling of the oxy-firing combustion products. One of the reasons is that the coefficients reported by Smith et al. (1982) were originally based on the charts of certain rates of molar fractions specified for air-fired combustion.

1.3 Outline of the work

The content of this research is divided into the following seven chapters.

The theory of the RTE solution methods, especially DOM, details of gray and non gray radiative heat transfer modeling, and the different quantitative spectroscopy databases for radiative properties of gases are discussed in Chapter 2.

The spectral predictions of two different formulations of the EWBM and their accuracy in the calculation of the total radiative properties are studied in Chapter 3. The available experimental data of the radiative properties of gases and the total emissivity obtained by the SNBM as a benchmark approach have been used for the accuracy analysis of different formulations of the EWBM.

The detailed description of the new logarithmic correlations for the total emissivity based on the SNBM for oxy-/air-fired combustion scenarios is reported in Chapter 4. These correlations can be implemented in any gray gas radiative heat transfer calculation of homogeneous and inhomogeneous media. The computational time and accuracy analysis for the new correlations is performed by comparing it with the other methods.

The establishing process of the new banded approach for non gray modeling of radiative heat transfer in homogeneous and inhomogeneous H_2O–CO_2 gas mixtures is included in Chapter 5. The theory of the banded approach, as an effective method for non gray modeling with its developed capability to be easily implemented in RTE solver, is formulated. The method is then validated by applying it to some standard benchmark problems.

The application of the new banded approach in gray and non gray modeling of a real industrial systems is described in Chapter 6.

The conclusions of the presented research are summarized in Chapter 7.

2 Radiative heat transfer

Radiative heat transfer is significantly important in a wide range of industrial applications. It is important in metallurgy and chemicals production, nuclear and industrial engineering, combustion and drying technologies, etc. Examples of thermal radiation in every day life include the heat from open fires and the sunshine on a clear sky. The nature of radiative heat transfer is that all materials continuously absorb and emit electromagnetic waves by changing their molecular energy levels. It is well known that the spectral range of the radiative heat transfer is located in ultraviolet, visible, and infrared parts of electromagnetic wave spectrum and limited by wavelengths in the range from 10^{-1} to 10^{2} μm. For example, the case of open fire consists of radiation including a small part of the ultraviolet range. One of the most significant factors affecting the emission by the wavelength and strength of the emitting media or material is the temperature. Generally, radiative heat transfer in the gas mixtures, for example combustion products, is a wavelength dependent phenomenon. It means that the strength of the participating gases in absorbing and emitting radiation rapidly changes with the wavelength in the spectrum (Modest and Zhang, 2002) which consists of thousands of absorption lines.

Two other modes of heat transfer are conduction and convection. Conduction heat transfer is energy transfer by photon interactions or by free electrons through the atomic grid. In liquid and gas media, energy transfer is carried out through molecule to molecule collisions (i.e., kinetic energy losses from faster to more slowly moving molecules). Convection heat transfer is similar and related to the replacement flow of molecules with high kinetic energy to low kinetic energy (colder media). In spite of radiative heat transfer, conduction and convection heat transfers require the medium presence in which the energy transfer is carried out. In its turn, the radiative heat transfer is carried out by photons flow, or electromagnetic waves, which can travel in vacuum. It is generally assumed that conductive and convection heat transfer rates are linearly proportional to differences in temperature while the radiative heat transfer rates are proportional to temperature differences in the fourth power. Thus, the dependency on high temperatures makes the radiative heat transfer important in industrial applications with high temperature ranges, especially in combustion applications (furnaces, engines, rocket nozzles, etc.). At very high temperatures the radiative heat transfer can be even dominant over conduction and convection which brings high importance to the radiative heat transfer in the design and analysis of industrial combustion systems.

Fuel combustion is one of major methods of producing both electrical and heat energy. The modern world-wide trend of CO_2 emission reduction requires significant improvements in the efficiency of the fuel combustion process. The increasing knowledge of radiative heat transfer behavior and the development of more powerful computers have increased the interest in the computational modeling of radiative heat transfer during the last decades. The numerical modeling has a significant role in the analysis and design of combustion systems. The modeling of radiative heat transfer is one of the most important aspects of the overall modeling process of combustion systems which is highly desired

for industrial purposes. Industrial modeling consists of quite large spaces and it should be supported by computationally efficient methods.

The analysis of radiative heat transfer is complicated by many factors, for example by the variation of radiative properties of different materials, especially the gas mixtures, with the wavelength. Heat transfer properties such as thermal conductivity, density, and kinematic viscosity related to the conduction and convection are clearly measurable and well behaved. However, radiative properties are difficult for measuring and their behavior is unsteady (Edwards, 1963). In the gas media, the radiative properties change rapidly with the wavelength and depend strongly on the pressure, temperature, and gas composition. This makes the radiative heat transfer analysis more complicated.

2.1 Theory of radiative heat transfer

Under the term of radiative transfer, the process of internal energy propagation by means of electromagnetic waves is considered. Electromagnetic waves propagate in a vacuum with the speed of light (3×10^8 m/s) from the radiating or emitting media. The electromagnetic waves absorbed by other media are converted into the energy of molecule motion.

The electromagnetic wave is produced by electromagnetic interaction of the photons. When photons pass through a media, the absorption and emission of photon energies occur in the atoms and molecules of that media. The absorption/emission of a photon is proportional to the change of rotational and (or) vibrational energy levels in molecules and atoms, or to the orbit changing of the electrons. These changes cause a modification in the intensity of the radiative energy resulting in spectral lines. It is known that every particle moves in 3-D space which has three types of freedom. A particle can change its place in the left-right, forward-backward, and (or) upward-downward directions. In the case of diatomic or polyatomic molecules which are connected with each other, each of the atoms lets the molecule have three types of freedom. In other words, a molecule consisting of N atoms has three types of transition freedoms and 3N-3 types of relative motion freedom between the atoms. These 3N-3 types of internal freedom could be further separated into the rotational and vibrational degrees of freedom. They are shown in Fig. 2.1 for a diatomic molecule and for linear/nonlinear triatomic molecules.

The diatomic molecule has three internal types of freedom. It could rotate around its center of gravity within the plane of the surface or perpendicularly to the surface, and it could also rotate around its own axis. Consequently, the last type of freedom between the two atoms is used for the vibrational motion. There are only two rotational modes for linear triatomic molecules gases, such as CO_2, N_2O, and HCN (Modest, 2003b). As shown in Fig. 2.1, since there are six internal types of freedom, there are four vibrational modes for linear triatomic molecules. A polyatomic molecule could have different moments of inertia depending on the axis of rotation for each of the three rotational modes. The molecule

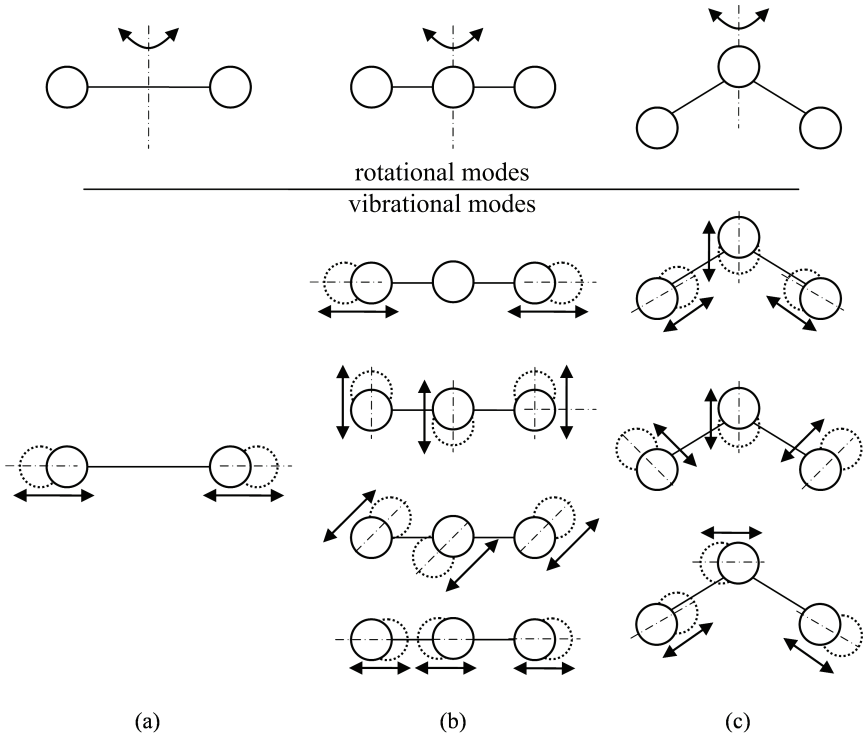

Figure 2.1: Diatomic (a), linear triatomic (b) and nonlinear triatomic molecules (c) of rotational and vibrational types of freedom.

is classified as a spherical top (for example, CH_4), in the case when all three moments of inertia are the same. The case of two same inertia moments is called a symmetric top (for example, NH_3, CH_3CL, C_2H_6, and SF_6), and if all three moments are different, it is called an asymmetric top (for example, H_2O, O_3, SO_2, NO_2, H_2S, and H_2O_2).

Usually, mono atomic and diatomic gases are transparent to radiation. Triatomic gases are considered to absorb and/or emit radiative energy. Differently from solids and liquids radiation, the gas radiation is volumetric by nature because the micro particles of the gas are involved in the thermal radiation. Thus, the emissivity/absorptivity of a single gas or gas mixture changes according to the thickness and density of its layer.

Greater absorptivity corresponds to large thickness and density of the layer. Gases absorb and/or emit radiative energy only in certain bands of wavelength spectrum which means that the gases are selective to radiation (Modest, 2003b). The absorption and emission of radiative energy by gases occurs only in certain wavenumber intervals. These intervals are known as bands. Within these bands, the absorption coefficient exhibits rapid changes. The parts of the spectrum which are outside of the bands might be absolutely

transparent to radiation. Thus, research is needed to obtain the absorption bands of gas mixtures corresponding the different conditions. In addition to radiative heat transfer in combustion gases, the features of radiative energy to/from/through luminous gas medium occur due to the presence of luminous particles of ash, coal, and soot (Isachenko et al., 1975). That kind of luminous gas medium can be easily observed as a flame. With the increasing number of suspended particles in the flame, the emission becomes higher.

The estimation of the spectral parameters of the combustion products in certain temperature, pressure, and gas composition conditions has a key role in the calculation of the radiation energy emitted or absorbed by a gas mixture. In turn, the combustion products represent the molecular fraction of each gas component composed during the thermal oxidation process. Moreover, the presence of more than one gas in the mixture has a great effect on the absorption coefficient. The changes in the absorption coefficient with the wavenumber for certain gases are obtained experimentally, and theoretically. Discussion about the different experimental data sources will follow later.

The interaction of radiative heat transfer with radiatively participating media is an important issue in the engineering applications. The general relationships of the radiative heat transfer behavior of an emitting, absorbing, and/or scattering media is developed through radiative energy balance. It is also known as radiative heat transfer equation (RTE) which describes the radiative intensity inside the enclosure as a function of spectral variable, direction, and location. For the estimation of the net radiative heat flux, the contributions of radiative energy must be integrated from all possible directions for all wavenumbers (for the whole spectrum of radiative energy). Further integration of the RTE over all directions and wavenumbers results in the conservation of radiative energy statement applicable to an infinitesimal volume (Modest, 2003b). The general RTE is highly dependent on the wavenumber. As the final step of the overall heat transfer calculations, the result of radiative heat transfer will be conjuncted with a balance for two other modes of energy transfer – conduction and convection, resulting in the overall conservation of energy equation.

In most of the energy transfer scenarios, the radiative heat transfer is usually combined with conduction and/or convection and its solution can be obtained using a non linear differential equation. The scattering of the media is one of the most difficult problems in solving the RTE, and it is generally assumed to be isotropic. The RTE for the non scattering media is simplified to a first order differential equation at the condition when the temperature profile is know. The evaluation of the temperature profile is the next significant problem in solving the RTE. Another problem in solving the RTE is related to the modern complex 3D geometries.

2.2 Solution methods of radiative transfer equation

The exact analytical solution of RTE is not available with the exception of some simple cases with several simplification assumptions. Thus, for solving radiative heat transfer

problems in real practical cases, numerical methods are used. Most of the cases with exact solutions are restricted to be used for gray media with constant properties (Shih and Chen, 1983) in simple one dimensional geometries.

The major solution methods of the RTE solver are the discrete ordinates (DOM), finite volume (FVM), $\mathrm{P_1}$, zonal, and Monte Carlo methods. The zonal method was developed for a non scattering emissive gray gas with the constant absorption coefficient, and extended later for an isotropically scattering media to work with non gray, and non uniform absorption coefficients by Hottel and Sarofim (1967). By-turn, the zonal method is presented by a finite number of surface areas, and isothermal volume zones that subdivide the enclosure. The exchange of radiative energy occurs between any two zones, creating so called exchange areas, obtaining an energy balance (Bordbar and Hyppänen, 2007, 2013). The original zonal method has been widely used as the solution of the RTE in the 1960s. Moreover, it is difficult to be used in complicated geometries, and almost useless in the presence of anisotropic scattering (Chu and Churchill, 1960). Based on the DOM, another method has been created by modifying its simple quadrature for angular discretization to a fully finite volume (Briggs et al., 1975; Murthy and Mathur, 1998). The method of finite volume (FVM) for radiative transfer utilizes the precise integration to estimate the integrals of solid angle, similarly to the estimation of volumes, and areas in the fluid flow of the finite volume approach (Chai et al., 1994). One of the popular methods because of its simplicity is the $\mathrm{P_1}$ approximation. In this method, the complicated spectral transfer equation in its integral form is changed to a partial differential equation, and keeping the applicability to non black surfaces, and anisotropic scattering (Park and Kim, 1993). However, the $\mathrm{P_1}$ approximation method can be inaccurate for optically thin media (Modest, 1989). This method apart from DOM, and FVM provides accurate results, and can easily be applied and solved in cold, and hot surroundings for very thick radiating media. The RTE can quite well be solved by one of the general Monte Carlo statistical methods which has a lot of applications. Thus, Monte Carlo methods presume tracing the history of photons related to the points from emission to absorption (Hammersley and Handscomb, 1964). The disadvantage of these methods is demonstrated in the statistical error, as in about all statistical methods.

The DOM is based on a discrete representation of the directional variation of the radiative intensity (Briggs et al., 1975; Murthy and Mathur, 1998). This $\mathrm{S_n}$ method was originally created by Chandrasekhar (1960) when he worked on stellar, and atmospheric radiation. The DOM solves the RTE for a certain number of discrete solid angles which are associated with a vector direction $\boldsymbol{s}$ fixed in the global Cartesian system (x, y, z). In the spatial Cartesian system, the DOM is used as a transport equation for radiation intensity. Thus, it solves as many transport equations as there are vector directions $\boldsymbol{s}$. The solution method is the same for the fluid flow, and energy equations. However, the DOM requires the absorption coefficient as an input parameter. The mean absorption coefficient can be a function of the local concentrations of $\mathrm{H_2O}$, $\mathrm{CO_2}$, path length, and total pressure in addition to the temperature. The original DOM suffers from ray effects, and false scattering. During the last thirty years, the DOM has been optimized to be used in radiative heat transfer prob-

lems by many researchers, including Carlson and Lathrop (1968), Hottel et al. (1968), Fiveland (1984), Truelove (1988), and Krishnamoorthy (2010).

The direction cosines ζ_{m}, ς_{m}, and μ_{m} of each ordinate direction m can be correlated with the following differential equation (Modest, 2003b)

$$\zeta_{\mathrm{m}}\frac{\partial \mathrm{I_m}}{\partial \mathrm{x}} + \varsigma_{\mathrm{m}}\frac{\partial \mathrm{I_m}}{\partial \mathrm{y}} + \mu_{\mathrm{m}}\frac{\partial \mathrm{I_m}}{\partial \mathrm{z}} = -\mathrm{K}\mathrm{I_m} + \mathrm{K}\mathrm{I_b}, \tag{2.1}$$

where $\mathrm{I_m}$ is the total radiation intensity, $\mathrm{I_b}$ is the blackbody radiation intensity, and K is the absorption coefficient.

Assuming that the bounding surfaces are gray, Eq. 2.1 can be solved with the boundary conditions as follows (Kayakol et al., 2000)

$$\mathrm{I_m} = \epsilon_{\mathrm{w}}\mathrm{I_{bw}} + \frac{1-\epsilon_{\mathrm{w}}}{\pi}\sum_{\mathrm{m'}}\omega_{\mathrm{m'}}\mu_{\mathrm{m'}}\mathrm{I_{m'}}, \tag{2.2}$$

where $\mathrm{I_{bw}}$ is the blackbody radiation intensity at the temperature of surface, ϵ_{w} is the wall emissivity, ω_{m} is the weight of angular quadrature, and m and $\mathrm{m'}$ are the outgoing and incoming directions, respectively.

The total radiative heat flux inside the medium or at the surface can be found as

$$\boldsymbol{q}(\boldsymbol{r}) = \int_{4\pi}\mathrm{I}(\boldsymbol{r},\hat{\boldsymbol{s}})\hat{\boldsymbol{s}}\,\mathrm{d}\Omega \approx \sum_{\mathrm{m}=1}^{\mathrm{n}}\omega_{\mathrm{m}}\mathrm{I_m}(\boldsymbol{r})\hat{\boldsymbol{s}}_{\mathrm{m}}, \tag{2.3}$$

where ω_{m} is associated with each direction $\hat{\boldsymbol{s}}_{\mathrm{m}}$, $\boldsymbol{r}$ is a position vector, and $\hat{\boldsymbol{s}}_{\mathrm{m}}$ are the different directions $\mathrm{m} = 1, 2, 3..., \mathrm{n}$.

The incident radiation is calculated as

$$\mathrm{G}(\boldsymbol{r}) = \int_{4\pi}\mathrm{I}(\boldsymbol{r},\hat{\boldsymbol{s}})\,\mathrm{d}\Omega \approx \sum_{\mathrm{m}=1}^{\mathrm{n}}\omega_{\mathrm{m}}\mathrm{I_m}(\boldsymbol{r}). \tag{2.4}$$

The choice of the angular scheme is random, although contingencies on the angular weights ω_{m}, and directions $\hat{\boldsymbol{s}}_{\mathrm{m}}$ can be obtained to satisfy certain conditions, such as symmetry. In general, the weights, and sets of directions are chosen as completely symmetric (Murthy and Mathur, 1998). Different weights, and sets of directions have a great effect on the accuracy, and they have been tabulated in the literature (Lee, 1962; Lathrop and Carlson, 1965; Truelove, 1987; Fiveland, 1987). The name $\mathrm{S_N}$ approximation indicates that N different direction cosines are applied for each number of direction (Murthy and Mathur, 1998). The range of quadrature discretization schemes are normally performed by $\mathrm{S_2}$-$\mathrm{S_8}$ in the DOM. More information concerning different angular discretization, and its accuracy of radiative heat transfer prediction can be found in the previously reported results by Jensen et al. (2007), and Hostikka (2008). The DOM has been used for produc-

ing results in all modeling simulations of the current research.

2.3 The Discrete Ordinates method

The discrete ordinates method (DOM) is the only method in the Fluent software package (Ansys, 2009) which can solve the radiative heat transfer equation (RTE) both in its gray, and non gray form (Stefanidis et al., 2007). For the gray modeling, the DOM utilizes the RTE as a field equation as (Raithby and Chui, 1990; Chui and Raithby, 1993)

$$\nabla \cdot (\mathrm{I}(\boldsymbol{r},\boldsymbol{s})\boldsymbol{s}) + (\mathrm{K}+\sigma_\mathrm{s})\mathrm{I}(\boldsymbol{r},\boldsymbol{s}) = \mathrm{Kn}^2\frac{\sigma \mathrm{T}^4}{\pi} + \frac{\sigma_\mathrm{s}}{4\pi}\int_0^{4\pi} \mathrm{I}(\boldsymbol{r},\boldsymbol{s}')\Phi(\boldsymbol{s}\cdot\boldsymbol{s}')\mathrm{d}\Omega', \qquad (2.5)$$

where $\boldsymbol{s}$ is a direction vector, σ_s is the scattering coefficient, n is the refractive index, and Φ is the scattering phase function.

The scattering effect is excluded from the presented thesis and the related term can be ignored from the RTE (the last term of integral is ignored). Thus, only gas radiation is taken into account. For the non gray radiative heat transfer modeling, the RTE should be solved in its spectral form as

$$\nabla \cdot (\mathrm{I}_\eta(\boldsymbol{r},\boldsymbol{s})\boldsymbol{s}) + (\mathrm{K}_\eta+\sigma_\mathrm{s})\mathrm{I}_\eta(\boldsymbol{r},\boldsymbol{s}) = \mathrm{K}_\eta \mathrm{n}^2\mathrm{I}_{\mathrm{b}\eta} + \frac{\sigma_\mathrm{s}}{4\pi}\int_0^{4\pi} \mathrm{I}_\eta(\boldsymbol{r},\boldsymbol{s}')\Phi(\boldsymbol{s}\cdot\boldsymbol{s}')\mathrm{d}\Omega', \quad (2.6)$$

where K_η is the spectral absorption coefficient, and $\mathrm{I}_{\mathrm{b}\eta}$ is the Planck distribution function.

To solve the RTE in its non gray form, the entire radiative spectrum can be divided into a number of wavelength/wavenumber intervals. The RTE is integrated over each spectral interval producing transport equations of the band quantity $\mathrm{I}_\eta \Delta\eta$, and each of the absorbing bands is treated as gray. The emission of black body over spectral interval per solid angle is estimated as (Modest, 1993)

$$\mathrm{I}_{\mathrm{b},\Delta\eta} = \left(f(\mathrm{n}\eta_\mathrm{u}\mathrm{T}) - f(\mathrm{n}\eta_\mathrm{l}\mathrm{T})\right)\mathrm{n}^2\frac{\sigma \mathrm{T}^4}{\pi}, \qquad (2.7)$$

where $f(\mathrm{n}\eta\mathrm{T})$ is the fractional black body function, and η_u and η_l are the upper and lower limits of the spectral interval, respectively.

The total intensity of each direction $\boldsymbol{s}$ considering position $\boldsymbol{r}$ is calculated as (Raithby and Chui, 1990)

$$\mathrm{I}(\boldsymbol{r},\boldsymbol{s}) = \sum_\mathrm{N} \mathrm{I}_\eta(\boldsymbol{r},\boldsymbol{s})\Delta\eta, \qquad (2.8)$$

where the summation is obtained over all selected spectral intervals.

The boundary conditions for the gray, and non gray modeling of DOM are applied on a band basis. In the non gray approach, the treatment within a spectral limit is the same as in the gray modeling. For the gray radiative modeling, the radiative flux leaving a surface is estimated as (Raithby and Chui, 1990; Chui and Raithby, 1993)

$$\mathrm{q_{out}} = (1 - \epsilon_\mathrm{w})\mathrm{q_{in}} + \mathrm{n}^2\epsilon_\mathrm{w}\sigma\mathrm{T}_\mathrm{w}^4, \tag{2.9}$$

where ϵ_w is the emissivity of a gray wall, and $\mathrm{q_{in}}$ is the incident radiation on the surface.

For the non gray radiative modeling, the radiative flux leaving a surface within a spectral limit $\Delta\eta$ is calculated as

$$\mathrm{q_{out,\Delta\eta}} = (1 - \epsilon_\mathrm{w,\Delta\eta})\mathrm{q_{in,\Delta\eta}} + \epsilon_\mathrm{w,\Delta\eta}\left(f(\mathrm{n}\eta_\mathrm{u}\mathrm{T}) - f(\mathrm{n}\eta_\mathrm{l}\mathrm{T})\right)\mathrm{n}^2\sigma\mathrm{T}_\mathrm{w}^4, \tag{2.10}$$

where $\epsilon_\mathrm{w,\Delta\eta}$ is the emissivity of a wall in the spectral interval, and $\mathrm{q_{in,\Delta\eta}}$ is the incident radiation on the surface within the spectral interval.

The incident radiation on the surface for the entire spectrum, and the selected spectral interval $\Delta\eta$ can be calculated as follows:

$$\mathrm{q_{in}} = \int_{\boldsymbol{s}\cdot\boldsymbol{n}>0} \mathrm{I_{in}}\boldsymbol{s}\cdot\boldsymbol{n}\mathrm{d}\Omega \tag{2.11}$$

and

$$\mathrm{q_{in,\Delta\eta}} = \Delta\eta\int_{\boldsymbol{s}\cdot\boldsymbol{n}>0} \mathrm{I_{in,\eta}}\boldsymbol{s}\cdot\boldsymbol{n}\mathrm{d}\Omega, \tag{2.12}$$

for the gray, and non gray radiative modeling, respectively.

2.4 Experimental quantitative spectroscopy

At a certain spectral position, a single spectral line is characterized by its intensity, and its line half-width. A vibration-rotation band has many closely spaced spectral lines that may overlap considerably. The absorption coefficient of an entire band is a sum of the absorption coefficient of the individual lines located in the band of each component contained in gas mixture at any spectral position (Denison and Webb, 1995; Modest, 2003b; Ströhle, 2008)

$$\mathrm{K}_\eta = \sum_j \mathrm{K}_{\eta j}, \tag{2.13}$$

where K_η is the spectral absorption coefficient, and j is a gas component of mixture.

It is shown in Figure 2.2, that unless the lines overlap very strongly, the function of spectral lines aims to strongly variate across the band.

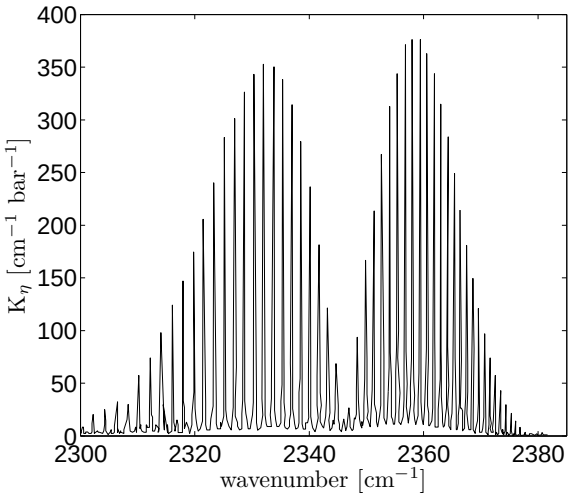

Figure 2.2: Spectral absorption coefficient of CO_2 in nitrogen with 4.3 μm band at $\mathrm{T} = 296$ K, and $\mathrm{P} = 1.0$ bar. Reproduced from Modest (2003b).

The fact that there could be tens of thousands of spectral lines makes the calculations of radiative transfer rather difficult, especially according to the tendency mentioned above. For the total intensity of spectral integration, the following equation can be used (Modest, 1991)

$$\mathrm{I}_\eta(\mathrm{s}) = \mathrm{I}_{\mathrm{bw}\eta}\exp\left[-\int_0^{\mathrm{s}} \mathrm{K}_\eta \mathrm{ds}'\right] + \int_0^{\mathrm{s}} \mathrm{I}_{\mathrm{b}\eta}(\mathrm{s}')\exp\left[-\int_{\mathrm{s}'}^{\mathrm{s}} \mathrm{K}_\eta \mathrm{ds}''\right]\mathrm{K}_\eta(\mathrm{s}')\mathrm{ds}' \ , \qquad (2.14)$$

where $\mathrm{I}_{\mathrm{bw}\eta} = \mathrm{I}_{\mathrm{b}\eta}(\mathrm{T}_\mathrm{w})$ is the intensity emitted into the medium from the black wall at $\mathrm{s} = 0$.

In Eq. 2.14, the first part on the right side is the contribution to the local intensity by the enclosure entering intensity at $\boldsymbol{s} = 0$ over the optical distance τ_η. The second part after the plus sign is the local emission contribution at τ'_η. Moreover, between the emission point, and the point under consideration $(\tau_\eta - \tau'_\eta)$ it is exponentially attenuated by self extinction over the optical distance. Finally, the integral sums the total contributions over the entire emission path.

The radiative heat flux is

$$\mathrm{q} = \int_0^\infty \int_{4\pi} \mathrm{I}_\eta(\boldsymbol{s})\boldsymbol{s}\mathrm{d}\Omega\mathrm{d}\eta, \qquad (2.15)$$

where q is the total radiative heat flux.

Depending on the described surface or the coordinate system used, the heat flux vector of radiative energy can be separated into normal, and tangential surface components or into the components of coordinate; for example, it can be a Cartesian system ($\mathrm{q_x}$, $\mathrm{q_y}$, $\mathrm{q_z}$) of coordinate.

The divergence of the heat flux can be expressed

$$\Delta \mathrm{q}_\eta = \mathrm{K}_\eta (4\pi \mathrm{I}_{\mathrm{b}\eta} - \int_{4\pi} \mathrm{I}_\eta \mathrm{d}\Omega) = \mathrm{K}_\eta (4\pi \mathrm{I}_{\mathrm{b}\eta} - \mathrm{G}_\eta), \tag{2.16}$$

where $\mathrm{I_b}$ is the blackbody intensity, and G is the incident radiation.

The physical base of Eq. 2.16 is that the net loss of radiative energy from a certain volume equals to the emitted energy excluding the absorbed energy. This integrated part of the heat transfer equation does not contain the coefficient of scattering because the scattering only redirects the photon stream. Thus, it does not affect the content of energy of any unit volume.

There are several experimental methods of determining the radiative properties of molecular gases. Because of the strongly changing values of the absorption coefficient, the problem of spectral radiative transfer must be solved for several hundred thousand wavenumbers which are followed by the spectrum integration. Differently from monochromators or spectrographs, FTIR spectrometers gather all wavelengths simultaneously. This method of experimental measurements is based on obtaining the infrared spectrum by collecting an interferogram of a sample signal through an interferometer. Finally, to obtain the spectrum, a Fourier transform is applied to the interferogram. Most common methods consist of measurements of gas properties by monochromators or Fourier transform infra red (FTIR) spectrometers, and they consist of a light source, a chopper, a test cell with the tested gas, a detector, associated optics, and an amplifier-recorder device (Modest, 2003b). A typical set-up unit is shown in Figure 2.3, and this kind of an apparatus scheme has been developed by Tien and Giedt (1965).

Usually, the chopper is used for two purposes. The first one is that a pyroelectric detector measures changes in the intensity but not the radiative intensity itself. The second one is that if the beam chopped before going through the tested gas, the incident light beam transmission can be measured by the difference in the intensity between the chopper open, and closed conditions. If a FTIR spectrometer is used, a chopper is not required due to the modulated light inside the unit.

The narrow band measurements, total band absorptance measurements or total emissivity/absorptivity measurements are obtained by hot window cell, cold window cell, nozzle seal cell, and free jet devices (Edwards, 1976). An isothermal gas within a vessel with closed ends at the same temperature as the gas is utilized in the hot window cell. Because the window must withstand both the high temperatures, and be transparent in the spectrum, its material presents a certain problem for obtaining the measurements. In the

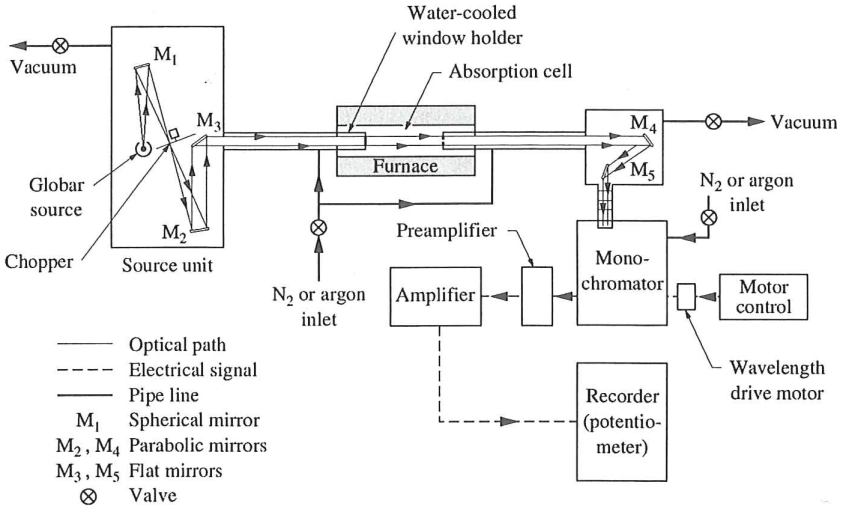

Figure 2.3: Apparatus unit of gas radiative measurements. Reproduced from Tien and Giedt (1965).

cold window cell, the windows through which the beam is passing are cooled by water. Thus, one of the problems of the previous method does not exist anymore. However, in the relatively small geometric path, the cold window cell method creates variations in temperature, and density along the path. The description of the apparatus of gas radiative measurements of the cold window cell method is shown in Figure 2.3, and more details can be found in the work presented by Tien and Giedt (1965). Nozzle seal cells (Hottel and Mangelsdorf, 1935) present open flow cells containing absorbing gas by layers on each end of an inert gas (N_2). Free jet devices are used for very high temperatures, and they introduce great opacity with respect to the density distribution, and gas temperature, and to the path length (Ferriso and Ludwig, 1964b).

Almost all measurements of gas properties are subject to significant experimental errors. In our days, the data measurements apparently have experimental errors less than 5% (Modest and Bharadwaj, 2002).

HITRAN (***H****igh resolution* ***Tran****smission*) represents a database of molecular spectroscopy the compilation of which consists of several units that are created as input codes for radiative transfer calculation. It includes parameters of the individual line for the micro-wave through the visible spectra of molecules in the gas phase. Also, it includes the absorption cross-sections for molecules having dense features of spectra; in other words, spectra in which the individual lines are not solvable, for example ultra-violet bands or refractive aerosols indices. The HITRAN database is recognized as an international standard (Rothman et al., 2005) which is used for a vast array of applications

including transmission simulations, terrestrial atmospheric remote sensing, basic laboratory spectroscopy data, monitoring of industrial process, and regulatory of pollution data. This kind of calculation can be the most accurate to date, but unfortunately, it requires a huge amount of computational resources. It is simply impossible to calculate in the nearest future because the HITRAN96 database is the result of many years of hard work, and is limited to atmospheric conditions with low partial pressures, and ambient temperature. Lately, a high temperature version of HITRAN96, called HITEMP by Rothman et al. (2009), has become available for CO_2 (including 1 million lines), and H_2O (including 1.2 million lines), and it has recently been updated by Rothman et al. (2010).

A number of investigators have created the total emissivity charts based on the integration of spectral data. Leckner (1972), and Ludwig et al. (1973) reported such charts which agree with each other well (Modest, 2003b). Using such charts, and other available experimental data, some empirical correlations have been reported for the total emissivity or absorptivity of the H_2O-CO_2 mixtures. They have been found based on correlating the available experimental data, and therefore, their accuracy depends on the accuracy of the experimental data, the form of the function used for the curve fitting, and the accuracy of fitting. One of the most famous ones was found by Leckner (1972), and it has been widely used in the engineering calculations of heat transfer in furnaces. Beside the Leckner method, one of the latest works of empirical correlations for the emissivities of the H_2O-CO_2 mixtures is provided by Green and Perry (2008). Based on the data provided in Hottel emissivity charts (Hottel and Sarofim, 1967), this empirical correlation was developed, and adjusted to the more recent data from RADCAL (Grosshandler, 1993). The constants of this empirical correlation are tabulated for $\mathrm{T} = 1000$ K, 1500 K, and 2000 K, and for $\mathrm{Pr} = 0$, 0.5, 1.0, 2.0, 3.0, and ∞ $\left(\mathrm{Pr} = \frac{\mathrm{p_{H_2O}}}{\mathrm{p_{CO_2}}}\right)$. For other T's, and Pr's, linear interpolation (extrapolation) of the constants is needed (Green and Perry, 2008).

2.5 Models for calculation of radiative properties in gases

The radiative heat transfer calculations are significantly different in industrial and meteorological contexts because of the differences in the total pressure. The calculation of larger pressures involving the entire spectrum is a really difficult task which has induced the development of the approximate spectral models (Modest, 2003b). There are three general model classes for the calculation of radiative properties of gas mixtures. In order of decreasing intricacy, they create the following list: the spectral line-by-line models (SLBLM), the spectral band models (SBM), and the gray gas models.

The SLBLMs estimate the radiative properties for each separate absorption line, and they are based on the HITRAN database. The rotational, and vibrational bands contain thousands of absorption lines. This kind of calculation is computationally expensive, and time consuming. The line-by-line portion of the HITRAN database contains spectroscopic parameters for 39 molecules. It is significant that the high resolution property of gas data resolution is better than $0.01\ \mathrm{cm}^{-1}$ which is the required accuracy for line-by-line calcu-

lations. The line-by-line model (LBLM) can be used for the accuracy testing of different approximate spectral models (Modest, 2003b). Węcel et al. (2010) has recently proposed new mathematical method to decrease the computational time of line-by-line calculations.

The SBM split up the whole wavelength spectrum into spectral bands. The SBM models can be classified into Narrow Band Models (NBM), and Wide Band Models (WBM), based on the spectral determination. NBM models divide the radiative heat transfer spectrum into narrow wavenumber intervals. Inside these intervals, the absorption coefficient is assumed to be constant, and it is estimated statistically. The emissivity, and the absorption coefficient of the narrow bands are obtained by using the experimental data of the mean intensity, and the spacing of individual absorption lines. The most widely used methods for calculating the narrow band properties are the Elsasser (Siegel and Howell, 1992; Modest, 2003b), and statistical models (Siegel and Howell, 1992; Soufiani and Taine, 1997; Modest, 2003b). In the first model, the lines within the narrow bands are assumed to be equally spaced with equal intensity. In the second model, the spectral lines are treated as randomly spaced. The main difference between these two methods is the way they treat the overlapping regions between bands (Modest, 2003b). In computational speed the NBM models are more efficient than the SLBLM; however, they need a larger number of bands compared to WBM. Thus, their computational costs are quite high. Theoretically, narrow band calculations can have almost the same accuracy as line-by-line calculations. The basic disadvantage of this kind of models is that they are not easy to apply to inhomogeneous gases (Soufiani and Taine, 1997; Park and Kim, 2002). Moreover, based on narrow band data, the calculations are limited to non scattering media within black-screened enclosures.

This statistical model is based on the exponential-tailed distribution function of line intensities. The narrow band properties are determined by the line property average with the probability density function. In the current research, the following formulation of the SNBM has been used to produce the databases of emissivities. The properties of the SNBM were obtained with a constant $25\ \mathrm{cm}^{-1}$ spectral width $\Delta\eta$ by using the LBLM based on the approximation of spectroscopic databases (Soufiani and Taine, 1997), including all of the lines of the HITRAN92 database. Riviére et al. (1994) reported that the spectral width of $25\ \mathrm{cm}^{-1}$ is narrow enough to assume a constant Planck function inside each absorption band in the temperature range of 300–2500 K. Soufiani and Taine (1997) have reproduced the calculations for $\mathrm{H_2O}$, $\mathrm{CO_2}$, and CO. The parameters of the model are also calculated using the line-by-line model. These values are tabulated for wavenumber intervals of $25\ \mathrm{cm}^{-1}$ (Soufiani et al., 1985). Further details of the SNBM can be found in the study of Soufiani and Taine (1997), and in Chapter 4 starting from page 69.

In general, the WBM equations are obtained by integrating the results of the NBM with adequate accuracy. Wide band calculations have been widely used due to the fast, and simple calculations. The WBM model is based on the absorption/emission of the infrared radiation by a molecular gas. The exponential wide band model (EWBM) is one of the famous models of its class. In the EWBM, extensive knowledge of the intensity, and posi-

tion of the rotational lines is found to be not so important because they can be reordered in the wavenumber space with the intensities of exponentially decreasing line stirring away from the head of the band. The band form is approximated by one of the three elementary exponential functions depending on upper or lower limits (see Figure 2.4). The wavenumber of the band center is also used to appoint the position of the band head (Cumber et al., 1998). Radiative properties are then obtained by specifying three model factors that characterize the given absorption band: the integrated band intensity (α), the mean line width to spacing parameter (β), and the band width parameter (ω). Variable values have been estimated for the number of bands of molecular gases by Edwards and Balakrishnan (1973). One of the simplest ways to approximate the effect of absoptive/emissive bands of gases, and their mixtures on radiative heat transfer calculations is the box model. In this model, the spectral absorption coefficient for a gas or gas mixture is calculated as a sum of all band absorption coefficient values which are assumed to be constant for each band.

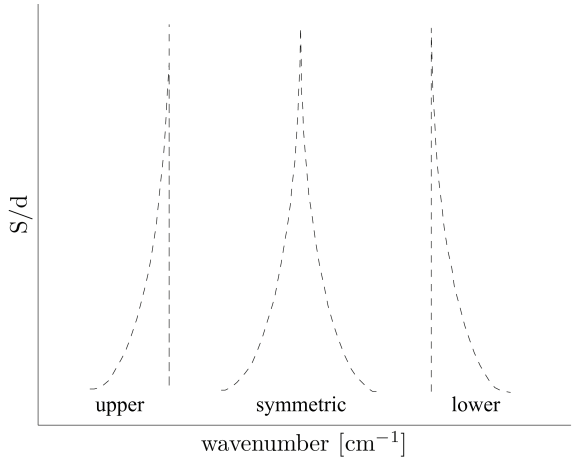

Figure 2.4: Exponential shapes of the bands.

Besides normal narrow band models (NBMs), there are more recent developments, such as the narrow band k-distribution methods (Modest, 2003a), and statistical narrow band correlated-k method (Liu and Smallwood, 2004). Moreover, band models are traditionally required to neglect the scattering, and this may affect the accuracy of modeling in general (Porter et al., 2010). Several methods are well established to provide results accurate enough for the modeling of the radiative properties of H_2O, and CO_2 as major combustion species. These methods are the spectral line based weighted sum of gray gases methods (SLWM) (Denison and Webb, 1995; Solovjov and Webb, 2000), and the full spectrum k-distribution methods (FSKM) (Modest, 2003a,b; Modest and Zhang, 2002). The FSKM is based on the reordering of the absorption coefficient subjection on wavenumber. For gases, the absorption coefficient may vary significantly in the spectrum, and be dependent on the pressure, and temperature. However, the other properties depending on the

wavenumber are constant, for example, the Planck distribution (Modest, 2003b). For several different wavenumbers, the equal absorption coefficient may be obtained over the narrow band. Thus, the distribution is reordered to k-distribution of the absorption coefficient, and it reduces the number of calculations resulting in more smooth dependence of the absorption coefficient on the cumulated function (Porter et al., 2010). Because the k-distributions are quite new, and they are difficult to apply to inhomogeneous media, they require more development in research. This exception has forced different researchers to create wide band k-distribution models based on EWBM correlation data. Wang and Shi (1988) have created a such model using the Malkmus narrow band model together with the exponentially decaying average of line strength. The Malkmus model is one of the most famous statistical models for the radiative calculations of gas mixtures. The wide band k-distribution method consists of numerical integration of the reordered absorption coefficient, obtained from the total band absorptance based on WBM parameters. For a homogeneous media, the k-distribution method demonstrates high accuracy compared to the LBL databases (Wang and Modest, 2005).

The box model (BM) is a very simple model in which the band is estimated by a rectangular box of the effective band width $\Delta\eta_{\mathrm{e}}$, and height $\bar{\mathrm{k}}$, as shown in Figure 2.5. The difference between the BM, and total properties model is that the last one supports full range radiative properties. Those values are received through the increasing sum weight of band properties over the full spectrum of wavelength. The most widely used gray gas models or models of total properties (Stefanidis et al., 2007) are the SLWM, and the weighted sum of gray gases model (WSGGM). These models are placed in order of accuracy of calculations, and decreasing complexity. The WSGGM (Hottel and Sarofim, 1967; Smith et al., 1982) is an engineering approximating method for the estimation of the absorption coefficient of gas mixtures. One of the most well known WSGGM coefficients are those presented by Smith et al. (1982). In their study, three gray gases, and one transparent gas were used to model the $\mathrm{H_2O}$-$\mathrm{CO_2}$ in air-fired combustion conditions. Originally, the WSGGM was proposed by Hottel and Sarofim (1967) in the framework of the radiative zone method to create a possibility to be applied to a non gray media with scattering. This feature is very important in furnace simulations when gas, and soot mixture are determinated by soot particles blackening furnace walls (Modest, 2003b).

In the non gray modeling, the media is assumed to involve various fractions of gray gases with the related partial values of absorption coefficient. In the case of non gray modeling, the RTE should be solved for each of these partial absorption coefficients, and the results should be summed up together using the blackbody fractional function of each value as the weighted factor. In the gray gas modeling, a single time solution of the RTE over the whole spectrum where the radiative heat transfer occurs employs an average absorption coefficient. This is the reason why the gray gas approach results in faster calculations of radiative heat transfer compared to the non gray approach. Because of the high importance of the computational time, the gray approach is the most widely used in industrial combustion systems of radiative heat transfer modeling.

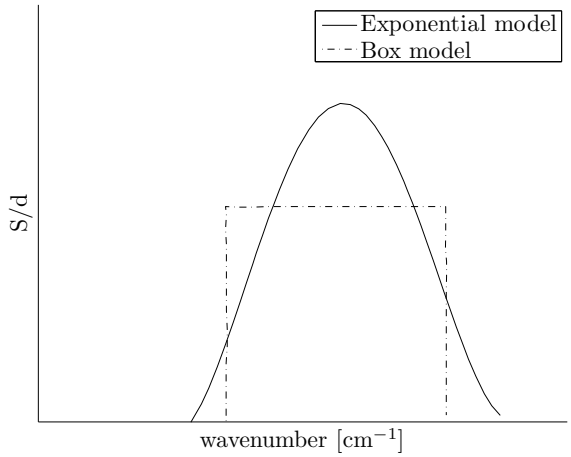

Figure 2.5: The exponential, and box models for the total band absorptance approximation.

The general supposition of the WSGGM is that the main emissivity of the gas over the center to center distance of the two radiative elements can be estimated by weighted summation of several gray gas emissivities (Hottel and Sarofim, 1967). The supposition of the model is right with the exception that the medium is optically thin and the temperature of the wall differs greatly from the temperature of the gas. The coefficients of the model are slowly changing functions of pressure P, optical path length L, and temperature T. The coefficients are obtained for different relative pressures of H_2O and CO_2 gases with the total pressure ($\mathrm{P_t}$) 1 bar. The WSGGM coefficients obtained by Smith et al. (1982) are in use for the limits: $0.001 \leq \mathrm{P_t L} \leq 10$ bar m, and $600 \leq \mathrm{T} \leq 2400$ K. For $\mathrm{T} \geq 2400$ K, updated coefficient values are suggested. The coefficients reported by Smith et al. (1982) were extracted from the EWBM with the band parameters reported by Edwards (1976). The accuracy of the WSGGM depends on the number of gray gases, database behind the model, and the accuracy of curve fitting.

2.6 The Wide Bands methods

Due to reasonable computational performance, the wide band models have been widely used to calculate the radiation properties of gases in the industrial combustion processes. Generally, this kind of methods treat the spectral range of the entire absorption bands (Modest, 2003b). The simplest wide band model is the box model developed by Penner (Penner, 1959) which approximates each gas absorption band as a rectangular box of certain width, and height. The accuracy of the box method is very sensitive to the correct choice of the effective band width, especially when the emission from a hot gas is desired (Modest, 2003b). However, the box model has been widely used in engineering applica-

tions because of its great simplicity.

A more complex wide band model is the exponential wide band model (EWBM). By reordering of wavenumbers, the EWBM assumes an exponential function for the mean line intensity to the line spacing ratio within each absorption band. In the EWBM, the radiative properties of each absorption band are characterized by three specifying factors: integrated band intensity, mean line width to spacing parameter, and band width parameter. These factors were obtained experimentally for a number of bands of molecular gases by Edwards and Balakrishnan (1973) to be used in a four-region equation which is proposed for obtaining the absorptivity of the bands.

As mentioned in the introduction part, the wide band interdependences are estimated by integrating the narrow band results across an entire band with a lower level of accuracy. Because of the fast, and simple calculations, the wide band models have been widely used. However, it is known that wide band predictions have a basic inaccuracy of $\pm 30\%$, and in some cases it can be as much as 70% (Modest, 2003b).

2.6.1 Exponential Wide Band Model (EWBM)

Kirchhoff's law designates the numerical relation between the absorptivity, and emissivity of black, and gray bodies. This kind of relation can be derived from the heat balance equation of the emitting system of several bodies with the walls non participating in radiative heat transfer. The radiative energy of each of the bodies is equal to the absorptive energy at the conditions of thermodynamic equilibrium as (Nadezin, 1986)

$$\frac{\epsilon_1(\eta, \mathrm{T})}{\mathrm{A}_1(\eta, \mathrm{T})} = \frac{\epsilon_2(\eta, \mathrm{T})}{\mathrm{A}_2(\eta, \mathrm{T})} = ... = \epsilon_{\mathrm{b}}(\eta, \mathrm{T}) = f(\eta, \mathrm{T}), \tag{2.17}$$

where ϵ is the emissivity, A is the absorptivity, ϵ_{b} is the radiative emittance of an absolute black body which is defined by the Planck law, and for absolute black body $\mathrm{A}(\eta, \mathrm{T}) = 1$.

Kirchhoff's law is correct both for the total radiation, and for the monochromatic radiation. Moreover, it can be concluded that at thermodynamic equilibrium, the monochromatic absorptivity A_η is identical to its monochromatic emissivity ϵ_η and does not depend on the surface properties ($\mathrm{A}_\eta = \epsilon_\eta$).

The phrase "gas emissivity" obviously represents the reference, meaning the emission from a volume unit of isothermal gas to a unit of its limiting surface. The gas emissivity is complying to a not moved beam length L (path length). It is correspondingly identical to the ratio of typical radiation onto a surface unit $\mathrm{dA_s}$ from a narrow beam of light of length L to radiation from blackbody with gas temperature.

By using the aforementioned definition, the Beer's law states that the monochromatic emissivity, and absorptivity are equal to each other

$$\epsilon_\eta = \mathrm{A}_\eta = 1 - \exp\left[-\mathrm{K}_\eta \mathrm{PL}\right], \tag{2.18}$$

where K_η is the spectral absorption coefficient, and L is the optical path length.

The total emissivity or absorptivity is obtained by integrating the spectral emissivity or absorptivity of all the wavenumbers as

$$\epsilon_\mathrm{g} = \frac{\int_0^\infty \epsilon_\eta \mathrm{E}_{\eta,\mathrm{g}} \mathrm{d}\eta}{\int_0^\infty \mathrm{E}_{\eta,\mathrm{g}} \mathrm{d}\eta} = \frac{1}{\sigma \mathrm{T}_\mathrm{g}^4} \int_0^\infty \epsilon_\eta \mathrm{E}_{\eta,\mathrm{g}} \mathrm{d}\eta, \tag{2.19}$$

$$\mathrm{A}_{\mathrm{g,s}} = \frac{\int_0^\infty \mathrm{A}_\eta \mathrm{E}_{\eta,\mathrm{s}} \mathrm{d}\eta}{\int_0^\infty \mathrm{E}_{\eta,\mathrm{s}} \mathrm{d}\eta} = \frac{1}{\sigma \mathrm{T}_\mathrm{s}^4} \int_0^\infty \mathrm{A}_\eta \mathrm{E}_{\eta,\mathrm{s}} \mathrm{d}\eta = \frac{1}{\sigma \mathrm{T}_\mathrm{s}^4} \int_0^\infty \epsilon_\eta \mathrm{E}_{\eta,\mathrm{s}} \mathrm{d}\eta, \tag{2.20}$$

where E is the blackbody monochromatic emissive power (Plank function), and T_g and T_s are the temperatures of gas and surface, respectively.

The absorption coefficient of the monochromatic cloud is independent on particle size, and proportional to the volume fraction (f_v) of area engaged by particles, and to the corresponding wavenumber (η). The emissivity is calculated then

$$\epsilon_\eta = 1 - \exp\left[-\mathrm{K} \mathrm{f}_\mathrm{v} \eta \mathrm{L}\right], \tag{2.21}$$

where f_v is the volume fraction ($\mathrm{f}_\mathrm{v} = \mathrm{C}_\mathrm{m}\rho$), C_m is the mass concentration, and ρ is the particle density.

The substitution of the Planck second radiation constant reduces the total emissivity (Hottel and Sarofim, 1967) to

$$\epsilon_\mathrm{g} = 1 - \left[\frac{1}{1 + \frac{\mathrm{K} \mathrm{f}_\mathrm{v} \mathrm{LT}}{\mathrm{C}_2}}\right]^4, \tag{2.22}$$

where C_2 is the Planck second radiation constant, and K is the absorption coefficient.

2.6.2 Formulations of the EWBM

The exponential wide band model (EWBM) was originally developed by Edwards and Balakrishnan (1973), and it was based on an analysis of physical gas absorption. The EWBM can easily be used for the prediction of the total radiative properties of gas mixtures for $\mathrm{H_2O}$, $\mathrm{CO_2}$, CO, NO, $\mathrm{SO_2}$, and $\mathrm{CH_4}$. The band parameters for these six gases have been obtained experimentally by Edwards and Balakrishnan (1973) for the original EWBM. Moreover, the model can be modified to work with other gases, and for that

purpose, the band parameters of the requested gases should be obtained. The EWBM is supposed to be used in a wide range of values, in comparison with the NBM; for example, the temperature range can be calculated from 300 to 3000 K, the total pressure from 0.5 to 20 bar, molar fractions of gases from 0 to 1, and the path length from 10^{-4} to 100 meters. The EWBM is less time consuming than the NBM (Lallemant and Weber, 1996) in the emissivity/absorptivity calculations.

One and two atom gases, such as helium, hydrogen, oxygen, and nitrogen, are practically transparent for radiation. Three and higher atom gases, such as CO_2, and H_2O, the possess greater emissivity, and absorptivity. Unlike most of the radiation of solid, and liquid bodies, the radiation of gases is volumetric, and all gas micro-particles are involved in it. Therefore, the absorptivity of gases depends on the density, and thickness of the gas layer. With the increase of density, and thickness of the gas layer, the absorptivity is increased (Isachenko et al., 1975). Gases absorb, and radiate only in certain intervals of wavenumbers, and in the other parts of a spectrum, they are transparent.

The states of photon vibrations interacting with the molecules are affecting the asymmetry shape of the band. In the case of a symmetrical band, the vibration of atoms does not produce an observable absorption band to increase, excluding the collisions that disturb the symmetry at high pressures (see Figure 2.4). Photon interacting with the molecules happens when the wavenumber of the photon is in the limit of vibration-rotational line, line width or two of wavenumber η_i. Then the photon energy $\mathrm{hc}\eta$ is almost equal to the difference between the energy E' in a quantified state of rotation, and vibration, and the molecular energy E'' in the original quantified state. These energy levels (Edwards, 1976) can be presented to the harmonic-oscillator, and rigid-rotator approximation as

$$\mathrm{E}' = \mathrm{hc}\eta \left(\vartheta' + \frac{1}{2}\right) + \mathrm{hcB}'\mathrm{J}'\left(\mathrm{J}' + 1\right), \tag{2.23}$$

$$\mathrm{E}'' = \mathrm{hc}\eta_0 \left(\vartheta'' + \frac{1}{2}\right) + \mathrm{hcB}''\mathrm{J}''\left(\mathrm{J}'' + 1\right), \tag{2.24}$$

$$\mathrm{hc}\eta = \mathrm{E}' - \mathrm{E}'', \tag{2.25}$$

where ϑ', and ϑ'' are the vibrational quantum numbers, J' and J'' are the rotational quantum numbers, η_0 is the vibrational constant, and B is the rotational constant which fixes the band location.

The integrated intensity equals to

$$\alpha = \int_0^\infty \left(\frac{\mathrm{S}}{\mathrm{d}}\right) \mathrm{d}(\eta_0 - \eta), \tag{2.26}$$

where α is the integrated intensity, and S/d is the leveled absorption coefficient.

The EWBM supports a mathematical model to estimate the experimental data to forecast

band properties. Edwards and Menard (1964) were the first who showed that three physical parameters are necessary to describe the total gas band absorptances over a wide range of temperature, pressure, and path length conditions: 1. The integrated band intensity – α; 2. The exponential decay width parameter – ω; and 3. The line-width-to-spacing parameter – β.

The line strength decreases exponentially in the band shapes remote from the band center. Edwards (1976) assumed that the leveled absorption coefficient S/d has the following shapes, shown in Figure 2.4:

$$\frac{\mathrm{S}}{\mathrm{d}} = \frac{\alpha}{\omega}\exp\left[-\frac{(\eta_{\mathrm{u}} - \eta)}{\omega}\right], \tag{2.27}$$

$$\frac{\mathrm{S}}{\mathrm{d}} = \frac{\alpha}{\omega}\exp\left[-\frac{2|\eta_{\mathrm{c}} - \eta|}{\omega}\right], \tag{2.28}$$

$$\frac{\mathrm{S}}{\mathrm{d}} = \frac{\alpha}{\omega}\exp\left[-\frac{(\eta - \eta_{\mathrm{l}})}{\omega}\right]. \tag{2.29}$$

The integrated absorption coefficient (K), that is the area under the curves in Figure 2.4, can be defined from the following equation

$$\mathrm{K} \equiv \int_0^\infty \mathrm{k}_\eta \mathrm{d}\eta = \int_0^\infty \left(\frac{\mathrm{S}}{\mathrm{d}}\right)_\eta \mathrm{d}\eta, \tag{2.30}$$

where k_η is the height of the band ($\bar{\mathrm{k}} = \frac{\mathrm{K}}{\Delta\eta_{\mathrm{e}}}$) which is shown in Figure 2.5.

In theory, α, β, and ω of each band are changing with pressure, and temperature. The effect of temperature is included in the EWBM formulations while the effect of pressure is involved by introducing the effective pressure (Stefanidis et al., 2007). The pressure dependence is considered with the effective pressure P_{e}, and it is calculated by equation

$$\mathrm{P}_{\mathrm{e},i} = \left[\frac{\mathrm{P}}{\mathrm{P}_0} + \frac{\mathrm{P}_i}{\mathrm{P}_0}(\mathrm{B}_i - 1)\right]^n, \tag{2.31}$$

where P_0 is the reference pressure (1 bar), P is the total pressure, P_i is the partial pressure of the absorbing gas, and B_i is the pressure self-broadening coefficient.

The other parameters of Eq. 2.31 are reported in the work of Edwards and Balakrishnan (1973) for each gas component as: b is the pressure broadening parameter which is calculated by $\mathrm{B} = 8.6\left(\frac{\mathrm{T}_0}{\mathrm{T}}\right)^{0.5} + 0.5$ for $\mathrm{H_2O}$ and for others gases, and their bands, there are known values which are obtained and tabulated; and n is the pressure broadening exponent (i.e., there are obtained and tabulated values for each gas component).

Equations for the functional dependence of α, β, and ω have been elaborated experimentally. These parameters for six different gases ($\mathrm{H_2O}$, $\mathrm{CO_2}$, CO, NO, $\mathrm{SO_2}$, and $\mathrm{CH_4}$) with

the reference temperature of $\mathrm{T}_0 = 100$ K are listed in the work by Edwards (1976).

The band absorption A (Edwards and Balakrishnan, 1973) is derived as

$$\mathrm{A}(\mathrm{X},\eta) = \int_0^{\infty} \left[1 - \exp\left[\frac{-\left(\frac{\mathrm{S}}{\mathrm{d}}\right)\mathrm{X}}{\left(1+\left(\frac{\mathrm{S}}{\mathrm{d}}\right)\frac{\mathrm{X}}{\zeta}\right)^{0.5}}\right]\right] \mathrm{d}(\eta_0 - \eta), \tag{2.32}$$

where $\zeta = \beta \mathrm{P}_\mathrm{e}$, and P_e is given by Eq. 2.31.

The exponential-tailed band model enables the using of a four-region equation for the determinations of non-dimensional band absorption which is defined as

$$\mathrm{A}^* = \frac{\mathrm{A}}{\omega}. \tag{2.33}$$

In this regard, the optical depth at the band head (with upper, lower, and symmetrical bands η_u, η_l, and η_c) equals to

$$\tau_\mathrm{H} = \frac{\alpha \mathrm{X}}{\omega}. \tag{2.34}$$

Then the dimensionless band absorption is estimated by the four-region equation (Edwards and Balakrishnan, 1973; Edwards, 1976):

The linear region for small optical depth, and high pressure as

$$\tau_{\mathrm{H,k}} \leq 1, \qquad \tau_{\mathrm{H,k}} \leq \gamma_\mathrm{k}, \qquad \mathrm{A}^*_\mathrm{k} = \tau_{\mathrm{H,k}}. \tag{2.35}$$

The square-root region for small to moderate optical depth, and low pressure as

$$\gamma_\mathrm{k} \geq \tau_{\mathrm{H,k}} \leq \frac{1}{\gamma_\mathrm{k}}, \qquad \tau_{\mathrm{H,k}} \leq 1, \qquad \mathrm{A}^*_\mathrm{k} = (4\gamma_\mathrm{k}\tau_{\mathrm{H,k}})^{\frac{1}{2}} - \gamma_\mathrm{k}. \tag{2.36}$$

The log-root region for large optical depth, and low pressure as

$$\frac{1}{\gamma_\mathrm{k}} \leq \tau_{\mathrm{H,k}} \qquad \tau_{\mathrm{H,k}} \leq 1, \qquad \mathrm{A}^*_\mathrm{k} = \ln(\tau_{\mathrm{H,k}}\gamma_\mathrm{k}) + 2 - \gamma_\mathrm{k}. \tag{2.37}$$

The log region for large optical depth, and high pressure as

$$\tau_{\mathrm{H,k}} \geq 1, \qquad \gamma_\mathrm{k} \geq 1, \qquad \mathrm{A}^*_\mathrm{k} = \ln\tau_{\mathrm{H,k}} + 1. \tag{2.38}$$

The four-region equation was found based on the experimental data. The best accuracy is obtained for the band absorption A calculations when the parameters of α, β, and ω are estimated together with the four-region equation (Edwards and Balakrishnan, 1973).

The main target of using the four-region equation is to analytically derive the upper limits to the spectrally-integrated band absorptance (A_Q). In that case, the band absorption is

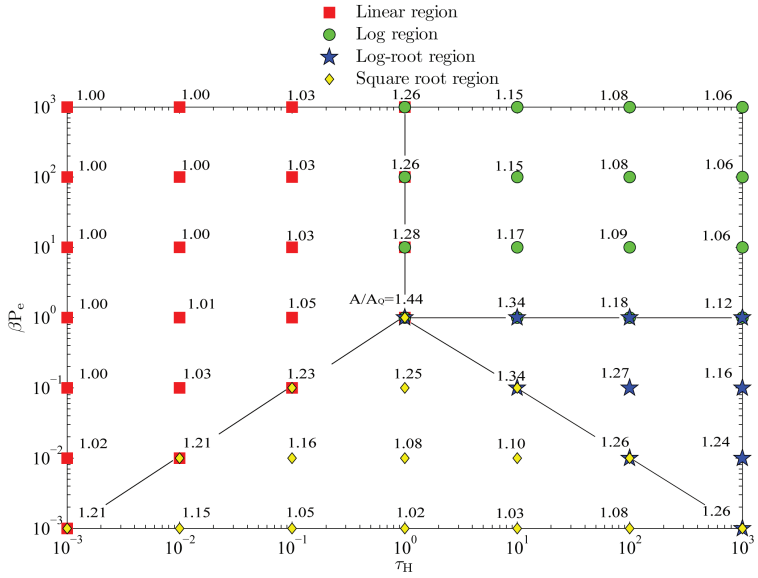

(a) 2D, reproduced from Edwards and Balakrishnan (1973)

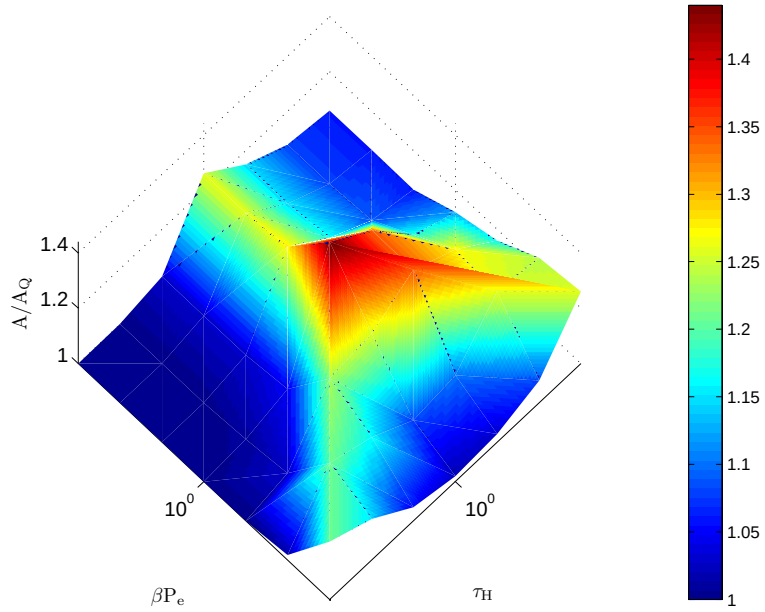

(b) 3D

Figure 2.6: The four-region equation chart for spectrally integrated band absorption.

found by the spectral quadrature

$$\mathrm{A}_{i,j} \equiv \int_0^\infty \alpha_{\eta,i,j} \mathrm{d}\eta. \tag{2.39}$$

As shown in Figure 2.6, $\mathrm{A_Q}$ is often 20% lower than the four-region value of A. In the original EWBM (Edwards and Balakrishnan, 1973), the following equations are used for considering the spectral quadrature value of $\mathrm{A_Q}$ with the band absorption A:

$$\alpha_0' = \alpha_0 \frac{\mathrm{A}}{\mathrm{A_Q}}, \tag{2.40}$$

$$\beta_0' = \beta_0, \tag{2.41}$$

$$\omega_0' = \omega_0 \frac{\mathrm{A}}{\mathrm{A_Q}}. \tag{2.42}$$

As mentioned above, to have good engineering equations, it is better to know how these three parameters (α, β, and ω) of different bands are changing with temperature, and pressure (Modest, 2003b). When the parameter of $\alpha(\mathrm{T})$ is stabilized by its value at some premise condition $\alpha(\mathrm{T_0}) = \alpha_0$, the equation founded on the harmonic-oscillator type of wave function can be written as (Edwards and Balakrishnan, 1973; Edwards, 1976)

$$\alpha_{ij} = \alpha_0 \frac{\left(1 - \exp\left[-\sum_{k=1}^{m} \pm \mathrm{u}_k \delta_k\right]\right) \Psi(\mathrm{T})}{\left(1 - \exp\left[-\sum_{k=1}^{m} \pm \mathrm{u}_{0,k} \delta_k\right]\right) \Psi(\mathrm{T_0})}, \tag{2.43}$$

$$\mathrm{u}_k = \frac{\mathrm{hc}\eta_k}{\mathrm{kT}}, \tag{2.44}$$

$$\mathrm{u}_{0,k} = \frac{\mathrm{hc}\eta_k}{\mathrm{kT_0}}, \tag{2.45}$$

$$\Psi(\mathrm{T}) = \frac{\prod_{k=1}^{m} \sum_{\eta_k=\eta_{0.k}}^{\infty} \frac{(\eta_k + \mathrm{g}_k + \delta_k - 1)!}{(\mathrm{g}_k - 1)! \eta_k!} \exp[-\mathrm{u}_k \eta_k]}{\prod_{k=1}^{m} \sum_{\eta_k=0}^{\infty} \frac{(\eta_k + \mathrm{g}_k - 1)!}{(\mathrm{g}_k - 1)! \eta_k!} \exp[-u_k \eta_k]}, \tag{2.46}$$

where c is the speed of light in vacuum, Ψ is the band intensity temperature variation parameter, and δ_k is the k mode transform in vibrational quantum number.

The selection of $\mathrm{T_0} = 100$ K extends the applicability range of the model to low temperatures.

Let $\eta_{0,k}$ indicate the probable lowest initial state as (Edwards, 1976)

$$\eta_{0,k} = 0 \ , \ \text{for} \ + \delta_k, \tag{2.47}$$

$$\eta_{0,k} = \delta_k \ , \ \text{for} \ - \delta_k. \tag{2.48}$$

Corresponding to the jth composition of δ_{k} values, the band source of the jth absorption band reveals at wavenumber

$$\eta_{0,j} = \sum_{k=1}^{m} \pm \delta_k \eta_k. \tag{2.49}$$

In turn, the jth band is called by the value of $\eta_{0,j}$ or the suitable value of $\lambda_{0,j}$

$$\lambda_{0,j} = \frac{1}{\eta_{0,j}}, \tag{2.50}$$

where λ is the wavelength.

The collection of $\eta_{0,j}$ can be defined j numbers in order of rising values (Edwards, 1976).

The line width $\gamma(\mathrm{T})$ can be calculated with the following equation

$$\gamma = \gamma_0 \left(\frac{\mathrm{T}}{\mathrm{T}_0} \right)^{0.5} \mathrm{P_e}, \tag{2.51}$$

where γ is the line width, and $\mathrm{P_e}$ is given by Eq. 2.31.

From Eq. 2.51, the relation for $\beta(\mathrm{T})$ becomes (Edwards and Balakrishnan, 1973)

$$\beta_{ij} = \beta_0 \left(\frac{\mathrm{T}_0}{\mathrm{T}} \right)^{0.5} \ , \ \exp \left[- \frac{\mathrm{hc}\eta_k}{\mathrm{kT}} \right] << 1 \ . \tag{2.52}$$

The equivalent line model approved that the same parameters of γ/d or $\beta = \pi\gamma/\mathrm{dP_e}$ are estimated by using the square of the square roots sum of the individual $(\mathrm{S/d})_\eta$, and β_η values (Edwards and Balakrishnan, 1973; Edwards, 1976). The equivalent value of $\mathrm{S/d}$ will then be converted into another form of the individual values $(\mathrm{S/d})_\eta$ as

$$\bar{\beta} = \frac{\left(\sum\limits_{\eta} \left(\dfrac{\mathrm{S}}{\mathrm{d}} \right)_\eta^{0.5} \beta_\eta^{0.5} \right)^2}{\sum\limits_{\eta} \left(\dfrac{\mathrm{S}}{\mathrm{d}} \right)_\eta} \ , \quad \left(\frac{\bar{\mathrm{S}}}{\mathrm{d}} \right) = \sum_{\eta} \left(\frac{\mathrm{S}}{\mathrm{d}} \right)_\eta . \tag{2.53}$$

It is an uncertain supposition that the spectral displacement of the disturbed bands at the initial state affects only to the line structure only, but not the band structure (Edwards, 1976). The pertinent intensities, which appeared in Eq. 2.46, are used in Eq. 2.53 for β_η to create (Weiner and Edwards, 1968)

$$\beta(\mathrm{T}) = \beta_0 \left(\frac{\mathrm{T}}{\mathrm{T}_0}\right)^{-0.5} \frac{\Psi(\mathrm{T})}{\Psi(\mathrm{T}_0)}, \tag{2.54}$$

where Ψ from Eq. 2.46 can be modified as

$$\Psi(\mathrm{T}) = \frac{\left[\prod_{k=1}^{m} \sum_{\eta_k=\eta_{0.k}}^{\infty} \left(\frac{(\eta_k + \mathrm{g}_k + \delta_k - 1)!}{(\mathrm{g}_k - 1)!\eta_k!} \exp[-\mathrm{u}_k \eta_k]\right)^{0.5}\right]^2}{\prod_{k=1}^{m} \sum_{\eta_k=0}^{\infty} \frac{(\eta_k + \mathrm{g}_k + |\delta_k| - 1)!}{(\mathrm{g}_k - 1)!\eta_k!} \exp\left[-\mathrm{u}_k \eta_k\right]}. \tag{2.55}$$

The calculation of the band parameters α, and (β for the 2.7 μm band of water vapor consists of three overlapping bands. In that case, the overall integrated band intensity is obtained by summing the three bands contributions (Lallemant and Weber, 1996), and it is estimated as

$$\bar{\alpha}_{2.7} = \sum_{j=1}^{3} \alpha_{2.7,j}, \tag{2.56}$$

$$\bar{\beta}_{2.7} = \frac{\sum_{j=1}^{3} \alpha_j \beta_j}{\bar{\alpha}_{2.7}}. \tag{2.57}$$

Because of the complexity, and high computational time required for the determination of $\Psi(\mathrm{T})$ with Eq. 2.55, Eq. 2.54 is not suitable for fast calculations. Thus, a more efficient equation should be used for the line-width to spacing parameter determination (β). In their work, Lallemant and Weber (1996) suggested another equation in a more approximated form

$$\beta_{ij}(\mathrm{T}) \cong \beta_0 \sqrt{\frac{\mathrm{T}_0}{\mathrm{T}}} \left(\sum_{\mathrm{k}=0}^{N} \mathrm{a_k T^k}\right), \tag{2.58}$$

where β_0 is the line-width to spacing parameter, T_0 is the reference temperature ($\mathrm{T} = 100$ K), T is the temperature, and $\mathrm{a_k}$ is the fitting coefficient for each band of each gas component.

The band width parameter ω for an absorption band is calculated as

$$\omega = 0.9\Gamma^2 \left(\frac{3}{4}\right) \left(\frac{2\mathrm{kTB}}{\mathrm{hc}}\right)^{0.5} \quad , \quad \omega(\mathrm{T}) = \omega_0 \left(\frac{\mathrm{T}}{\mathrm{T}_0}\right)^{0.5}, \tag{2.59}$$

where Γ is the gamma function, B is the rotational constant, k is the Boltzmann constant, h is the Planck constant, c is the speed of light, and ω_0 is the band absorption parameter.

The ideal gas law is sufficiently correct for the density times path length calculation (Edwards, 1976)

$$\rho \mathrm{L}_i = \frac{\mathrm{P}_0 \mathrm{L}_0 \mathrm{MG}_i}{\mathrm{RT}_\mathrm{g}}, \tag{2.60}$$

where P_0 is the gas reference pressure (1.0 bar), L_0 is the reference zone length (1.0 m), MG is the molar mass, R is the gas constant ($\mathrm{R} = 8.205 \times 10^{-5}\ \mathrm{m^3\ bar\ K^{-1}\ mole^{-1}}$), and T_g is the gas temperature.

The effective bandwidth A, or in other words the band absorption, can be explained as a completely absorbing band, or the width of a black band, centered approximately in the middle of the real band that generates the same absorption (Stefanidis et al., 2007).

The optical depth (the value of τ_H) at the top (band head) or center of the band in the highest absorption range for a non-dimensional is calculated as

$$\tau_{\mathrm{H},i,j} = \frac{\alpha_{i,j} \rho_i \mathrm{L}}{\omega_{i,j}}. \tag{2.61}$$

The value of the total optical depth parameter τ can be calculated as (Edwards and Balakrishnan, 1973)

$$\tau = \tau_{i,j} \mathrm{X}_i \left(\frac{\mathrm{PL}}{\mathrm{P}_0 \mathrm{L}_0} \right), \tag{2.62}$$

where X is the absorber density path length product, P_0, and L_0 are the reference values equaled to $\mathrm{P}_0 = 1$ bar, and $\mathrm{L}_0 = 1$ m, respectively.

The band absorption ratio from the four-region equation (see Eqs. 2.35–2.38) was estimated previously. The next step is the calculation of the band transmittance. The gray gas assumption in the band is not valid in the small beam length. The solution of this problem was proposed by Edwards and Balakrishnan (1973) in the form of a suggested upper limit for the band transmissivity as

$$\tau_{\mathrm{g},i} = \frac{\tau_{\mathrm{H},i}}{\mathrm{A}_i^*} \frac{\mathrm{dA}_i^*}{d\tau_{\mathrm{H},i}} \leq 0.90. \tag{2.63}$$

The band width (Edwards, 1976) can be calculated by

$$\Delta \eta_i = \frac{\mathrm{A}_i}{1 - \tau_{\mathrm{g,i}}}. \tag{2.64}$$

Many researchers, including Hottel and Sarofim (1967), Leckner (1972), and Edwards and Balakrishnan (1973), have been researching the effect of overlapping bands on the total radiative properties of gas mixtures. When two or more absorption bands overlap, a new single band is created through their transmissivity product. Edwards, and Balakrishnan showed this kind of overlapping solution to be in good agreement with their experiment

data. This commonly used solution for supporting overlapping bands is also used in two formulations of the EWBM of this research. The solution was obtained from the quantum mechanics theory, and can be expressed by the transmissivity or emissivity of the overlapping bands (Edwards and Balakrishnan, 1973; Felske and Tien, 1974; Edwards, 1976; Ströhle and Coelho, 2002; Runstedtler and Hollands, 2008):

$$\tau_{\mathrm{k,t}} = \prod_{\mathrm{m=1}}^{\mathrm{N}} \tau_{\mathrm{k,m}} \qquad \text{or} \qquad \epsilon_{\mathrm{k,t}} = \sum_{\mathrm{m=1}}^{\mathrm{N}} \epsilon_{\mathrm{k,m}} - \prod_{\mathrm{m=1}}^{\mathrm{N}} \epsilon_{\mathrm{k,m}}, \tag{2.65}$$

where N is the component number or band number (generally, overlapping may happen in a single gas as well).

It should be mentioned here that the above solution is widely used in radiation models as a highly accurate method for supporting overlapping bands. In general, the overlapping solution justifies the physical background of the overlapping bands. Physically, when two or more bands overlap, the emission of the mixture is smaller than the summation of the emissions of individual components, due to the higher self-absorption. If the overlapping solution were interpreted by using the band emissivity, that is the second part of Eq. 2.65, the second term on the right-hand side would act as a correction factor when considering the above-mentioned physical phenomenon.

As a final calculation step for be following "block approximation" for the total emissivity of a gas at the surface temperature $\mathrm{T_s}$ (Edwards, 1976)

$$\epsilon_{\mathrm{t}} \cong \sum\nolimits_{k=1}^{N} (1 - \tau_{k,t}) \left[\mathrm{F}\left(\frac{\mathrm{T_s}}{\eta_k}\right) - \mathrm{F}\left(\frac{\mathrm{T_s}}{\eta_{k+1}}\right) \right], \tag{2.66}$$

where N is the number of bands, and F is the blackbody fractional function for the lower limit η_{k}, and the upper limit $\eta_{\mathrm{k+1}}$ in each band k (or wavenumber interval in the case of spectral calculations).

Siegel and Howell (1981) reported the following correlation for the black body fractional function

$$\begin{cases} \mathrm{F}_{0-\lambda \mathrm{T}} = 1 - \dfrac{15}{\pi^4}\eta^3 \left[\dfrac{1}{3} - \dfrac{\eta}{8} + \dfrac{\eta^2}{60} - \dfrac{\eta^4}{5040} + \dfrac{\eta^6}{272160} - \dfrac{\eta^8}{272160} \right], & \eta < 2; \\ \mathrm{F}_{0-\lambda \mathrm{T}} = \dfrac{15}{\pi^4} \displaystyle\sum_{m=1,2,\ldots} \dfrac{\exp\left[-m\eta\right]}{m^4} \left[\left(\left[m\eta + 3 \right] m\eta + 6 \right) m\eta + 6 \right], & \eta \geq 2. \end{cases} \tag{2.67}$$

To calculate the upper, and lower limits in Eq. 2.66 for symmetric bands ($\eta_{\mathrm{c,k}}$) only, the following equations are used:

$$\eta_{\mathrm{u},k} = \eta_{\mathrm{c},k} + \frac{\Delta\eta_k}{2}, \tag{2.68}$$

$$\eta_{\mathrm{l},k} = \eta_{\mathrm{c},k} - \frac{\Delta\eta_k}{2}. \tag{2.69}$$

All bands used by the EWBM are symmetric except the 4.3 μm band $\mathrm{CO_2}$ with an upper limit. In the case of an asymmetric band, the band limit is set by the following correlation:

$$\eta_{\mathrm{u},k} - \eta_{\mathrm{l},k} = \Delta\eta_k. \tag{2.70}$$

In conclusion, to calculate the total absorption coefficient, the Beer's law is employed as

$$\mathrm{K} = -\ln\left(\frac{1-\alpha}{\mathrm{L}}\right). \tag{2.71}$$

As it was mentioned, three kinds of band shapes are assumed for the absorption bands in the EWBM (Edwards and Balakrishnan, 1973): with upper/lower limit head, and symmetric. In both methods, the exponential form is assumed for the bands; the difference is in how they calculate the absorptivity of the band. In the EWBM-4RE, the four region equation is used while in the EWBM-IM, the direct integration of the exponential curves of the bands is used. According to Figure 2.4, the leveled absorption coefficient (S/d) has three shapes for the absorption bands, and the integrating S/d in the band width can be used with an alternative approach. It is possible to calculate those shapes, as is shown in the top graphs of Figures 2.7, 2.8, and 2.9 by using the following equation from Edwards and Balakrishnan (1973):

$$\tau_\eta = \exp\left[\frac{-\left(\frac{\mathrm{S}}{\mathrm{d}}\right)\mathrm{X}}{\left(1+\left(\frac{\mathrm{S}}{\mathrm{d}}\right)\mathrm{X}/\beta\right)^{0.5}}\right], \tag{2.72}$$

where X is the absorber density path length product, β is the mean line-width-to-spacing parameter $\beta = \pi\gamma_0/\mathrm{d}$, and τ_η is the spectral transmittance of the band at wavenumber η.

The entire spectrum can be divided into several wavenumber intervals. In each interval, the equivalent transmissivity can be calculated by integrating the spectral transmittance over the wavenumber interval (Ströhle and Coelho, 2002) as

$$\tau_{\mathrm{k}} = \frac{1}{\Delta\eta}\int_{\Delta\eta}\tau_{\eta,\mathrm{b}}\mathrm{d}\eta. \tag{2.73}$$

The last two equations form the basis of the integration method which was first proposed by Cumber et al. (1998). The original correlations of the EWBM-IM can be found in the works og Edwards and Balakrishnan (1973), and Edwards (1976). Moreover, this method has been extensively documented by other researches (Ströhle and Coelho, 2002).

For modeling the band transmittance, the gray band supposition required in estimating the absorption of the band using the four-region equation is consequently avoided by using the analytic equations, such as Eq. 2.32, and its variations. For gas mixtures, the spectral transmittance is estimated as (Cumber et al., 1998)

$$\tau_{\mathrm{g},\eta} = \exp\left[-\sum_{ij} \frac{\left(\frac{\mathrm{S}}{\mathrm{d}}\right)_i \mathrm{X}_j}{\left(1+\left(\frac{\mathrm{S}}{\mathrm{d}}\right)_i \left(\frac{\mathrm{X}}{\beta}\right)_j\right)^{0.5}}\right], \tag{2.74}$$

where i is the particular gas band, and j is the participating species.

By dividing the whole radiative spectrum into a certain number of wavenumber intervals (blocks), the corresponding number of values of the partial or band emissivity can be obtained. Moreover, they can be selected in a such manner that it would be possible for the user to select the real absorption bands of the gas mixture with the following calculation. For this purpose, the Eq. 2.19 of the total emissivity integration is transformed into

$$\epsilon = \frac{\int_{\eta_{\mathrm{b,b}}}^{\eta_{\mathrm{e,b}}} \epsilon_\eta \mathrm{E}_\eta \mathrm{d}\eta}{\int_{\eta_{\mathrm{b,b}}}^{\eta_{\mathrm{e,b}}} \mathrm{E}_\eta \mathrm{d}\eta} = \frac{1}{\sigma \mathrm{T_g}^4} \int_{\eta_{\mathrm{b,b}}}^{\eta_{\mathrm{e,b}}} \epsilon_\eta \mathrm{E}_{\eta,\mathrm{g}} \mathrm{d}\eta, \tag{2.75}$$

where $\eta_{\mathrm{b,b}}$ and $\eta_{\mathrm{e,b}}$ are the beginning, and end of the wavenumber block, E_η is the black-body emissive power (Planck function) at wavenumber η, η is the wavenumber, T is the gas temperature, and σ is the Stefan-Boltzmann constant.

For this case, the wavenumber of the block end $(\eta_{\mathrm{e,b}})$ is estimated through the summation of the beginning band width $\eta_{\mathrm{b,b}}$, and the wavenumber average of the block $\Delta\eta$

$$\eta_{\mathrm{e,b}} = \eta_{\mathrm{b,b}} + \Delta\eta. \tag{2.76}$$

The data for the leveled absorption coefficients $(\mathrm{S/d})$ for each gas component ($\mathrm{H_2O}$, $\mathrm{CO_2}$, CO, NO, $\mathrm{SO_2}$, and $\mathrm{CH_4}$) presented in Figures 2.7, 2.8, and 2.9 are taken from the study of spectral location parameters by Edwards and Balakrishnan (1973). In these three figures, there are five temperature cases: 800 K, 1000 K, 1200 K, 1400 K, and 1600 K. The parameters of the total pressure $(\mathrm{P_t})$, characteristic length (L), and density path length $(\mathrm{X_i})$ for these cases equals to 1 bar, 100 cm, and 1.0, respectively. In the upper graphs of Figures 2.7, 2.8, and 2.9, the leveled absorption coefficient $(\mathrm{S/d})$ has three different shapes: band with upper limit head, symmetric band, and band with lower limit head, respectively. It should be mentioned that only the 4.3 μm band of $\mathrm{CO_2}$ gas has an upper limit which equals to 2410 $\mathrm{cm^{-1}}$, and the rotational band of $\mathrm{H_2O}$ gas has a lower limit which equals to 0 $\mathrm{cm^{-1}}$ (Edwards and Balakrishnan, 1973).

It is shown in Figures 2.7, and 2.9 that the band shapes are asymmetric, and they do not have a symmetric band. The other bands of $\mathrm{H_2O}$, and $\mathrm{CO_2}$ and other mentioned gases are symmetric, like the one in Figure 2.8.

The spectral values represented from the centers of the bands $(\eta_{\mathrm{c,k}})$ are taken from the

study by Edwards and Balakrishnan (1973), and upper/lower limits are calculated by Eqs. 2.68, and 2.69, respectively. Regarding to the middle graph in the triple pictures, it has been reported by Ströhle and Coelho (2002) that the band spectral transmittance (in the middle graphs τ_η) is calculated with Eq. 2.72, where η is a wavenumber.

The lowest graph in the triple Figures 2.7, 2.8, and 2.9 reflects the idea of the band (block) estimation. In these three figures, the absorbing gases are presented with five different temperatures, and different band shapes. Thus, in Figure 2.7, a band of CO_2; in Figure 2.8, a band of H_2O; and in Figure 2.9, a band of H_2O are presented corresponding to the bands with upper shape, with symmetric shape, and with lower shape, respectively. Each rectangle colored band with temperatures 800 K, 1000 K, 1200 K, 1400 K, and 1600 K is calculated from their own interval limits, by Eqs. 2.68, and 2.69 in the case of symmetric bands, and by Eq. 2.70 in the case of asymmetric bands (Nilsson and Sundén, 2003).

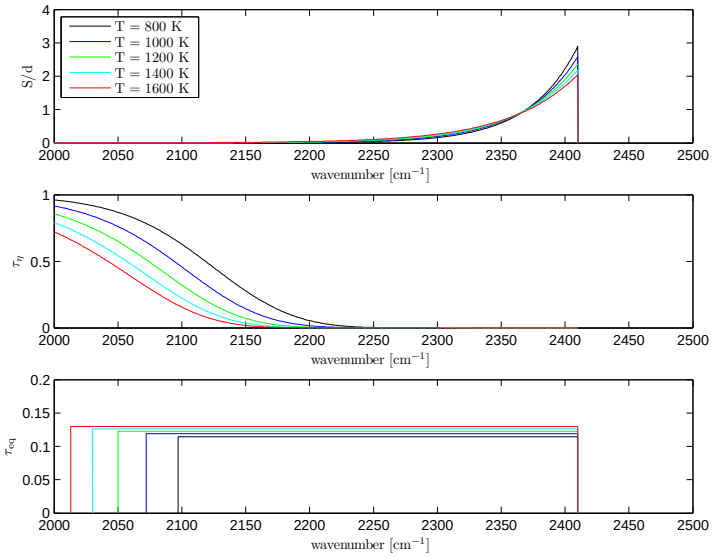

Figure 2.7: The predictions of EWBM for a band with upper limit; gas composition: pure CO_2, $P_t = 1$ bar, $L = 1$ m.

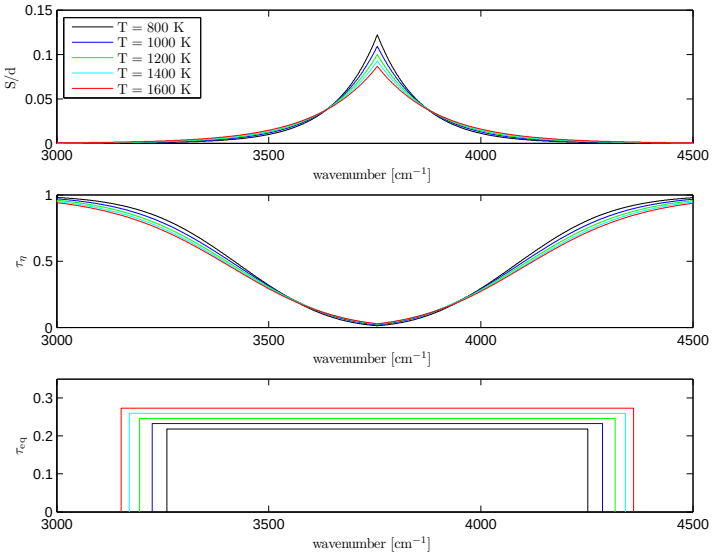

Figure 2.8: The predictions of EWBM for a symmetrical band; gas composition: pure H_2O, $P_t = 1$ bar, $L = 1$ m.

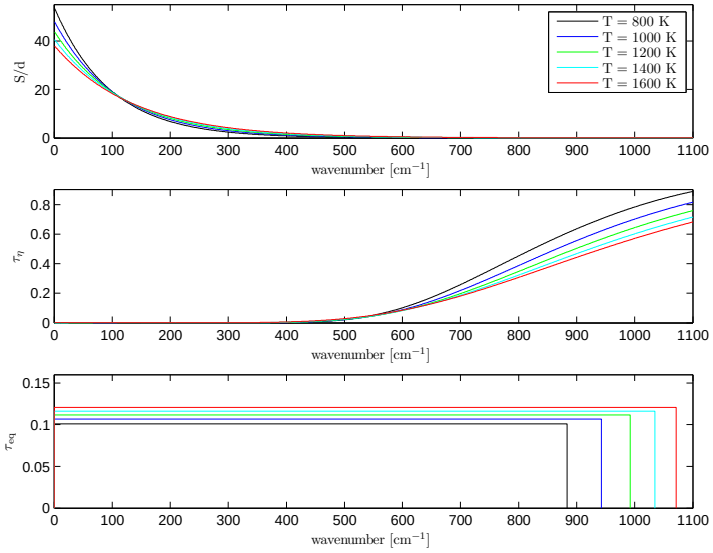

Figure 2.9: The predictions of EWBM for a band with lower limit; gas composition: pure H_2O, $P_t = 1$ bar, $L = 1$ m.

3 Analysis of two formulations of the EWBM

This chapter describes the particular analyses concerning the comparison of the spectral and total radiative properties for the two different formulations of the exponential wide band model (EWBM) in H_2O–CO_2 mixtures under the air-fired conditions (Maximov et al., 2012). The first one is the original wide band method with the four region equation (EWBM-4RE) and the second is the numerical integration method (EWBM-IM).

Using the statistical narrow band model (SNBM) as a benchmark together with some experimental data, the accuracy of the two implementations of the EWBM can be analyzed. Generally, the EWBM-IM has more potential for spectral predictions. As opposite to the EWBM-4RE, the EWBM-IM approximately reproduces the shape of spectrum. Therefore, it will be discussed whether the accuracy of the EWBM-IM of total properties calculations could be improved by deriving new spectral parameters for the EWBM-IM instead of using those which were developed to be used in the original EWBM-4RE. The original EWBM-4RE accompanied with the original spectral parameters can be found as a more accurate model for obtaining total property calculations. Because of the underpredicted behavior of the EWBM-IM of total properties calculations, the model will show better conformity with the non gray benchmark solutions compared with the original EWBM.

3.1 Spectral analysis of different formulations

For the demonstration of the spectral behavior of the EWBM-4RE and EWBM-IM, two experimental profiles have been chosen. For the first comparison, a $6.3 - \mu$m band of water vapor was selected. Figure 3.1 shows the profile of the spectral emissivity of a symmetrical band of H_2O at $T = 1111$ K, $P = 2$ bar, and $L = 6.096$ m (20 feet). The predictions of the two EWBM formulations and the SNBM are compared with the experimental data presented by Ludwig et al. (1973).

Figure 3.1 conforms that the spectral emissivity computed from the EWBM-4RE is in fair agreement with the experimental data. However, the EWBM-4RE obviously cannot predict the shape of the spectra. The SNBM predicts the band shape which is close to the experimental profile as well as the roughly replicated profile of the EWBM-IM. By graphical integration it has been found that the SNBM slightly underpredicts the spectral emissivity (the area below the curve) with the experimental profile compared to the overpredicted results of the EWBM-IM.

The second experimental profile in Figure 3.2 of the $2.7 - \mu$m fully overlapped bands of H_2O and CO_2 has been modeled for a mixture of $Pr = 1$ $\left(Pr = \frac{p_{H_2O}}{p_{CO_2}}\right)$ at the temperature of $T = 1500$ K and pressure path length product of $P_{w+c}L = 0.00936$ bar m ($P_{w+c} = p_{H_2O} + p_{CO_2}$). Figure 3.2 shows the difference in the band shape behavior predicted by the EWBM-4RE and EWBM-IM. The band shape predictions of the two methods were compared with the experimental data presented by Ferriso and Ludwig (1964a).

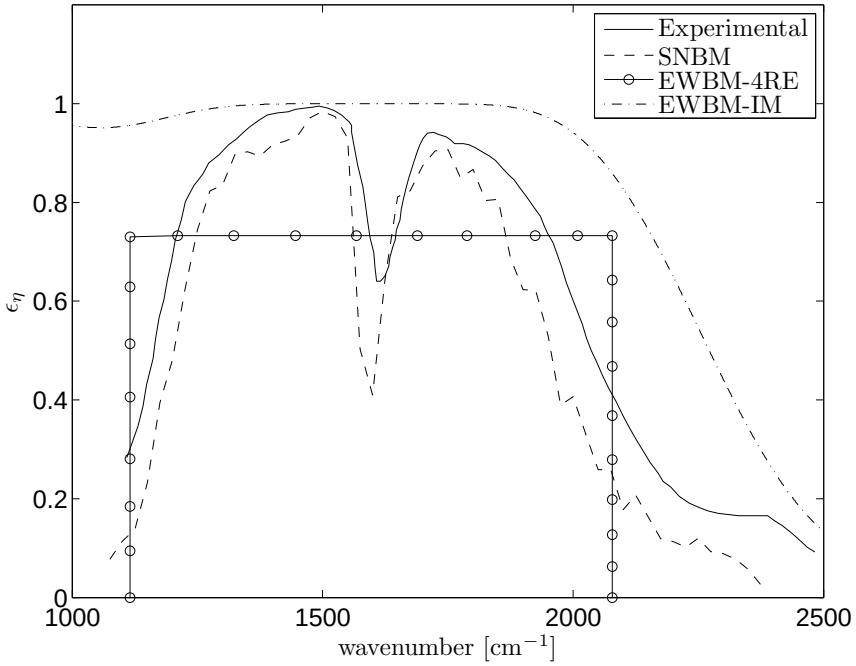

Figure 3.1: The spectral emissivity obtained by the EWBM-4RE, the EWBM-IM and the SNBM compared with the experimental data reproduced from Ludwig et al. (1973).

It can be seen that the results of the EWBM-4RE are in reasonable agreement with the experimental data, apart from the shift of the bands to higher wavenumbers. However, the EWBM-4RE obviously cannot predict the shape of the spectra. The EWBM-IM predicts a band shape that is similar to the experimental profile. Generally, the nature of the EWBM-IM has more ability for band predictions, but the current values of the band parameters were introduced to be used for the EWBM-4RE. Nevertheless, the accuracy of the EWBM-IM can be improved by obtaining new band parameters specifically found for being used in the EWBM-IM. In the current results of the EWBM-IM, the value of ω, reported by Edwards (1976) for being used in the EWBM-4RE, has been increased by 20% to be suitable for being implemented in the EWBM-IM.

In order to consider the behavior of the different models in gas mixtures, the spectral emissivity calculated by the EWBM-4RE and the EWBM-IM are compared with the SNBM results (Soufiani and Taine, 1997). The two emissivity profiles at the temperatures 800 K and 1800 K of the H_2O–CO_2 gas mixture under air-fired conditions and atmospheric pressure are shown in Figure 3.3.

The figure confirms that the spectral emissivity profiles presented by the EWBM-IM roughly reproduce the shape of the spectrum presented by the benchmark. However, the

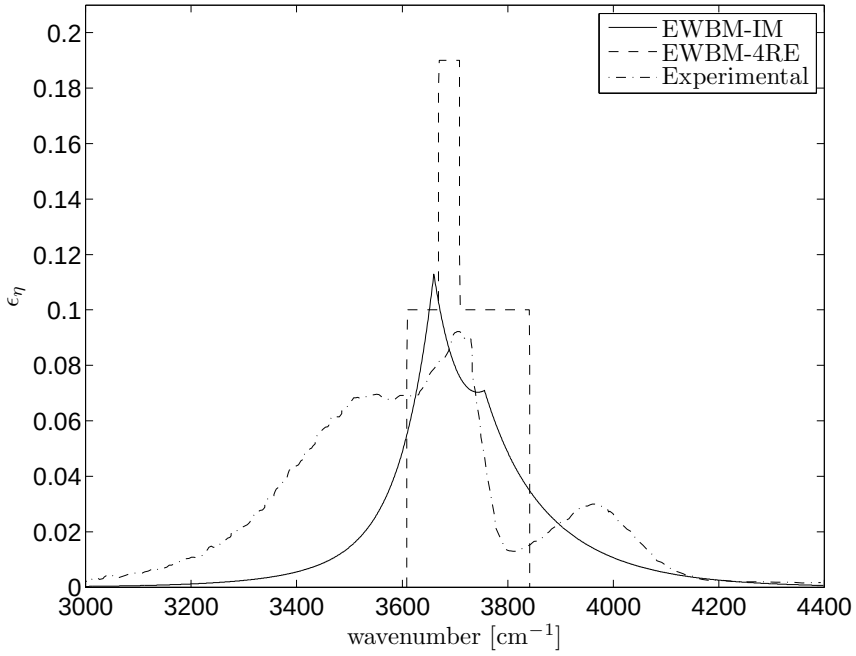

Figure 3.2: The spectral emissivity calculated by the EWBM-4RE and the EWBM-IM compared with the experimental data reproduced from Ferriso and Ludwig (1964a).

EWBM-4RE is producing rectangular boxes of the absorption bands. Figure 3.3a shows that at low temperatures, the EWBM-IM insignificantly underpredicts the height of the absorption bands presented by the SNBM. At high temperatures (see Figure 3.3b), the EWMB-IM produces results closer to the benchmark profile.

The EWBM-4RE produces band boxes with narrower widths for the lower temperature (Figure 3.3a) and significantly wider widths for the higher temperature (Figure 3.3b). The fact that the band widths produced by the EWBM-4RE are much wider compared to the ones produced by the SNBM creates some inaccuracies in EWBM-4RE predictions. This can be observed in the total transmissivity obtained by the EWBM-4RE for gas mixtures in the overlapping bands and spectral windows. In the case of overlapping bands, the EWBM-4RE produces higher values for the transmissivity of the overlapping zones than was estimated by the SNBM. In the case of spectral windows, the wider band boxes produced by the EWBM-4RE cause extra absorption regions in the spectrum which are actually transparent.

3.2 Total radiative properties comparison

For the evaluation of the accuracy of the two different implementations of the EWBM, the SNBM developed by Soufiani and Taine (1997) has been used as a benchmark method as suggested by Chu et al. (2011). In all cases, the temperatures of the gas and radiation source were assumed to be equal. Therefore, the absorption coefficient is termed as the "local absorption coefficient".

The changes in the local mean absorption coefficient with the temperature of the gas mixture in a moderate $\mathrm{P_{w+c}L}$ are shown in Figure 3.4 for the EWBM-4RE and the EWBM-IM. The condition of this figure is as follows: molar fractions ratio $\mathrm{Pr} = 2$, source temperature $\mathrm{T_s} = \mathrm{T_g}$, and $\mathrm{P_{w+c}L} = 0.12$ bar m. As the figure shows, the EWBM-4RE generally predicts a more accurate result than the EWBM-IM at certain $\mathrm{P_{w+c}L}$. As the gas temperature increases above 1200 K, the predictions of the EWBM-4RE approach the SNBM results.

The changes of the local mean absorption coefficient with $\mathrm{P_{w+c}L}$ of a gas mixture in a certain temperature are shown in Figure 3.5. For this figure, both models have been applied to a mixture of $\mathrm{Pr} = 2$ at $\mathrm{T_g} = 1500$ K and a varying $\mathrm{P_{w+c}L}$ between 0.0003 and 3 bar m. The EWBM-4RE shows a better conformity with the prediction of the SNBM in the large $\mathrm{P_{w+c}L}$ region. In the small $\mathrm{P_{w+c}L}$s, the difference between the predictions of the two implementations of the EWBM and the SNBM increases.

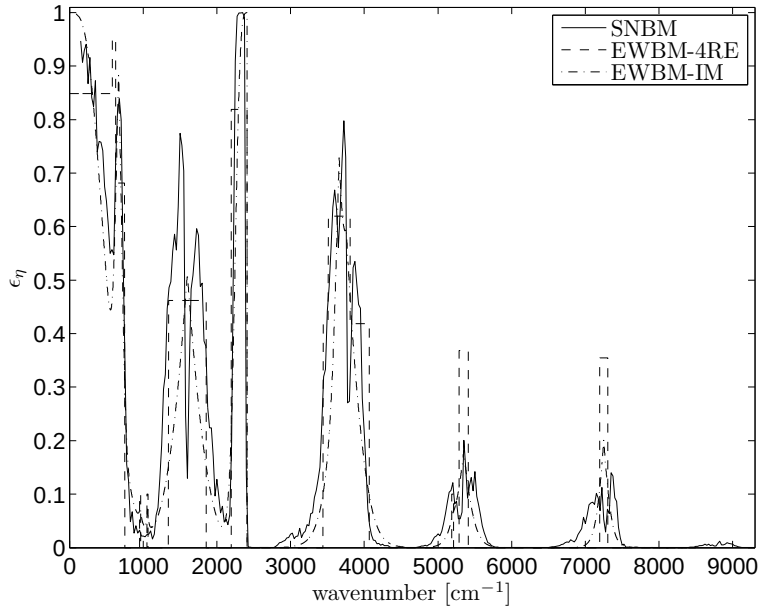

(a) T = 800 K

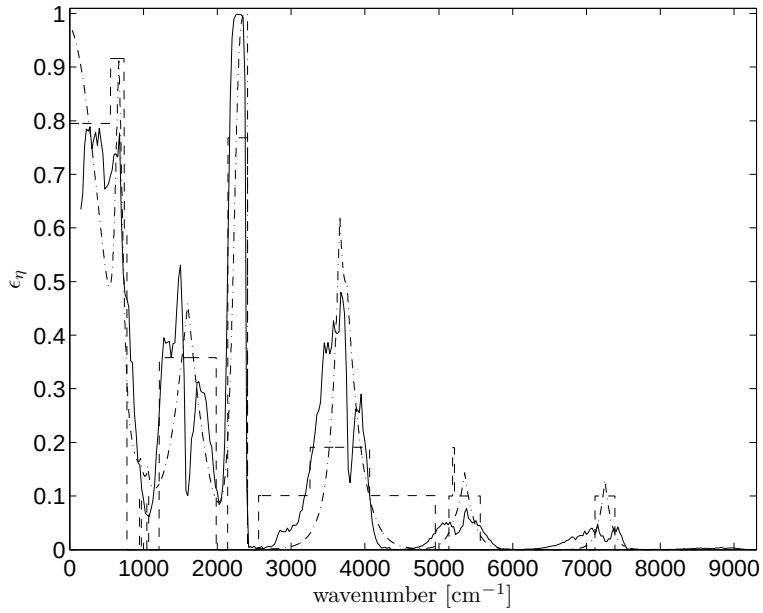

(b) T = 1800 K

Figure 3.3: Predictions of spectral emissivity calculated by two EWBM formulations compared with the SNBM as a benchmark.

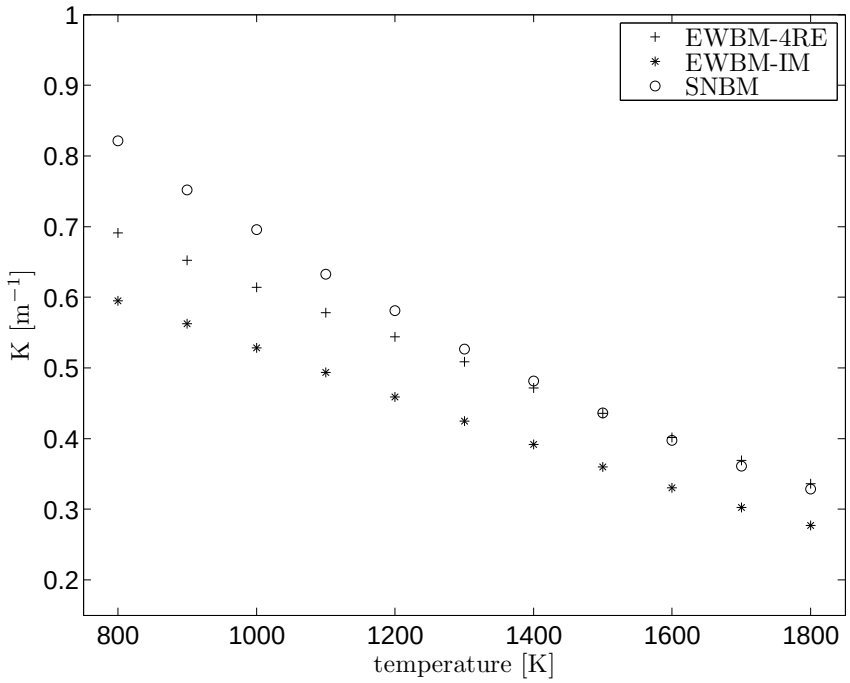

Figure 3.4: The absorption coefficient vs. the temperature for a H_2O–CO_2 gas mixture at molar fractions ratio $\mathrm{Pr} = 2$ and $\mathrm{P_{w+c}L} = 0.12$ bar m.

For the smallest $\mathrm{P_{w+c}L}$, a 1.6% difference was observed for the EWBM-4RE and an 8.7% difference for the EWBM-IM. The high error in the thin optical thickness results from assuming the upper limit of 0.9 for the transmissivity of bands. As mentioned before in the case of optically very thin media, the gray gas assumption is broken in the bands. To solve this problem, Edwards suggested an upper limit for the band transmissivity.

Using an upper limit for the band transmissivity may introduce serious errors if the recurrence relation is used, leading to a strong dependence on the grid resolution (Ströhle and Coelho, 2002). The suggested solution of the problem consists of obtaining a fixed band width for all the absorption bands by using the average properties of the whole computational domain in the preprocessing step.

To present results which can be useful for industrial modeling, the gas mixtures under air-fired condition were selected as $\mathrm{Pr} = 1/2$, $2/3$, 1, $4/3$, $3/2$, and 2. The temperature range 800 K $\leq \mathrm{T_{s,g}} \leq 1800$ K and the $\mathrm{P_{w+c}L}$ range 0.001 bar m $\leq \mathrm{P_{w+c}L} \leq 10$ bar m were selected as additional effective parameters. For the accuracy comparison of the two implementations of the EWBM for all ranges of $\mathrm{P_{w+c}L}$ and T, the predictions for a known gas composition were compared with the SNBM through a deviation plot, as shown in Figure 3.6.

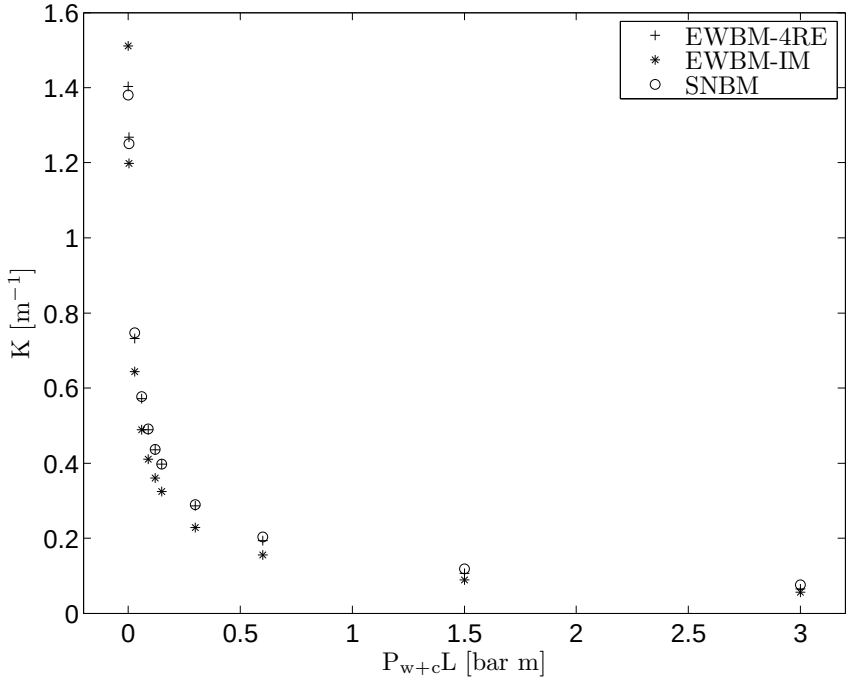

Figure 3.5: Changes of the absorption coefficient (K) with the $\mathrm{P_{w+c}L}$ from the EWBM-4RE and the EWBM-IM of a H_2O–CO_2 mixture at molar fractions ratio $\mathrm{Pr} = 2$ and $\mathrm{T_g} = 1500$ K.

The figure confirms that the predictions of the EWBM-4RE are much closer to the SNBM results. For other ranges of gas composition, the deviation plots (not reported here) show almost the same higher level of accuracy for the EWBM-4RE. By analyzing the results shown in the last two figures, one can conclude that the EWBM-4RE generally provides more accurate total properties than the EWBM-IM.

In order to investigate the accuracy of the radiative heat transfer calculation in a real-participating gas mixture, two different benchmarks have been used. Each benchmark has been solved using a ray tracing method of the RTE solver accompanied with the SNBM results (Ludwig et al., 1973; Soufiani and Taine, 1997). In the current work, for both benchmark solutions the participating gas is chosen as homogeneous gas mixture of 20% H_2O, 10% CO_2, and 70% N_2 on a mole basis. These benchmarks are somehow representing the condition of a flame combustion inside the furnace as a result of the specialized "flame" temperature distribution profile.

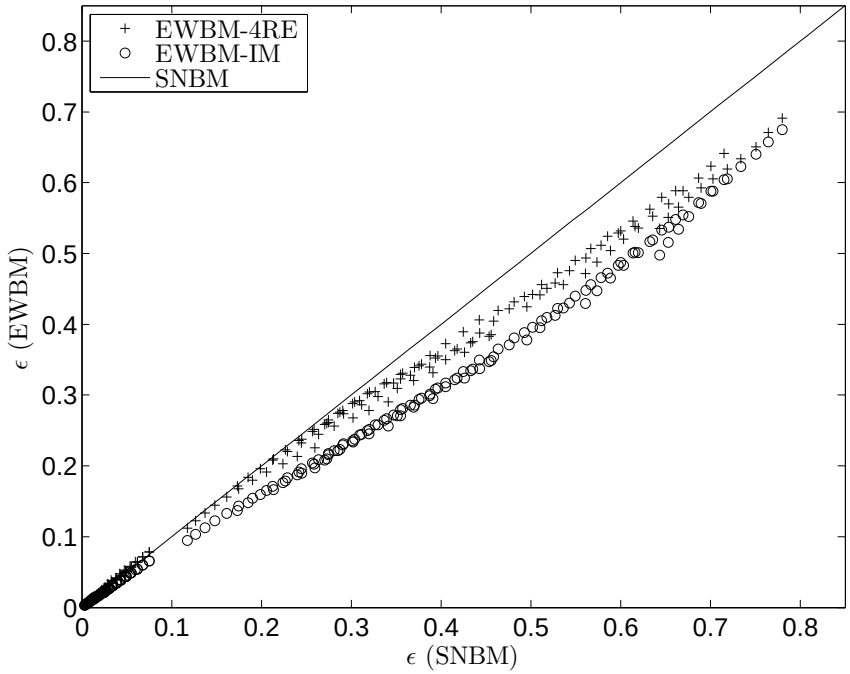

Figure 3.6: The deviation plot of comparing the total emissivity predicted by the EWBM-4RE and EWBM-IM from the predictions of the SNBM. The middle diagonal shows the perfect agreement region with the SNBM results.

3.2.1 2D benchmark of homogeneous H_2O–CO_2 mixture

Discrete ordinate method (DOM) has been used to solve the radiative heat transfer equation (RTE) for the gray radiative heat transfer modeling of the benchmarks. Different radiative properties models including the SNBM and the standard WSGGM have been implemented by DOM. The first benchmark presented by Goutiere et al. (2000) is a 2D rectangular enclosure (1 m $\times$ 0.5 m) with a known temperature field shown in Figure 3.7. In the present work, the grid mesh size is kept the same as the one originally used to solve the benchmark. The flame profile has been obtained through the certain temperature distribution defined by the following expressions

$$\mathrm{T(x,y)} = (14000\mathrm{x} - 400)(1 - 3\mathrm{y}_0^2 + 2\mathrm{y}_0^3) + 800 \quad \text{for} \quad \mathrm{x} \leq 0.1, \tag{3.1}$$

$$\mathrm{T(x,y)} = -\frac{10000}{9}(\mathrm{x} - 1)(1 - 3\mathrm{y}_0^2 + 2\mathrm{y}_0^3) + 800 \quad \text{for} \quad \mathrm{x} \geq 0.1, \tag{3.2}$$

where $\mathrm{y}_0 = \mid 0.25 - \mathrm{y} \mid /0.25$.

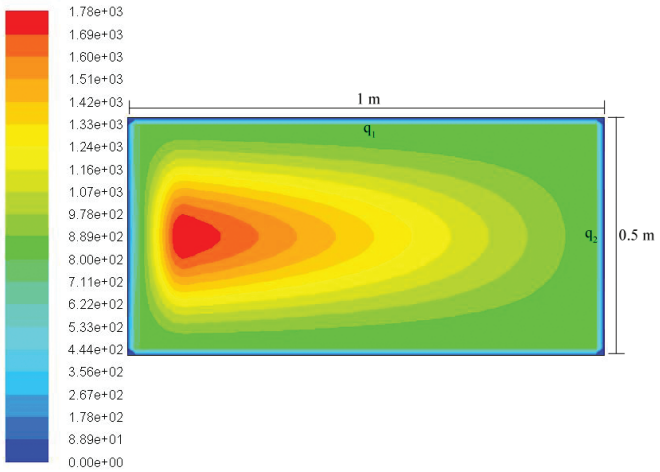

Figure 3.7: Contours of temperature of the 2D benchmark presented by Goutiere et al. (2000) in which the temperature of the walls is 0 K, and they are black.

For obtaining results of the 2D benchmark of the homogeneous H_2O–CO_2 mixture with the certain temperature distribution, the values of the absorption coefficient for different models have been integrated into the Fluent DOM solver through the user defined function (UDF) defined by cubical polynomial fitting as a function of temperature. Using the total emissivity/transmissivity, the values of the mean absorption coefficient have been calculated by means of the Beer's law. Matlab software has been used in the fitting process, and due to its simple realization and insignificant scientific value, the fitting coefficients are not reported. The path length used in WSGGM calculations has been calculated as the domain based mean beam length.

The calculated heat fluxes of the top wall (q_1) and the side wall (q_2) are shown in Figures 3.8a and 3.8b, respectively.

Figure 3.8 confirms that the EWBM-4RE overpredicts the radiative heat flux as opposed to the underprediction of the results by the EWBM-IM. Figure 3.8a shows that the predicted results of the radiative heat flux at the top wall (q_1) obtained by the EWBM-IM the closest to the exact benchmark solution. However, for the radiative heat flux at the side wall (q_2) (Figure 3.8b), the EWBM-4RE presents twice more diverse results to a benchmark data than the EWBM-IM. One of the sufficient justifications for the difference between the behaviors of q_1 and q_2 can be found by obtaining the total properties which are for the 800 K and 1800 K cases shown in Figure 3.3. For these cases, the relative error is 13.7% and 11.8% for the EWBM-4RE; 24.3% and 6.7% for the EWBM-IM, at low and high temperatures, respectively. Therefore, both formulations of the EWBM underpredict the total emissivity compared to the results presented by the SNBM which is used as the benchmark. It can be concluded that for the used effective parameters, the EWBM-IM

can produce calculations of the total properties accurately enough at low temperatures.

3.2.2 3D benchmark of homogeneous H_2O–CO_2 mixture

The second benchmark, presented originally by Liu (1999), presents a 3D rectangular enclosure study (2 m $\times$ 2 m $\times$ 4 m) shown in Figure 3.9. In obtaining the results for this benchmark, the domain based path length has been used. In this benchmark, the temperature distribution is symmetrical about the geometry center line and specified as

$$\mathrm{T} = (\mathrm{T_c} - \mathrm{T_e})\mathrm{f}\,(\mathrm{r/R}) + \mathrm{T_e}, \tag{3.3}$$

where $\mathrm{T_c}$ is the gas temperature along the geometry center line and $\mathrm{T_e}$ is the temperature at the geometry exit at z $= 4$ m.

The variation of gas temperature inside the geometry is defined by the circular cross section as

$$\mathrm{f}\,(\mathrm{r/R}) = 1 - 3\,(\mathrm{r/R})^2 + 2\,(\mathrm{r/R})^3\,, \tag{3.4}$$

where r is the distance from the geometry center line and R is the radius of the circular region ($\mathrm{R} = 1$ m).

For obtaining results of the 3D benchmark of a homogeneous H_2O–CO_2 mixture with a certain temperature distribution, the values of the absorption coefficient for different models have been integrated into the DOM through the UDF defined by the forth degree polynomial fitting as a function of temperature. Using the total emissivity/transmissivity, the values of the mean absorption coefficient have been calculated by means of the Beer's law. Matlab software has been used in the fitting process, and due to its simple realization and insignificant scientific value, the fitting coefficients are not reported here for the current and following benchmark problems. The path length used in WSGGM calculations has been calculated as the domain based mean beam length.

Outside the circular region, the gas mixture temperature is treated as uniform at the temperature of $\mathrm{T_e}$. The center line temperature is assumed to increase linearly from the inlet at z $= 0$ m of 400 K to 1800 K at z $= 0.375$ m and then to decrease linearly to the exit of 800 K. By using the SNBM, Liu solved the radiative transfer equation by employing the ray tracing method. In the present work, the uniform grid distribution is used, and the mesh size is kept the same as the one originally used to solve the benchmark. The calculated results of the heat flux density of different models are shown in Figure 3.10.

Figure 3.10 shows that because the EWBM-IM to underpredicts the radiative heat flux calculations, this model presents the closest results to the benchmark solution with an average relative error of 18.5%. The differences between the benchmark solution and the Leckner method, EWBM-4RE, and WSGGM equal to 32.3%, 34.8%, and 40.1%, respectively.

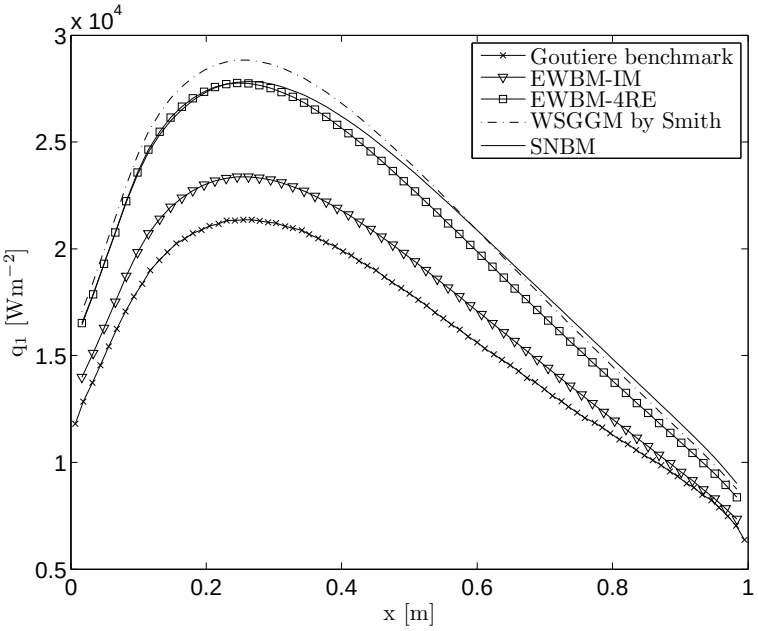

(a) Radiative heat flux $\mathrm{q_1}$

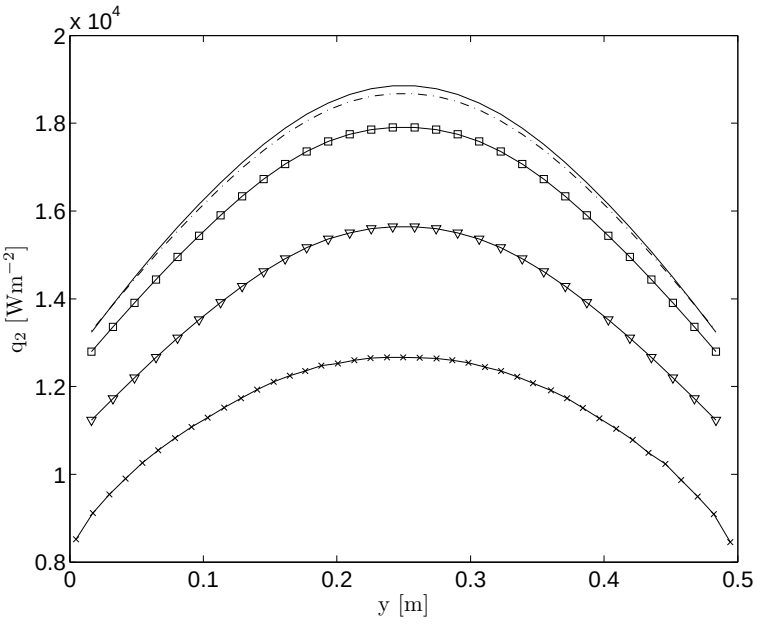

(b) Radiative heat flux $\mathrm{q_2}$

Figure 3.8: Calculated results of heat fluxes for a H_2O–CO_2 gas mixture of $\mathrm{Pr} = 2$, pressure path length product $\mathrm{P_{w+c}L} = 0.201$ bar m at: a) top wall; b) side wall. A comparison between the predictions of the radiative heat fluxes by different methods with a benchmark, reproduced from Goutiere et al. (2000).

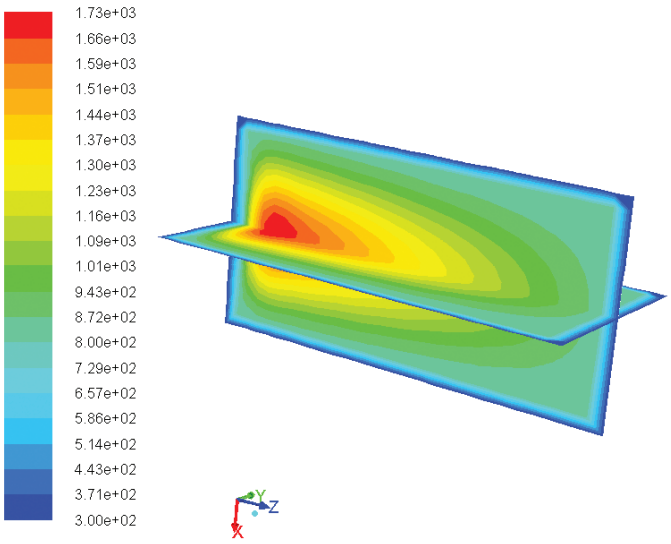

Figure 3.9: Contours of temperature of the 3D benchmark, presented originally by Liu (1999), in which the temperature of the walls is 300 K and the walls are black.

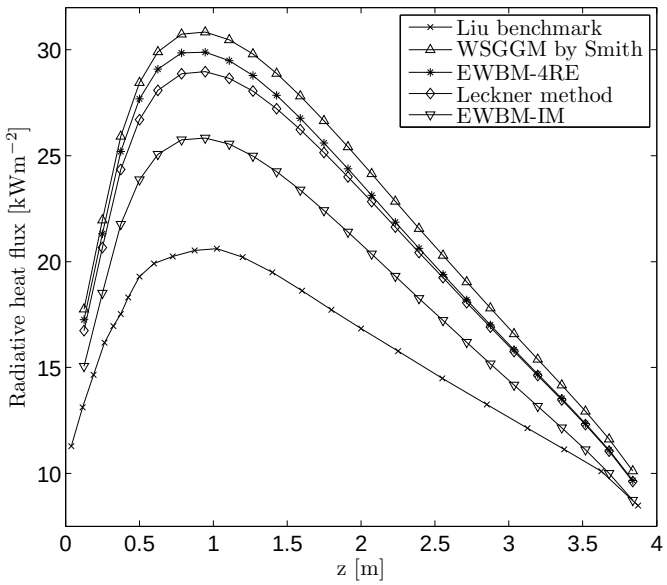

Figure 3.10: Distribution of the radiative heat flux along 2 m, 1 m, and z for a H_2O–CO_2 mixture. A comparison between the predictions of the different models with a benchmark solution from the work presented by Liu (1999).

3.3 Summary

Two implementations of the EWBM (EWBM-4RE and EWBM-IM) have been spectrally analyzed and compared with the available experimental data and the SNBM as the benchmark method. The EWBM treats the properties of the absorption bands by an exponential function. The EWBM-IM treats the properties of the absorption bands for each wavenumber separately with further integration, whereas in the EWBM-4RE, the absorption bands are approximated by rectangular boxes with the constant absorption coefficient of each box. As opposed to the EWBM-4RE, the EWBM-IM roughly reproduces the shape of spectrum, and by nature, this method has more ability for spectral predictions. However, the accuracy of the EWBM-IM in the calculations of the total properties can be improved by obtaining new spectral parameters for the EWBM-IM instead of using those which were originally developed to be used in the EWBM-4RE. A comparison of these methods with the SNBM as the benchmark method showed the EWBM-4RE with its originally developed parameters to be a more accurate model for obtaining total properties. However, the EWBM-IM provides as twice less accurate solutions for two benchmarks compared with the original EWBM-4RE of the total properties calculations in 2D and 3D rectangular enclosures.

4 Correlations based gray modeling of radiative heat transfer in homogeneous and inhomogeneous H_2O–CO_2 mixtures

The main focus of the present chapter is on proposing some useful correlations for the total emissivity of homogeneous and inhomogeneous H_2O–CO_2 mixtures which in turn will be used for gray gas radiative heat transfer modeling. Discrete ordinate method (DOM) has been used to solve the radiative heat transfer equation (RTE) in its gray form in the benchmarks. Different models of obtaining radiative properties have been implemented to the DOM through the polynomial fitting of the mean absorption coefficient values for a certain gas composition and path length as a function of temperature. The gray gas assumption presents a single value of the absorption coefficient averaged over the entire radiative spectrum. In gray gas models, the RTE is solved once by using the mean absorption coefficient. By using the emissivity databases obtained by the statistical narrow band model (SNBM), a correlation of the total emissivity can be found as a function of effective parameters, that is gas composition, temperature, and pressure path length product for being used in the gray gas modeling. The comparison of the obtained correlation with other widely used methods is performed to present the accuracy level and computational effectiveness of the new correlation based gray approach.

Narrow Band models (NBM) are well known for the spectral behavior of gas molecules. In NBMs, the entire radiative heat transfer spectrum is divided into narrow wavenumber intervals in which the absorption coefficient is assumed constant and evaluated statistically. The absorption coefficient and the emissivity of the narrow bands are obtained by using the experimental data of the spacing and the mean intensity of individual absorption lines. The most widely used methods for calculating the narrow band properties are the Elsasser (Siegel and Howell, 1992; Modest, 2003b), in which the equal intensity lines are assumed equally spaced within the narrow bands, and the statistical models (Siegel and Howell, 1992; Soufiani and Taine, 1997; Modest, 2003b), in which random spacing of the spectral lines is considered.

The SNBM is a sub-model of the NBMs. This model assumes that the absorption lines are located randomly in the bands, and their line intensity yields to a statistical distribution law. In the SNBM used in this research by applying the Malkmus model (Ludwig et al., 1973) with the Lorentz line shapes (Goody, 1964), the transmissivity averaged over a wide spectral interval of a homogeneous and isothermal slab of a gas is given as (Soufiani and Taine, 1997)

$$\bar{\tau}^{\Delta\eta} = \exp\left[-2\frac{\zeta_{\mathrm{M}}}{\delta}\left(\sqrt{1+\mathrm{xPLk}^{*}\frac{\bar{\delta}}{\zeta_{\mathrm{M}}}}-1\right)\right], \tag{4.1}$$

where L is the path length (cm), P is the total pressure (bar), x is the molar fraction, and k^{*} ($\mathrm{cm}^{-1}\mathrm{bar}^{-1}$), $\bar{\delta}$ (cm^{-1}), and ζ_{M} (cm^{-1}) are the parameters of the SNBM model.

The exponential-tailed $(1/\mathrm{S})$ distribution or the Malkmus model is calculated as

$$\mathrm{p(S)} = \frac{1}{\bar{\mathrm{S}}} \exp\left[-\frac{\mathrm{S}}{\bar{\mathrm{S}}}\right] \quad , \qquad 0 \leq \mathrm{S} < \infty, \tag{4.2}$$

where $\mathrm{p(S)}$ is a probability density function and $\bar{\mathrm{S}}$ is the line intensity average.

Integration of Eq. 4.2 for the Lorentz profile produces (Modest, 2003b)

$$\frac{\bar{\mathrm{W}}}{\mathrm{d}} = \frac{\pi \bar{\mathrm{b}}_{\mathrm{L}}}{2\mathrm{d}} \left[\left(1 + \frac{4\bar{\mathrm{S}}\mathrm{X}}{\pi \bar{\mathrm{b}}_{\mathrm{L}}}\right)^{0.5} - 1\right] = \frac{\beta}{2} \left[\left(1 + 4\frac{\tau}{\beta}\right)^{0.5} - 1\right], \tag{4.3}$$

where $\bar{\mathrm{W}}$ is an average over N lines included in the spectral interval and d is the average line spacing ($\mathrm{d} = \Delta\eta/N$). The SNBM parameters $\bar{\mathrm{b}}_{\mathrm{L}}/\mathrm{d}$ and $\bar{\mathrm{S}}/\mathrm{d}$ are obtained from experimental data or from high-resolution spectral databases such as HITRAN.

The presented formulation of the SNBM has been used to produce databases of the total emissivity for obtaining new correlations. In addition, the SNBM was used as a benchmark method as suggested in the literature (Soufiani and Djavdan, 1994; Parthasarathy et al., 1996; Bedir et al., 1997; Liu, 1999; Chu et al., 2011).

4.1 Emissivity database for homogeneous and inhomogeneous oxy- and air-fired combustion

Simple, fast, and sufficiently accurate models are highly necessary to obtain the radiative properties of combustion products. For improving the computational performance of the SNBM (Soufiani and Taine, 1997) by means of curve fitting process of the total emissivity of H_2O–CO_2 mixtures, the fitted correlations can be obtained. Therefore, for a database creation, the range of effective parameters, that is gas composition, pressure, path length and temperature, should be selected to satisfy the industrial oxy/air-fired combustion requirements. These correlations, which are based on the SNBM, can be used to calculate the total emissivity of H_2O–CO_2 mixtures in a faster and simpler manner than the conventional formulation of the SNBM with almost the same level of accuracy. Moreover, the obtained correlations should reduce the computational time and provide better accuracy compared to other methods.

By using the SNBM (Soufiani and Taine, 1997), the databases of the total emissivity have been generated. To do the SNBM calculations, a modified, publicly accessible version of the excel spreadsheet originally coded by professor Paul D. Ronney (2010), has been used. The SNBM can be used to calculate the radiative properties of gas mixtures to produce almost as accurate solutions as LBLM calculations (Chu et al., 2011). While the review process about to begin, it was found out that the updated version (Ronney, 2012) of the SNBM spreadsheet had become available. However, it was decided to keep the

previous version for presenting the results of gray modeling and use the latest version for producing the correlations supporting the non gray modeling in this thesis.

Generally, in the air-fired combustion, the molar ratios of H_2O and CO_2 are relatively small and the main component is N_2. The following four different gas mixtures are assumed to cover most of the possible conditions in the homogeneous air-fired combustion scenario systems: Case 1 – 10% H_2O, 10% CO_2 –; Case 2 – 10% H_2O, 20% CO_2 –; Case 3 – 20% H_2O, 10% CO_2 –; and Case 4 – 20% H_2O, 20% CO_2. For each of the listed cases of gas composition case, the following ranges of effective parameters are selected: the temperature T_g ranges from 500 K to 2200 K with a step of 100 K the source temperature T_s equals to T_g, and the values of the pressure path length product P_tL at atmospheric pressure ($P_t = 1$ bar) equal to 0.001, 0.01, 0.1, 0.2, 0.3, 0.4, 0.5, 1, 2, 5, and 10 bar m.

In the following, another emissivity database is produced using the SNBM to produce some other correlations for supporting the gray gas modeling in the oxy-fired systems. In this regard, by assuming that the whole mixture consists only of H_2O and CO_2, the total emissivity is assumed to be a function of the three main parameters only: molar fractions ratio of H_2O and CO_2, temperature, and pressure path length product. Fifteen different gas compositions have been considered to support all the possible conditions which may occur in oxy-fired systems.

4.2 General form of correlation

In order to select a suitable form for the correlation, a 3D graphical analysis of the total emissivity values calculated by the SNBM at the selected ranges of temperature, pressure, and optical path length has been carried out. Figure 4.1 shows the behavior of the total emissivity at atmospheric pressure calculated by the SNBM for 20% H_2O, 10% CO_2 (Case 3) as a function of T and P_tL. For the other three cases, the profiles of the total emissivity showed similar behavior, and therefore, the figures are not reported here.

By analyzing Figure 4.1, various forms of mathematical functions have been tested and, finally, the following general logarithmic type showed promising behavior to be selected as the form of the correlation of the total emissivity in the fixed gas compositions

$$\epsilon = a_1 + a_2 \ln(T) + a_3 \ln(P_tL) + a_4[\ln(T)]^2 + a_5[\ln(P_tL)]^2 + a_6 \ln(T)\ln(P_tL), \quad (4.4)$$

where T is the temperature, P_t is the total pressure ($P_t = 1$ bar), and L is the optical path length.

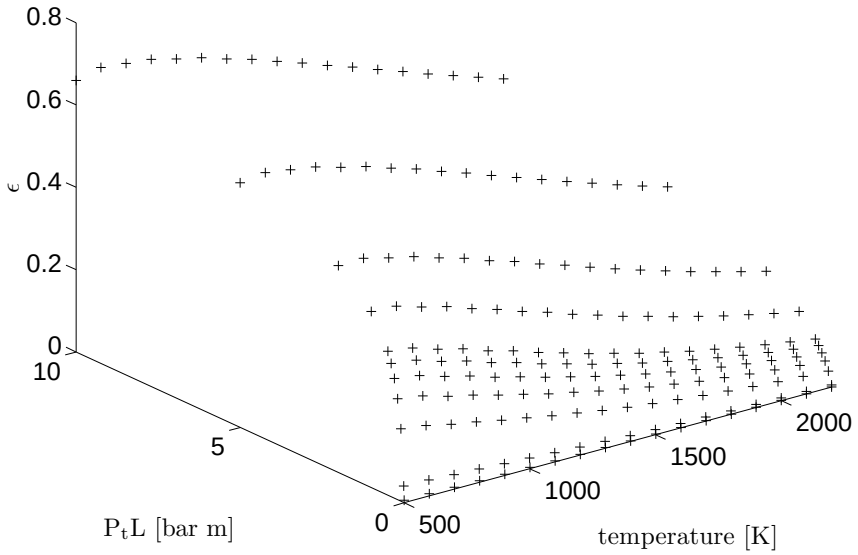

Figure 4.1: The changes of total emissivity (ϵ) with temperature and pressure path length product for a homogeneous H_2O–CO_2 gas mixture of 20% H_2O, 10% CO_2 (Case 3).

4.3 Description of curve fitting process

The minimization of the nonlinear data fitting was solved by the *lsqcurvefit* function in the Matlab R2010b software. The algorithm of this function is based on the least-squares mathematical method. The following equation is used in the same software (MathWorks, 2010) represented by a widely used method of least-squares

$$\min_{\epsilon} f(\epsilon) = \min_{\epsilon} \sum_{i} \left[\mathrm{F}(\epsilon, \epsilon\mathrm{data}_i) - \epsilon'\mathrm{data}_i \right]^2, \tag{4.5}$$

where $\epsilon\mathrm{data}$ and $\epsilon'\mathrm{data}$ are matrices: $\epsilon\mathrm{data}$ is the given input data by SNBM and $\epsilon'\mathrm{data}$ is the observed output data by Matlab. F (ϵ, $\epsilon\mathrm{data}$) is a matrix valued function of the equal size as $\epsilon'\mathrm{data}$ and $\epsilon'\mathrm{data}$ is defined by Eq. 4.4.

The function *lsqcurvefit* is trying to find a solution of the minimum values through the squared difference (see Eq. 4.5). For that solution, the function uses a math controller which checks the absolute errors between the given input and the observed data in a certain $\pm$ error range. However, that kind of a solution, because of the absolute error fitting structure, creates a certain discrepancy at small values of the initial fitting data presented in databases. The solution of this problem is found by moving from the absolute to the relative fitting structure. Thus, Eq. 4.5 is modified to

$$\min_{\epsilon} f(\epsilon) = \min_{\epsilon} \sum_{i} \left[\frac{\epsilon' \mathrm{data}_i - \mathrm{F}(\epsilon, \epsilon \mathrm{data}_i)}{\mathrm{F}(\epsilon, \epsilon \mathrm{data}_i)} \times 100 \right]^2 . \tag{4.6}$$

4.4 The correlation of total emissivity for homogeneous air-fired combustion product

By implementing the least-squares method for multivariate regression, the corresponding coefficients for the general logarithmic correlation in each of four cases of air-fired combustion have been found. However, to produce better accuracy, the $\mathrm{P_tL}$ range was divided into two smaller ranges, and for each of them, the coefficients of the correlation were obtained. The considered ranges correspond to the optically thin and optically thick media as $\mathrm{P_tL}$ was 0.001 bar m $\leq \mathrm{P_tL} \leq 1$ bar m and 1 bar m $\leq \mathrm{P_tL} \leq 10$ bar m, respectively. The coefficients for the four different cases accompanied by the normal residuals are presented in Table 4.1. This kind of correlation of the total emissivity can be used in models employing the ray tracing method, and through the Beer's law, in any radiative model that utilizes the gray gas assumption of air-fired combustion.

Table 4.1: Coefficients of the logarithmic correlation (Eq. 4.4) for the calculation of total emissivity based on the SNBM. Range 1 is 0.001 bar m $\leq \mathrm{P_tL} \leq 1$ bar m and Range 2 is 1 bar m $\leq \mathrm{P_tL} \leq 10$ bar m.

	10% H_2O, 10% CO_2		10% H_2O, 20% CO_2		20% H_2O, 10% CO_2		20% H_2O, 20% CO_2	
	Range 1	Range 2	Range 1	Range 2	Range 1	Range 2	Range 1	Range 2
a_1	0.4801	−4.0835	0.3179	−4.2019	0.3916	−5.2036	0.2519	−5.2330
a_2	0.0836	1.4383	0.1404	1.4784	0.1650	1.7962	0.2146	1.8115
a_3	0.2481	0.2173	0.2535	0.2530	0.3069	0.1085	0.3109	0.1378
a_4	−0.0171	−0.1166	−0.0215	−0.1196	−0.0255	−0.1435	−0.0295	−0.1448
a_5	0.0059	0.0040	0.0059	0.0043	0.0077	0.0008	0.0075	0.0014
a_6	−0.0250	−0.0163	−0.0255	−0.0216	−0.0303	0.0007	−0.0308	−0.0038

To show the accuracy of the multivariate regression, the predictions of the correlation were compared with the original data found by the SNBM through a deviation plot, as shown in Figure 4.2. The figure confirms that the data for both sources agree reasonably well within $\pm 5\%$. The middle diagonal (solid line) is the perfect agreement region, while the upper and lower diagonals (dotted lines) are the regions of $+5\%$ and -5% difference, respectively. Figure 4.2 confirms that the agreement is fairly good, especially for optically thick gas mixtures.

By performing a linear 2D interpolation/extrapolation, a single correlation was obtained which includes the effect of gas composition in addition to that of T and $\mathrm{P_tL}$. For better clarification in the system of too complex correlations, the notation "single correlation" is used in this work. The range of gas composition varies from 5% to 30% for each gas component. The form of this correlation is the same as that shown in Eq. 4.4; however, the

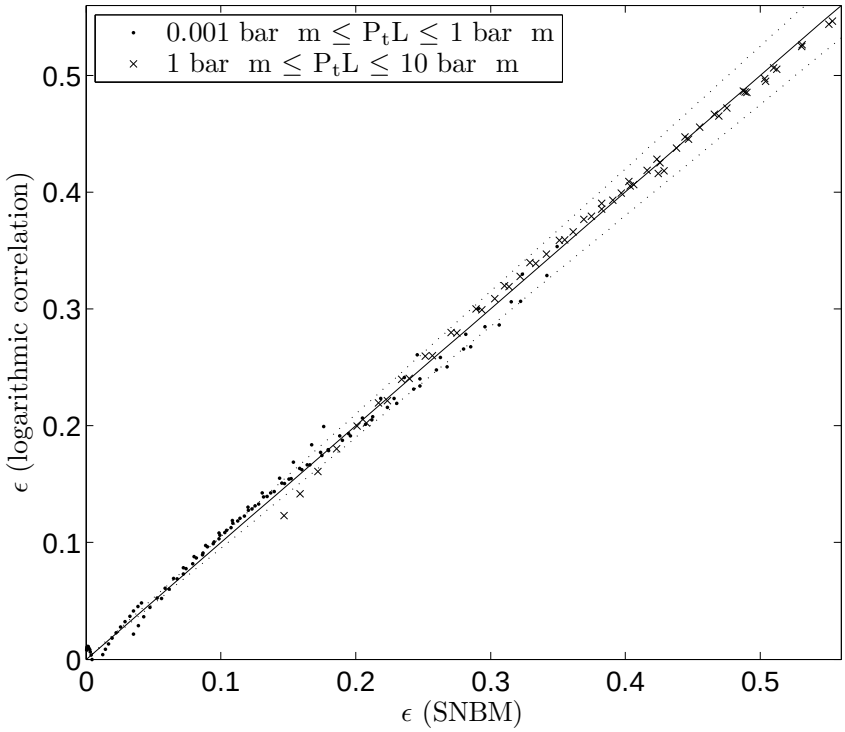

Figure 4.2: Deviation of the total emissivity predicted by the SNBM versus the logarithmic correlation (Eq. 4.4). Gas composition $H_2O = 20\%$, $CO_2 = 10\%$; temperature range $500\ \mathrm{K} \leq T_g \leq 2200\ \mathrm{K}$; and $0.001\ \mathrm{bar\ m} \leq P_tL \leq 10\ \mathrm{bar\ m}$.

effect of gas composition is manifested through its coefficients. The modified coefficients are calculated with the following equation

$$a_i = a_{10,i} + a_{11,i}x_{H_2O} + a_{12,i}x_{CO_2} + a_{13,i}x_{H_2O}x_{CO_2}, \tag{4.7}$$

where i is the number of coefficients ($i = 1, 2, 3...6$), and x_{H_2O} and x_{CO_2} are the molar fractions of H_2O and CO_2, respectively.

In Table 4.2, the coefficients of the single correlation (combination of Eqs. 4.4 and 4.7) are given based on the SNBM.

4.4.1 Accuracy comparison

Figure 4.3 shows the changes in the total emissivity with the gas temperature, based on the prediction of three different approaches: the single correlation, the Leckner method (Leck-

Table 4.2: Coefficients of the single correlation for the calculation of total emissivity based on the SNBM.

	0.001 bar m $\leq \mathrm{P_tL} \leq 1$ bar m				1 bar m $\leq \mathrm{P_tL} \leq 10$ bar m			
	$\mathrm{a_{10}}$	$\mathrm{a_{11}}$	$\mathrm{a_{12}}$	$\mathrm{a_{13}}$	$\mathrm{a_{10}}$	$\mathrm{a_{11}}$	$\mathrm{a_{12}}$	$\mathrm{a_{13}}$
$\mathrm{a_1}$	0.7533	-1.11	-1.847	2.25	-2.756	-12.091	-2.074	8.9
$\mathrm{a_2}$	-0.0618	0.886	0.64	-0.72	1.0155	3.827	0.649	-2.48
$\mathrm{a_3}$	0.1825	0.602	0.068	-0.14	0.284	-1.024	0.421	-0.64
$\mathrm{a_4}$	-0.0039	-0.088	-0.048	0.04	-0.085	-0.286	-0.047	0.17
$\mathrm{a_5}$	0.0039	0.02	0.002	-0.02	0.0104	-0.067	-0.016	0.19
$\mathrm{a_6}$	-0.0192	-0.053	-0.005	0.0	-0.0272	0.162	-0.061	0.08

ner, 1972), and the SNBM as the benchmark. For obtaining results of this comparison, the values of the mean absorption coefficient calculated by applying Beer's law into total transmissivity obtained by SNBM and Leckner method have been integrated into the Fluent DOM through the user defined function (UDF) implementing the cubical polynomial fitting in a range of temperatures. Using the total emissivity, the values of the absorption coefficient have been calculated by means of the Beer's law. As the figure shows, for most cases, the single correlation by the combination of Eqs. 4.4 and 4.7 provides closer results to the SNBM at the specified parameters of gas composition, pressure, path length, and temperature, especially at middle and lower temperatures. As the temperature of the gas increases, the predictions obtained through both methods approach the values of the SNBM.

For the accuracy demonstration of the multivariate regression, Figure 4.4 shows the deviation plot of the total emissivity in the specified T and $\mathrm{P_tL}$ ranges for the present single correlation and Leckner (1972) method with the SNBM as a benchmark. Figure 4.4 shows that the present single correlation provides closer predictions to the SNBM results, especially for optically thick gas mixtures. The single correlation can be easily implemented in the simulation methods of radiative transfer in $\mathrm{H_2O}$ and $\mathrm{CO_2}$ mixtures of gray gas modeling.

By accurately measuring the CPU time of the different approaches under identical conditions, that is computational power, software, and computational sample, it was found out that the present single correlation decreases the CPU time by a factor of at least ten with better accuracy than the Leckner approach. However, the Leckner method is also a quite fast and accurate approach, especially for optically thin media. It should be noticed that the Leckner method was obtained based on the available emissivity databases at 1970's and it produced quite fast and useful results for engineering applications at that time. The method was belonging to one of the two reliable models for calculating the total emissivities of $\mathrm{H_2O}$–$\mathrm{CO_2}$ mixture, even when it was used outside of its path length applicability domain (Lallemant et al., 1996).

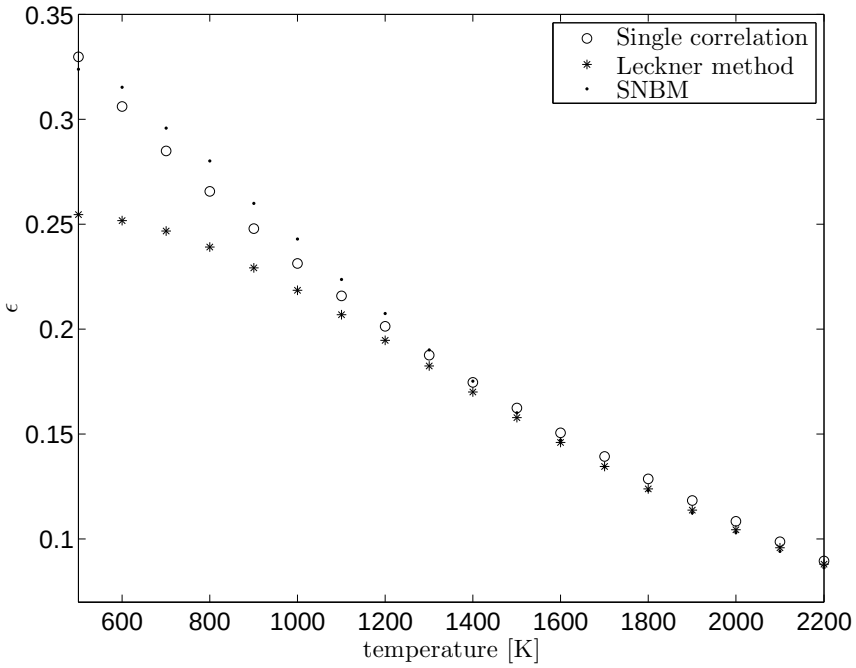

Figure 4.3: Comparison between emissivities obtained by the single correlation, Leckner method, and SNBM as a benchmark for gas composition $H_2O = 20\%$, $CO_2 = 10\%$; the temperature range 500 K $\leq T_g \leq 2200$ K; and $P_tL = 0.4$ bar m.

4.5 Total emissivity correlation for inhomogeneous oxy-fired combustion product

The combustion process of different types of fuels in pure O_2 as the primary oxidant, instead of air mixture which is used in air-fired combustion, is termed as oxy-fired combustion. Because the air component N_2 is not participating in the oxy-fired combustion process, the fuel consumption is significantly lower compared with air-fired scenario. Moreover, the range of flame temperatures is larger. The economical barrier of the oxy-fired combustion is contained in the system costs compared with the traditional air-fired scenario. One of the main problems is connected to the separation of O_2 from the air mixture. The separation of O_2 is an energy consuming process, and about 15% of power production can be consumed. However, a modern technology which is called the chemical looping combustion has been developed to reduce these costs (Pröell et al., 2009). There might not be a significant alternative to the oxy-fired combustion for the CO_2 emission reductions. Because of the modern straggle with emission reductions and higher heat rate production, the oxy-fired combustion is competitive with traditional air-fired scenario (Myöhänen et al., 2009). Furthermore, homogeneous gas composition is practically impossible in industrial combustion systems, especially in the part of the systems

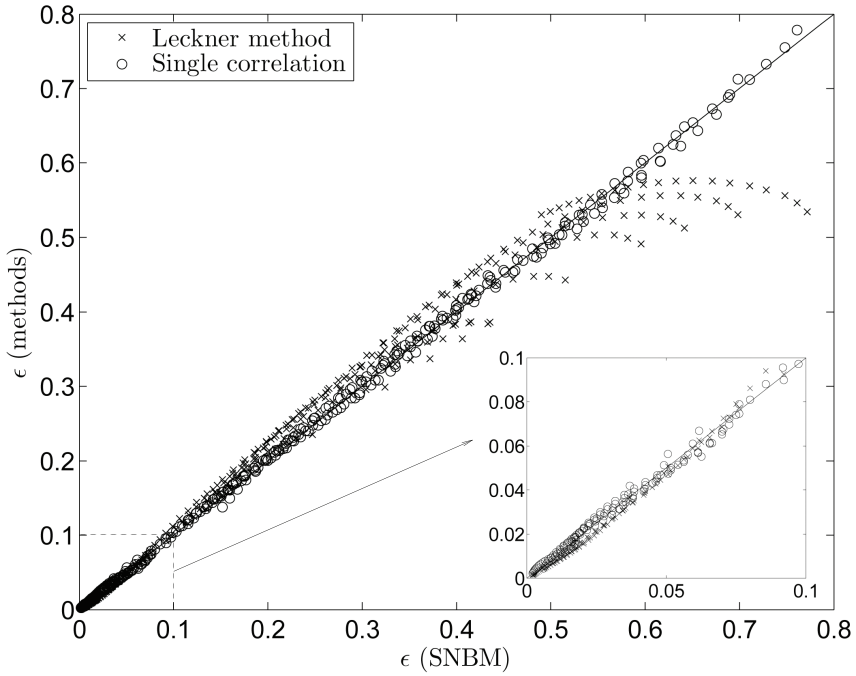

Figure 4.4: Deviation of the total emissivity predicted by the SNBM versus the single correlation for air-fired combustion (Eq. 4.4) and the Leckner method. Gas composition $H_2O = 20\%$, $CO_2 = 10\%$; temperature range $600\ \text{K} \leq T_g \leq 2500\ \text{K}$; and $0.001\ \text{bar m} \leq P_t L \leq 10\ \text{bar m}$.

in which the combustion is not completed yet and is still improving. Therefore, there is a clear need for methods which could support the oxy-fired combustion and inhomogeneous conditions. For this reason, this part of the research has been developed.

Hydrocarbon fuel combustion produces several species as combustion products. The absorbing or emitting species of oxy-fired combustion have been simplified to be composed only of H_2O and CO_2 species. These species have a significant share of the combustion products, especially in industrial oxy-fired systems, and the effect of the other species can be assumed to be neutral in radiation. For obtaining the correlations of the total emissivity calculation, as previously for air-fired combustion, the SNBM has been used to produce the needed database for the range of the effective parameters covering the oxy-fired combustion at atmospheric pressure.

4.5.1 Three effective parameters – Pr, $P_{w+c}L$, and T

The general logarithmic correlation (see Eq. 4.4) is used to calculate the total emissivity as a function of T and P_tL in a constant fixed gas composition representing the homogeneous media in the air-fired systems. For the case of air-fired combustion, the single correlation (Eq. 4.4) includes the effect of gas composition by substituting coefficients of Eq. 4.7 with Eq. 4.4. Particularly, the effect of gas composition is included by p_{H_2O} and p_{CO_2} fractions individually. Thus, a single correlation is obtained for the total emissivity calculations as a function of four parameters: p_{H_2O}, p_{CO_2}, T, and L.

For oxy-fired combustion at atmospheric pressure, the share of other gas species excluding H_2O and CO_2 is quite small compared to H_2O and CO_2. Thus, it can be assumed that the whole mixture consists of H_2O and CO_2 and the effect of other gases is negligible. The same assumption has been done in the previous models obtained for calculating radiative properties of combustion product in oxy-fired systems (Johansson, 2008; Johansson et al., 2010; Yin et al., 2010; Johansson et al., 2011). By this assumption, $P_{w+c} = p_{H_2O} + p_{CO_2}$ equals to 1 bar, and therefore, by introducing three parameters as $Pr = p_{H_2O}/p_{CO_2}$, T, and $P_{w+c}L = (p_{H_2O} + p_{CO_2})\,L$, the emissivity can be assumed to be a function of only these three parameters.

The ranges of the set parameters have been selected taking into account the requirements of the industrial needs. In the case of equal Pr ratios of gas compositions, the $P_{w+c}L$ parameter is intended to complement the difference. Thus, the ratio of molar fractions can be presented in different ways resulting in the same Pr. However, the originality of one or another molar ratio is represented by $P_{w+c}L$ where the summation of molar fractions is obtained.

4.5.2 New correlation of total emissivity

For producing the total emissivity database based on the SNBM of the oxy-fired scenario, the following conditions have been considered. The chosen molar fractions ratios of H_2O and CO_2 at the total pressure of 1 bar were selected as $Pr = 1/8$, $1/4$, $1/2$, $3/4$, $1/1$, $2/1$, $3/2$, $5/2$, $3/1$, $7/2$, and $4/1$. The following effective parameters were selected: temperature range 600 K $\leq T_g \leq 2800$ K with a step of 100 K, source temperature $T_s = T_g$, and the $P_{w+c}L$ range 0.001 bar m $\leq P_{w+c}L \leq 10$ bar m. The values of $P_{w+c}L$ equal to 0.001, 0.003, 0.005, 0.007, 0.009, 0.01, 0.1, 0.2, 0.3, 0.4, 0.5, 1, 2, 3, 5, and 10 bar m.

The profile of the total emissivity as a function of Pr, $P_{w+c}L$, and T has sensibly identical behavior to the previously presented air-fired combustion scenario (see Figure 4.1). Thus, a modified version of the general logarithmic correlation (Eq. 4.4) is used to correlate the new database with the three effective parameters of the total emissivity under oxy-fired combustion scenario. The modification of the term of correlation P_tL into $P_{w+c}L$ results in

$$\epsilon = \mathrm{a}_1 + \mathrm{a}_2 \ln(\mathrm{T}) + \mathrm{a}_3 \ln(\mathrm{P_{w+c}L}) + \mathrm{a}_4[\ln(\mathrm{T})]^2 + \mathrm{a}_5[\ln(\mathrm{P_{w+c}L})]^2 + \mathrm{a}_6 \ln(\mathrm{T}) \ln(\mathrm{P_{w+c}L}). \tag{4.8}$$

Because of the highly complex behavior of the emissivity, the $\mathrm{P_{w+c}L}$ range was divided into three smaller ranges with further obtaining the coefficients for each of three ranges. The considered ranges for $\mathrm{P_{w+c}L}$ are 0.001 bar m $\leq \mathrm{P_{w+c}L} \leq 0.01$ bar m, 0.01 bar m $\leq \mathrm{P_{w+c}L} \leq 0.5$ bar m, and 0.5 bar m $\leq \mathrm{P_{w+c}L} \leq 10$ bar m which correspond to the definition of optically thin, moderate optical thickness, and thick optical thickness, respectively.

The multivariate regression for the fitting of the new correlation into the emissivity database has been done in two steps. In the first step of developing the new correlation, the values of the coefficients (a_i) have been obtained for each Pr. The minimization of the data fitting was solved by the *lsqcurvefit* function in the Matlab R2010b software based on the least-squares method. It has been done by minimizing the deviation with the relative fitting (Eq. 4.6) between the total emissivity calculated by Eq. 4.8 and the emissivity database obtained by the SNBM. In the next step, the functionally dependence on Pr is included by

$$\mathrm{a}_i(\mathrm{Pr}) = \mathrm{b}_{1,i}(\mathrm{Pr})^4 + \mathrm{b}_{2,i}(\mathrm{Pr})^3 + \mathrm{b}_{3,i}(\mathrm{Pr})^2 + \mathrm{b}_{4,i}\mathrm{Pr} + \mathrm{b}_{5,i}, \tag{4.9}$$

where i is the number of a coefficients ($i = 1, 2, 3...6$).

In the second step, the coefficients (b_j) have been obtained by minimizing the values of (a_i) given by Eq. 4.9 and those obtained in the first step. Thus, the effect of Pr is considered in the overall calculation of the emissivity by substituting Eq. 4.8 with Eq. 4.9. By this, there is no need for presenting several sets of the coefficients for each Pr, as they have been produced in the previously published methods, such as the WSGGM by Smith et al. (1982) and the empirical correlation by Green and Perry (2008). In those methods, inter/extrapolations are needed for the not tabulated $\mathrm{Pr}'\mathrm{s}$ causing some inaccuracies and extra computational time. In this work, a unique set of coefficients is presented for the whole range of $\mathrm{Pr}'\mathrm{s}$.

The new correlation (Eq. 4.9) for the calculation of the total emissivity $\mathrm{H_2O}$–$\mathrm{CO_2}$ mixtures under oxy-fired condition can be used in any radiative model with the gray gas assumption. The coefficients of the new correlation are given in Tables 4.6–4.8.

4.5.3 Accuracy and computational time

The accuracy comparison was done through a deviation plot, as shown in Figure 4.5, between the new correlation, Green and Perry empirical correlation (Green and Perry, 2008), WSGGM by Smith et al. (1982), WSGGM by Johansson et al. (2011), the EWBM (Edwards and Balakrishnan, 1973), and the original results of the SNBM (Soufiani and Taine, 1997) as the benchmark. The figure confirms that the data presented by the new

correlation agree reasonably well within $\pm 5\%$, especially for optically thick gas mixtures.

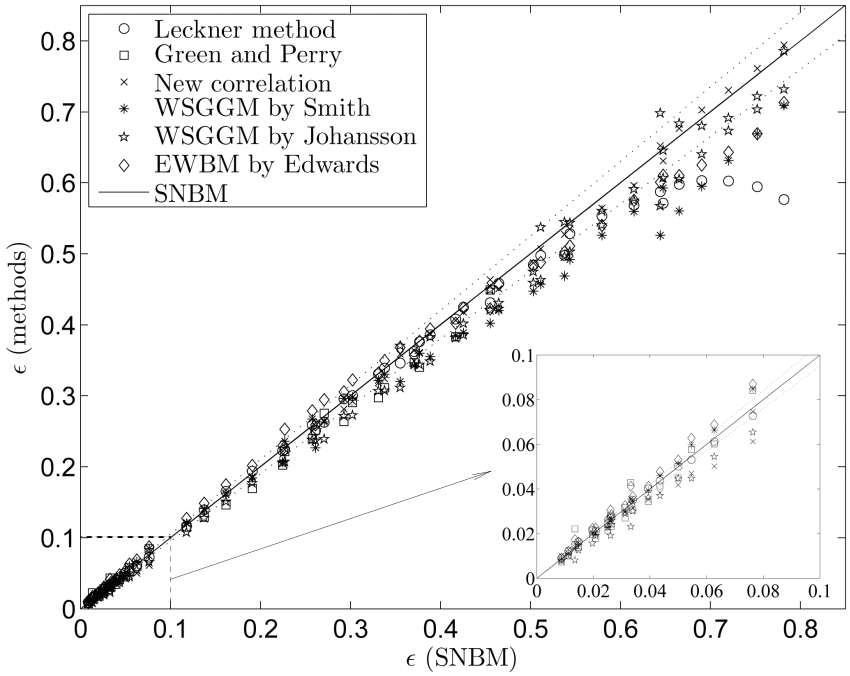

Figure 4.5: The deviation plot of comparing the total emissivity predicted by the new correlation (Eq. 4.9) and other methods. Molar fractions ratio $\mathrm{Pr} = 2$, temperature range $800\ \mathrm{K} \leq \mathrm{T_g} \leq 1800\ \mathrm{K}$, and $0.001\ \mathrm{bar\ m} \leq \mathrm{P_{w+c}L} \leq 10\ \mathrm{bar\ m}$.

Figure 4.5 shows that the proposed new correlation provides better accuracy, especially for optically thick media at the specified Pr. By calculating the average of the relative errors at a certain Pr, the values of different methods were obtained in Table 4.3. For the presented new oxy-fired correlation, the average relative error was obtained as an average error of three $\mathrm{P_{w+c}L}$ intervals. The comparison of other reported Pr's showed a similar level of deviation for different methods.

Table 4.3: Comparison of the average relative errors of total properties calculation for different methods (SNBM used as a benchmark).

Calculated sample	$\mathrm{Pr} = 2$; $800\ \mathrm{K} \leq \mathrm{T_g} \leq 1800\ \mathrm{K}$; $0.001\ \mathrm{bar\ m} \leq \mathrm{P_{w+c}L} \leq 10\ \mathrm{bar\ m}$					
Method	New correlation (Tables 4.6–4.8)	Leckner	WSGGM by Smith	EWBM	WSGGM by Johansson	Green and Perry
$\mathrm{Error_{Av.Rel}}$ [%]	4.3	4.7	6.2	7.1	10.6	7.8

The computational efficiency (CPU) and the accuracy are the most important factors, when solving the radiative heat transfer problems, especially in engineering calculations.

To provide a quantitative view of the computational costs of each model, the CPU time measurement of different methods has been performed under the identical conditions, that is the calculated sample, software, and computational power. The calculations were carried out using a DELL Optiplex 755E6750 with Intel® Core$^{\mathrm{TM}}$ 2 Duo processor at 2.66 GHz with 3.072 GB of RAM. All calculations of this work were carried out using the listed computer facilities. The results of the CPU time of the different methods for the same number of executions are listed in Table 4.4. The table shows that the new correlation (Eq. 4.9) is one of the fastest methods, yielding the first position to Green and Perry empirical correlation. However, the fastest method is less accurate. It should be mentioned that the CPU time needed for the interpolation/extrapolation of the coefficients for the not tabulated cases of Green and Perry (2008) empirical correlation and various WSGGMs is taken into account.

Table 4.4: Comparison of the CPU times for different methods of total properties calculation accompanied with the average relative errors (SNBM used as a benchmark).

Calculated sample	$0.125 \leq \mathrm{Pr} \leq 4$; 800 K $\leq \mathrm{T_g} \leq 1800$ K; 0.001 bar m $\leq \mathrm{P_t L} \leq 10$ bar m					
Method	New correlation (Tables 4.6–4.8)	Leckner	WSGGM by Smith	EWBM	WSGGM by Johansson	Green and Perry
CPU time [s]	30.36	879.36	37.33	156250.0	57.42	27.72
$\mathrm{Error_{Av.Rel}}$ [%]	4.4	5.6	7.1	6.6	10.5	13

4.5.4 3D benchmark of homogeneous $\mathrm{H_2O}$–$\mathrm{CO_2}$ mixture

The main target of this section is to validate the correlation of total properties, which is implemented in gray gas radiative heat transfer, by comparing it to a benchmark. Benchmark has been solved using a ray tracing method of the RTE solver accompanied with the SNBM results of Soufiani and Taine (1997). Liu (1999) presented a benchmark which is a rectangular enclosure with dimensions of 2 m $\times$ 2 m $\times$ 4 m and black walls at 300 K. The concentration of $\mathrm{H_2O}$ and $\mathrm{CO_2}$ equal to 20% and 10% by molar fraction. The temperature profile within the 3D enclosure is modeled to be of a flame shape. This benchmark has been introduced in Chapter 3.2.2 starting from page 64.

Widely used DOM is one of the methods for the approximate solution of the radiative transfer equation (RTE). This method utilizes an approach of splitting up the solid angle into a number of discrete directions. Moreover, within each division of the solid angle, the radiative intensity is supposed to be constant. Thus, the RTE must be solved for the equal number of discrete angles with the weights of each discrete direction. For obtaining results in this section, one of the highest discretization schemes $\mathrm{S_8}$, has been used. The analysis of the obtained results with the benchmark can show the effect of using different discretization schemes in the DOM and their effect on the performed accuracy.

The comparison of total properties calculations for the correlation (Eq. 4.4) with coefficients listed in Table 4.1 and the different methods with the benchmark are shown in

Figure 4.6. The maximum and average relative errors are listed in Table 4.5.

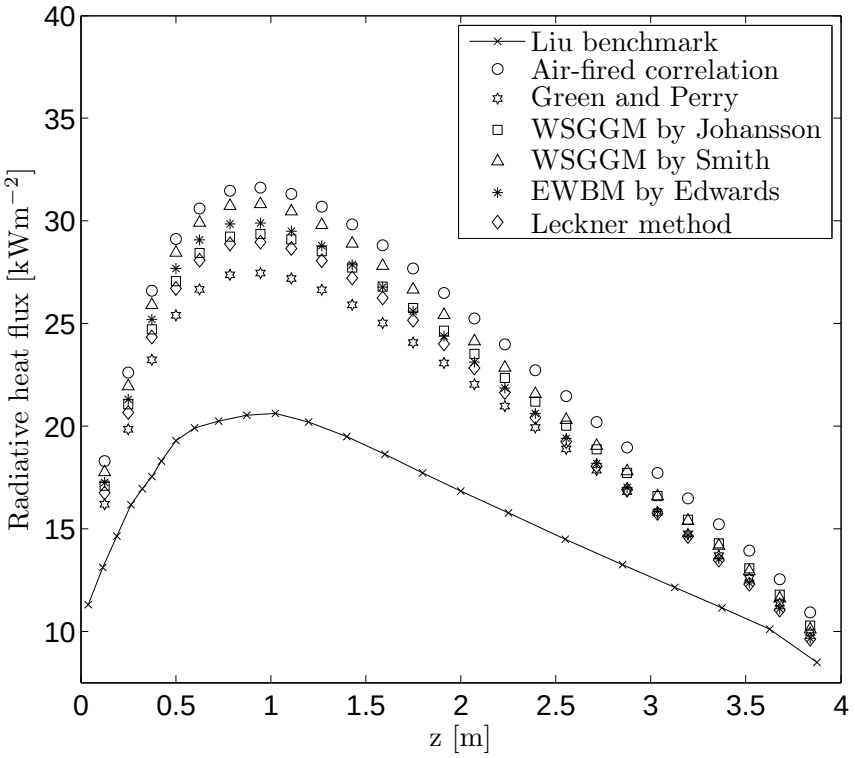

Figure 4.6: A comparison between the predictions of gray modeling of different methods and the air-fired correlation (Eq. 4.4) with coefficients listed in Table 4.1 with a benchmark solution by Liu (1999). Distribution of radiative heat flux along a side wall (2 m, 1 m, z) for H_2O–CO_2 mixture of $\mathrm{Pr} = 2$ at temperature range $300\ \mathrm{K} \leq \mathrm{T} \leq 1800\ \mathrm{K}$ and pressure path length product $\mathrm{P_{w+c}L} = 0.432$ bar m.

Table 4.5: Maximum and average errors of the distribution of radiative heat flux along a side wall (2 m, 1 m, z) for H_2O–CO_2 mixture of $\mathrm{Pr} = 2$ at temperature range $300\ \mathrm{K} \leq \mathrm{T} \leq 1800\ \mathrm{K}$ and pressure path length product $\mathrm{P_{w+c}L} = 0.432$ bar m for different methods; Liu (1999) solution used as a benchmark.

Calculated sample	$\mathrm{Pr} = 2$; $300\ \mathrm{K} \leq \mathrm{T_g} \leq 1800\ \mathrm{K}$; $\mathrm{P_{w+c}L} = 0.432$ bar m					
Method	Air-fired correlation	Leckner	WSGGM by Smith	EWBM	WSGGM by Johansson	Green and Perry
$\mathrm{Max.Error_{Rel}}$ [%]	54.2	41.1	50.2	46.1	43.5	34.1
$\mathrm{Error_{Av.Rel}}$ [%]	46.5	32.3	40.1	34.8	36.6	28.9

By analyzing Figures 4.6 and 4.5, one can conclude that by presenting the results of gray gas modeling calculations, some of the listed radiative models with higher levels of un-

derestimation of total emissivity, as a result, provide a better concurrence with a non gray benchmark solution in which the spectral radiative properties are considered carefully. The source of difference of the air-fired correlation (Eq. 4.4) and other presented methods of the total properties approximation is located in different spectrum profiles accompanied by the blackbody radiation distribution providing different averaging of emissivity values. It is well known that the SNBM is one of the most accurate models being almost as accurate as LBLM. Thus, the air-fired correlation calculates the spectral features at a very high level while the other methods are neglecting the spectral effects. Because of the fact that the other methods have errors of underestimation of total properties, it gives smaller values of total properties approximation and, as a result, closer to a non gray benchmark solution.

Analyses of the results of different methods for the gray modeling by using the air-fired correlation with the coefficients reported in Table 4.1 show a high difference with the benchmark with an average relative error of about 46%. The different versions of gray modeling of WSGGM by Smith and by Johansson, the Leckner method, and the empirical correlation by Green and Perry provide results with an average relative error of approximately 30%. However, the comparison of different methods utilizing the total properties (gray gas assumption) with a non gray exact solution, presented in Figure 4.6, is not the main target of the current research, and it can be considered in future studies.

4.5.5 3D benchmark of homogeneous H_2O–CO_2 mixture for oxy-fired combustion

In order to validate the new correlation which is going to be used in engineering CFD calculations under oxy-fired conditions it must be compared with much higher concentrations of participating species, especially CO_2. Therefore, the oxy-fired benchmark by Porter et al. (2010) with the same geometry (2 m $\times$ 2 m $\times$ 4 m with black walls at 300 K) with the known flame temperature profile has been used. The concentrations of the gases equal to 10% H_2O, 85% CO_2, and 5% N_2 by mole basis and the partial pressures ratio is $\mathrm{Pr} = 0.1176$. The benchmark is solved using the ray tracing method together with SNBM (Soufiani and Taine, 1997).

The results of gray modeling of the benchmark by using the new correlation (Eq. 4.9) with coefficients listed in Tables 4.6–4.8 have been compared with those of using other methods. One of the highest discretization scheme S_8 of DOM has been used for obtaining results. For other radiative models, the values of absorption coefficient have been defined by cubical polynomial fitting in the range of temperatures for listed gas composition and path length. Figure 4.7 shows the radiative heat flux on a side wall along z direction of the geometry at $x = 0$ and $y = 1$. The figure shows that the WSGGM with air-fired coefficients predicts the radiative heat flux significantly better in oxy-fired solutions at certain effective parameters.

It can be clearly seen from Figure 4.7 that the heat flux profile using the WSGGM is cal-

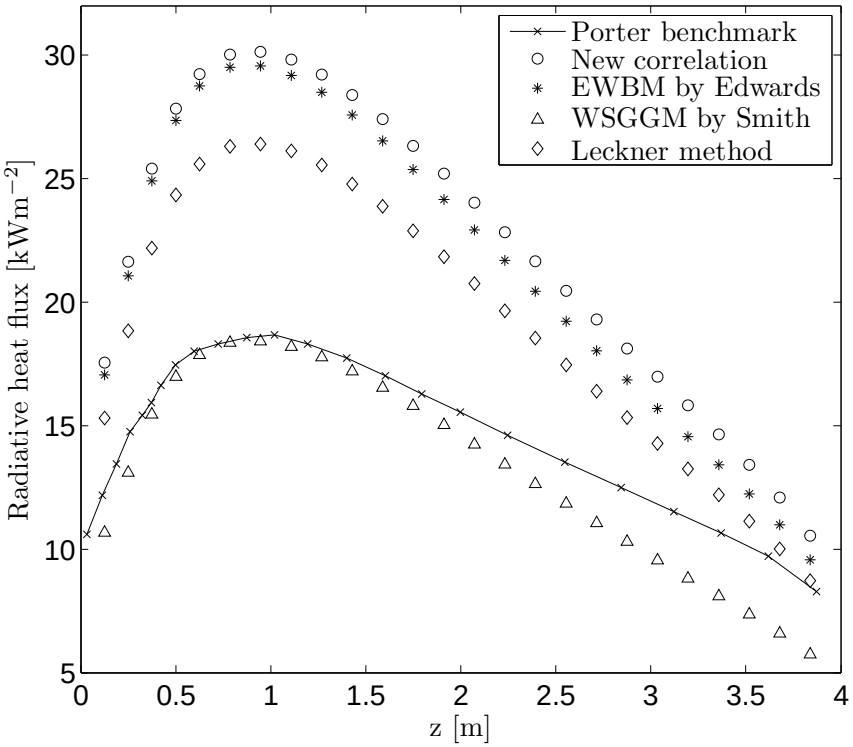

Figure 4.7: A comparison between the predictions of gray modeling of different methods and the new correlation with coefficients presented in Table 4.8 with a benchmark solution by Porter et al. (2010). Distribution of radiative heat flux along a side wall (0 m, 1 m, z) for H_2O–CO_2 mixture of $\mathrm{Pr} = 0.1176$ at temperature range $300\ \mathrm{K} \leq \mathrm{T} \leq 1800\ \mathrm{K}$ and pressure path length product $\mathrm{P_{w+c}L} = 1.368$ bar m.

culated very close to the benchmark solution, especially at high temperatures. This "accurate" solution is obtained due to underpredicted radiation values near the wall. Moreover, similar behavior of the WSGGM with the air-fired coefficients in oxy-fired combustion has been investigated and described by Porter et al. (2010). If the distance is increasing from the high flame temperature region to the wall, the accuracy of the radiative heat transfer prediction leads to significant errors. The figure shows that kind of an error at the end of the modeled enclosure.

4.6 Summary

A correlation for the total emissivity of air-fired combustion products is presented in the form of a general logarithmic correlation as a function of $\mathrm{P_tL}$ and T for four different gas

compositions, and the coefficients are presented in Table 4.1. Moreover, a single correlation is obtained by linear interpolations/extrapolations which additionally includes the effect of gas composition. The coefficients of a single correlation are presented in Table 4.2. The reported correlation for the total emissivity of air-fired combustion products provides more accurate, simpler, and faster calculations than the other similar correlation based methods available for calculation of total emissivity of H_2O–CO_2 mixtures. The suggested correlations decrease the CPU time with a small reduction in the accuracy of the total emissivity calculation compared with the original SNBM data. Nonetheless, the coefficients of the single correlation are suitable for a range of gas compositions variable from 5% to 30% for each component, thus characterizing it for a limited usage in homogeneous and inhomogeneous systems of the air-fired combustion.

In order to propose an effective correlation for the total emissivity with a wide range of applicability for the oxy-fired systems, it has been shown that the total emissivity of H_2O–CO_2 mixtures in the atmospheric pressure can be interpreted as a function of only three parameters of Pr, T, and $\mathrm{P_{w+c}L}$. The SNBM has been used to produce databases of the total emissivity of H_2O–CO_2 mixtures for the range of effective parameters: Pr, T, and $\mathrm{P_{w+c}L}$, corresponding to oxy-fired combustion scenario. Based on the profiles of emissivity as a function of T and $\mathrm{P_{w+c}L}$ at a certain Pr, the general logarithmic form is obtained for the new correlation. By applying the least-squares method for multivariate regression, the coefficients of the new correlation have been derived. The new correlation calculates the total emissivity as a function of three effective parameters, that is Pr, T, and $\mathrm{P_{w+c}L}$, and its coefficients are listed in Tables 4.6–4.8.

The new SNBM based correlation obtained for the calculation of the total radiative properties of the oxy-fired combustion products (Tables 4.6–4.8) provides more accurate, simpler, and fast enough calculations of the total emissivity compared with the EWBM, various formulations of the WSGGM, and the other correlation based approaches in this field. The new correlation decreases the CPU time with almost no change in the accuracy of the total emissivity calculations compared with the original SNBM data.

The suggested correlations can be simply implemented in gray radiative heat transfer modeling and in any commercial CFD code, such as Fluent or CFX, resulting in more computationally efficient, accurate, and simple calculations.

Table 4.6: Coefficients of the new correlation for the calculation of total emissivity under oxy-fired condition for 0.001 bar m $\leq P_{w+c}L \leq 0.01$ bar m.

	b_1	b_2	b_3	b_4	b_5
a_1	-0.015282	0.16798	-0.65142	0.99094	0.89121
a_2	0.0030685	-0.033837	0.13237	-0.20884	-0.11625
a_3	-0.0011482	0.01246	-0.047226	0.066122	0.11322
a_4	-0.00015358	0.0016951	-0.0066839	0.010972	0.0021576
a_5	$-2.0618e-005$	0.00021657	-0.00079996	0.0011132	0.0020393
a_6	0.00011577	-0.0012686	0.0048561	-0.0069105	-0.010616

Table 4.7: Coefficients of the new correlation for the calculation of total emissivity under oxy-fired condition for 0.01 bar m $\leq P_{w+c}L \leq 0.5$ bar m.

	b_1	b_2	b_3	b_4	b_5
a_1	-0.049421	0.53038	-2.0435	3.5205	1.1072
a_2	0.0086047	-0.094673	0.37513	-0.67482	-0.092097
a_3	-0.0072315	0.072959	-0.26094	0.40169	0.25102
a_4	-0.00033794	0.0039128	-0.016384	0.031912	-0.0041642
a_5	-0.00019445	0.0019716	-0.0071378	0.0114	0.0053602
a_6	0.00073246	-0.0073525	0.026039	-0.039143	-0.025775

Table 4.8: Coefficients of the new correlation for the calculation of total emissivity under oxy-fired condition for 0.5 bar m $\leq P_{w+c}L \leq 10$ bar m.

	b_1	b_2	b_3	b_4	b_5
a_1	0.045068	-0.46171	1.7339	-3.0187	1.6547
a_2	-0.015736	0.1604	-0.59326	0.99421	-0.19373
a_3	0.013191	-0.13512	0.49832	-0.81572	0.52082
a_4	0.0012206	-0.012392	0.045363	-0.074097	-0.0002397
a_5	$3.7967e-005$	-0.00056815	0.0031857	-0.0086675	0.012006
a_6	-0.0019818	0.020245	-0.074369	0.12101	-0.060572

5 The Banded Approach for non gray modeling of radiative heat transfer in inhomogeneous H_2O–CO_2 mixtures

This chapter describes a new approach towards the non gray radiative heat transfer modeling of H_2O–CO_2 mixtures. The new approach is based on dividing the wavenumber spectrum into some limited wavenumber intervals in which the spectral radiative properties are averaged and the RTE is solved. In each interval, the transmissivity of the mixture is obtained using the SNBM (Soufiani and Taine, 1997). Using the transmissivity of each narrow band interval, the values of the spectral absorption coefficient have been calculated by means of the Beer's law. For obtaining the correlation of the local absorption coefficient for each wavenumber interval in oxy-fired combustion systems, the local absorption coefficient database is obtained for the ranges of effective parameters, that is Pr, T, and $\mathrm{P_{w+c}L}$, by using the SNBM. The least-squares method for the multivariate regression of the local absorption coefficient database has been used to establish suitable correlations for the absorption coefficients in each of the wavenumber intervals. The ranges of the effective parameters are selected according to the industrial needs of oxy-fired combustion scenario for a wide range of industrial applications.

The new approach for non gray modeling is validated by applying it to some benchmarks of oxy- and air-fired combustion scenarios. By the spectral analysis of the wavenumber spectrum and the results of benchmarks analyses, the suitable number of wavenumber intervals and their limits are obtained. For obtaining results of oxy-/air-fired benchmarks of homogeneous H_2O–CO_2 mixtures, the values of the absorption coefficient have been implemented by the Fluent discrete ordinate method (DOM) through the user defined function (UDF). The three order polynomial is used to interpret the changes of the band absorption coefficient with temperature in a fixed gas composition and path length of the benchmarks.

The results of using the new non gray approach in modeling the benchmarks have been compared with those of other methods and the exact solutions reported for the benchmarks. The correlations of the local absorption coefficient provide faster and simpler calculations than the conventional SNBM with the almost same level of accuracy. The presented correlations can be easily implemented in any CFD code for non gray radiative heat transfer modeling.

5.1 Banded Approach

To support the non gray radiative heat transfer modeling in combustion products, the SNBM (Soufiani and Taine, 1997) has been used to calculate the transmissivity of each narrow band. The values of the spectral absorption coefficient of each narrow band have been calculated by means of the Beer's law. The SNBM with a narrow band resolution of $25\ \mathrm{cm^{-1}}$ has been implemented to calculate the local absorption coefficient in a certain number of wavenumber intervals – the so-called "band absorption coefficient". The

properties of the narrow bands in each wavenumber interval were integrated to gain the band absorption coefficient. The band absorption coefficient corresponding to each interval is obtained by the integration of the absorption coefficient narrow bands over the wavenumber interval as (Modest, 2003b)

$$\mathrm{K}_{\eta_1-\eta_2} = \frac{\int_{\eta_1}^{\eta_2} \mathrm{I}_{\mathrm{b}\eta}\mathrm{K}_{\eta}\mathrm{d}\eta}{\int_{\eta_1}^{\eta_2} \mathrm{I}_{\mathrm{b}\eta}\mathrm{d}\eta}, \tag{5.1}$$

where $\mathrm{I}_{\mathrm{b}\eta}$ is the spectral blackbody intensity (Planck function) and K_{η} is the spectral absorption coefficient calculated by the SNBM.

The spectral absorption coefficient for the mixture is calculated as (Denison and Webb, 1995; Runstedtler and Hollands, 2008; Ströhle, 2008)

$$\mathrm{K}_{\eta(\mathrm{H_2O-CO_2})} = \mathrm{K}_{\eta(\mathrm{H_2O})} + \mathrm{K}_{\eta(\mathrm{CO_2})}, \tag{5.2}$$

where $\mathrm{K}_{\eta(\mathrm{H_2O})}$ and $\mathrm{K}_{\eta(\mathrm{CO_2})}$ are the spectral absorption coefficients of the individual gas components, respectively.

Eleven absorption bands of H_2O and CO_2 are considered: 1 rotational band and 10 vibrational bands. In these bands, carbon dioxide and water vapor absorb and emit radiation. These bands consist of $667\ \mathrm{cm}^{-1}$, $960\ \mathrm{cm}^{-1}$, $1060\ \mathrm{cm}^{-1}$, $2410\ \mathrm{cm}^{-1}$, $3660\ \mathrm{cm}^{-1}$, $5200\ \mathrm{cm}^{-1}$ of carbon dioxide and to the rotational band, $1600\ \mathrm{cm}^{-1}$, $3760\ \mathrm{cm}^{-1}$, $5350\ \mathrm{cm}^{-1}$, and $7250\ \mathrm{cm}^{-1}$ of water vapor.

Based on the knowledge of the spectral analysis, the part of wavenumber spectrum in which the radiative heat transfer occurs has been divided into a number of wavenumber intervals. The division has been done in such a way that each of the intervals includes some parts of the above mentioned eleven absorption bands of H_2O and CO_2 and the entire radiative heat transfer spectrum, that is the region from ultraviolet to mid-infrared, is fully covered by a certain number of wavenumber intervals.

To find the optimal division form, the non uniform division of the wavenumber spectrum with various numbers of wavenumber intervals has been considered in this research. The non uniform dividing has been done in such a way that each "non uniform" interval includes at least parts of the above mentioned absorption bands of H_2O and CO_2. On the other hand, by using the term "uniform" intervals, the division of the entire spectrum (i.e., $0 - 9300\ \mathrm{cm}^{-1}$) to a number of equal wavenumber intervals is supposed. The discussion concerning the uniform division of the spectrum will follow after the presentation of the two benchmarks.

For the gray modeling, the solution of the RTE is obtained once for entire radiative spectrum by using the pre-calculated mean absorption coefficient (see Eq. 2.5). Nevertheless, for the non gray modeling, by using the pre-calculated band absorption coefficients, the RTE must be solved for each of these intervals of non uniform division (see Eq. 2.6). The

non gray modeling is done by using the spectral absorption coefficient values through a summation of the each interval results accompanied with the blackbody fractional function (Planck distribution) as the weighted factors. The theoretical aspects of the gray and non gray interpretations used by the DOM is presented in Chapter 2.3 starting from page 29.

Figure 5.1 presents an example of how the eleven absorption bands of H_2O and CO_2 considered in this study are located and how the non uniform division is typically carried out together with the blackbody emissivity function (BBEF) representing the Planck function.

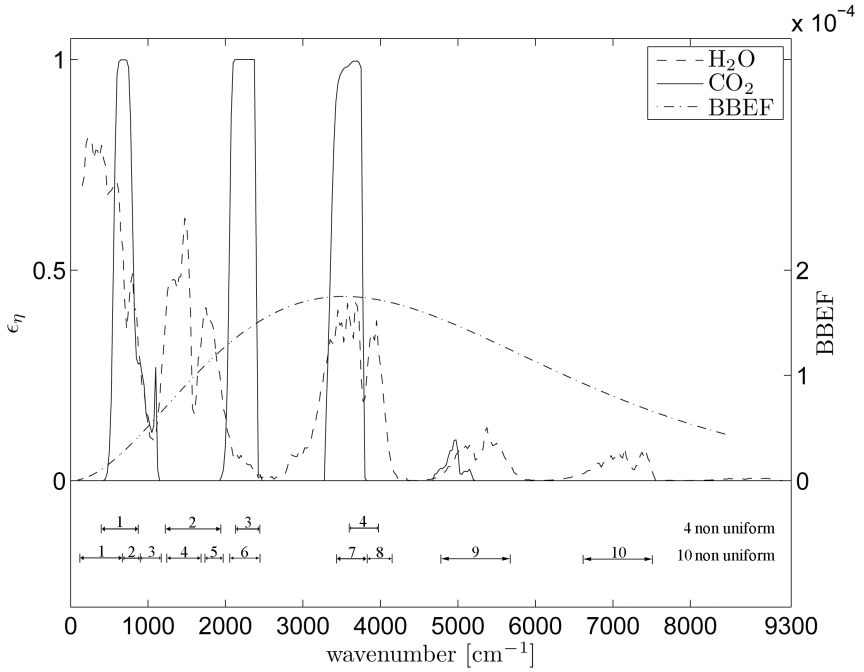

Figure 5.1: The spectral band emissivity of H_2O–CO_2 mixture calculated by the SNBM for an entire spectrum accompanied with the BBEF. The band shape is produced by the SNBM in the following conditions: molar fractions ratio $\mathrm{Pr} = 0.1176$, temperature $\mathrm{T_s} = \mathrm{T_g} = 1800$ K, and $\mathrm{P_{w+c}L} = 1.368$ bar m.

According to Stefanidis et al. (2007), the most important emission occurs in five absorption bands of H_2O and CO_2, two of which are fully overlapped, and by losing little accuracy, one can ignore the effect of the other bands. The considered bands in the study of Stefanidis et al. (2007) were for CO_2 667 $\mathrm{cm^{-1}}$, 2410 $\mathrm{cm^{-1}}$, and 3660 $\mathrm{cm^{-1}}$ and for H_2O 1600 $\mathrm{cm^{-1}}$ and 3760 $\mathrm{cm^{-1}}$. For producing the non gray radiative heat transfer modeling, Stefanidis et al. (2007) considered four non uniform wavenumber intervals to support the effect of these five absorption bands as shown in Figure 5.1. However, to avoid losing

accuracy, in the present work, all the absorption bands of H_2O and CO_2 are taken into account and these bands are located in ten non uniform wavenumber intervals. Ignoring some bands in radiative heat transfer calculations may cause a significant underestimation of the absorptivity, especially at high values of effective parameters, that is Pr, T, and L.

The benchmarks analyses were aimed to validate the suggested banded approach idea. With oxy-/air-fired benchmarks the appropriate number of wavenumber intervals can be obtained. Moreover, with the exact solutions of radiative heat transfer, the accuracy of the banded approach can be addressed. Further comparison shows the advantage of the suggested banded approach compared with the widely used WSGGM in its gray and non gray configuration. By analyzing the spectra of absorptivity/emissivity in averaged properties of the computational domain, a number of spectral wavenumber intervals along with their limits are carefully selected for the non uniform division of spectrum. Benchmark analysis has been done to present a suitable solution for the non gray modeling by the proposed banded approach using the non uniform spectral division.

5.2 Verification of the Banded Approach by benchmark analyses

In order to validate the proposed banded approach and also to obtain the optimal solution for dividing the radiative heat transfer spectrum, the spectral properties obtained by the SNBM have been used in the simulation of two radiative heat transfer benchmarks of 3D rectangular enclosure. The solution of the first benchmark has been reported by Liu (1999) and the second one by Porter et al. (2010) representing the air-fired and oxy-fired combustion scenario, respectively. The exact solution of these benchmarks has been obtained by using the ray tracing approach for solving the RTE together with the SNBM for calculating the gas radiative properties. The difference of these two benchmarks is in the gas composition of the participating media which fills up the same geometry with the same thermal conditions. The air-fired benchmark represents a solution of radiative heat transfer in a homogeneous gas mixture of 20% H_2O, 10% CO_2, and 70% N_2 on a molar basis. The oxy-fired benchmark is fulfilled with a homogeneous gas mixture of 10% H_2O, 85% CO_2, and 5% N_2 on a molar basis. Both benchmarks have been solved using the same mesh structure. The geometry details of the two benchmarks as well as the description of the previously reported solution is presented in Chapter 3.2.2 starting from page 64 for the air-fired scenario and in Chapter 4.5.5 starting from page 83 for the oxy-fired scenario.

5.2.1 3D benchmark of homogeneous H_2O–CO_2 mixture for air-fired combustion

DOM has been used as the RTE solver for gray and non gray radiative heat transfer modeling of the benchmarks. Different radiative property models including the non gray banded approach and the standard WSGGM have been implemented by DOM. The radiative heat fluxes on the center line of a side wall of the enclosure (2 m, 1 m, z) of this benchmark (see Chapter 3.2.2) calculated by using the non gray banded approach with different num-

ber of non uniform spectral intervals and the WSGGM by Smith et al. (1982) in its gray implementation are compared in Figure 5.2. The calculations were performed using one of the highest angular discretizations of the DOM, that is S_8, to damp the effect of inaccuracy in DOM calculation.

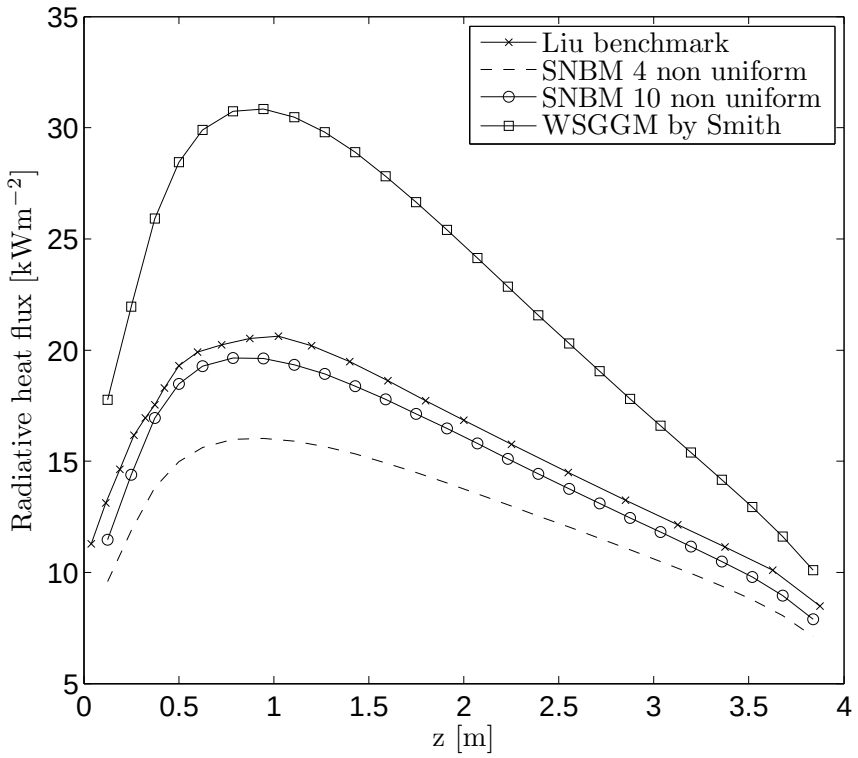

Figure 5.2: Distribution of radiative heat flux along a wall (2 m, 1 m, z) for a $\mathrm{H_2O}$–$\mathrm{CO_2}$ mixture of $\mathrm{Pr} = 2$ at the temperature range of $300\ \mathrm{K} \leq \mathrm{T} \leq 1800\ \mathrm{K}$ and pressure path length product $\mathrm{P_{w+c}L} = 0.432$ bar m. The predicted values by DOM using S_8 angular discretization together with the banded approach using the non uniform interval divisions; a benchmark solution presented by Liu (1999).

Figure 5.2 confirms that the relative average differences between the benchmark solution and the predicted radiative heat flux of the presented banded approaches of four and ten non uniform wavenumber intervals equal to 19.5% and 5.7%, respectively. Both the non uniform divisions with different numbers of intervals give relatively accurate values of radiative heat flux as opposed to the original WSGGM the average relative error of which is 40%. The level of difference between the two banded solutions of non uniform intervals, introduced in Figure 5.1, is significant. The CPU time of the original WSGGM in its gray form equals to 0.29 s and the computational power facilities have been described

previously. Theoretically, the CPU time of the radiative heat transfer calculation using DOM with the banded approach is proportional to the number of intervals because the RTE must be solved for each interval. Therefore, if all the mathematical functions used in the correlations of gray and non gray approaches would be the same, the CPU time of non gray banded approach using ten non uniform intervals is expected to be ten times greater than CPU time of the gray calculations. However, due to some differences between the form of correlations used in the gray and non gray modeling the measured value of non gray modeling show faster calculations as was expected. The CPU time for four non uniform intervals with five clear windows and ten non uniform wavenumber intervals (clear windows excluded) are 1.16 s and 1.45 s, respectively. Generally, one can say that, with the current available computational resources, these methods are quite fast and computationally efficient be used in modeling of large scale combustion systems.

5.2.2 3D benchmark of homogeneous H_2O–CO_2 mixture for oxy-fired combustion

DOM has been used as the RTE solver for gray and non gray radiative heat transfer modeling of the benchmarks. Different radiative property models including the non gray banded approach and standard WSGGM have been implemented by DOM. In this benchmark, the gas composition is a homogeneous gas mixture of 10% H_2O, 85% CO_2, and 5% N_2 at non uniform temperature distribution, similarly to the air-fired benchmark. The radiative heat fluxes on the center line of a side wall of the enclosure (0 m, 1 m, z) of the oxy-fired benchmark (see Chapter 4.5.5), calculated by using the non gray banded approach with a different number of non uniform intervals and the WSGGM by Smith et al. (1982) in its gray modeling are compared in Figure 5.3. The calculations were performed using the S_8 angular discretization of DOM, to damp the effect of inaccuracy in the DOM calculation.

Figure 5.3 confirms that the presented banded approach with the ten non uniform intervals of the entire spectrum provides accurate results in oxy-fired combustion with the average relative error of 8.3%. The solution presented by four non uniform intervals predicts the radiative heat flux different from the benchmark solution with the average relative error of 23.4%. However, the solution of the WSGGM in its gray implementation produces a profile that is closer to the exact benchmark data than the four non uniform intervals at certain parameters of Figure 5.3 with the average relative error of 10.9%.

The original WSGGM (Smith et al., 1982) was develop based on the emissivity charts of the partial pressures defined by air-fired combustion scenario with two specified gas compositions ($\mathrm{Pr} = 1$ and $\mathrm{Pr} = 2$). For other Pr's, the interpolation and/or extrapolation are applied to obtain the model coefficients for the specified gas mixture. Generally, the concentration of CO_2 for oxy-fired combustion is presented by very high concentrations, and for benchmark presented by Porter et al. (2010), the partial pressures ratio is presented by a smaller value of Pr ($\mathrm{Pr} = 0.1176$). The original WSGGM simply cannot support such high concentrations of CO_2 since they are far from the valid range of Smith's parameters. Porter et al. (2010) reports that the predictions of the source term of the oxy-fired benchmark for using WSGGM could lead to large errors in the modeling of the flame and

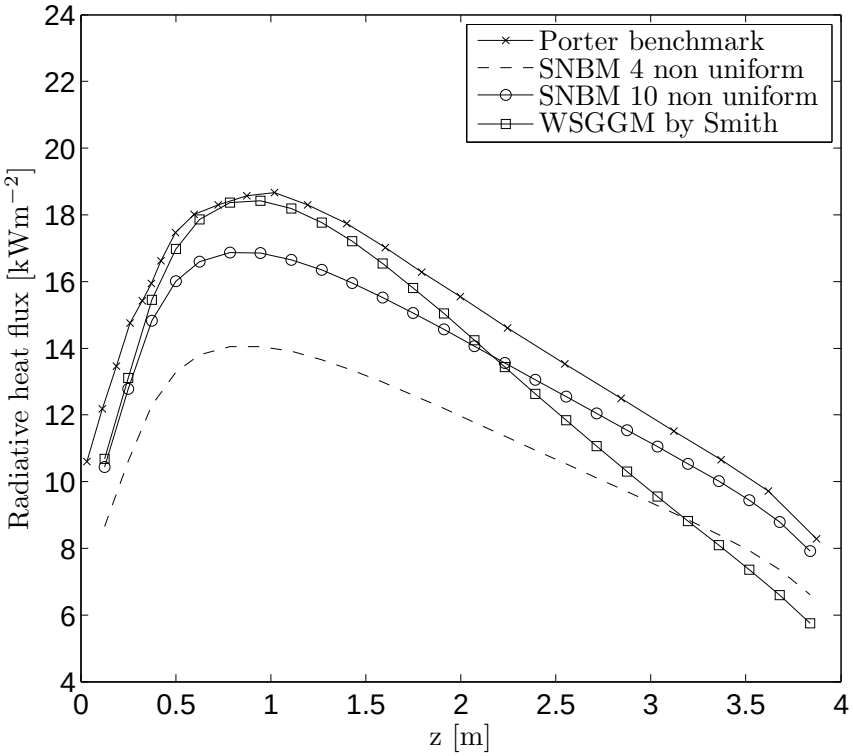

Figure 5.3: Distribution of radiative heat flux along a wall (0 m, 1 m, z) for a H_2O–CO_2 mixture of $\mathrm{Pr} = 0.1176$ at the temperature range of $300\ \mathrm{K} \leq \mathrm{T} \leq 1800$ K and pressure path length product $\mathrm{P_{w+c}L} = 1.368$ bar m. The predicted values by DOM using S_8 angular discretization together with the banded approach using the non uniform interval divisions; a benchmark solution presented by Porter et al. (2010).

surrounding temperature. Figure 5.3 shows that the results of gray modeling for oxy-fired benchmark with WSGGM happen to be accurate. These accurate results are obtained because of the errors from the emissivity database which was suited for air-fired combustion of the original WSGGM are compensated by an opposite sign error of ignoring the gas radiative spectral features in gray modeling.

Using the standard WSGGM with the air-fired coefficients for the calculation of the radiative properties of oxy-fired combustion produces underpredicted results of the absorption coefficient. Porter et al. (2010) reported that the original WSGGM in gray form has an ability of correct predictions for the heat fluxes along the walls at high temperature regions due to contributing factors of the model to the underprediction tendency. At low temperature regions, when the heat source is far from the walls, the incorrect prediction of the absorptive properties leads to significant differences.

The width of the absorption bands is varying with effective parameters, and since one of the aims of this work is to obtain correlations for the ranges of Pr, T, and L, the limitations of effective absorption bands are quite variable in the analysis. Thus, by selecting fixed starting and ending limits for the non uniform wavenumber intervals, the effect of some of absorption lines is missed in the calculations resulting in a slightly lower accuracy. This dependence of the limits on the effective parameters causes uncertainties in the selection of the non uniform bands. The benchmarks analyses show that the solution of ten non uniform divisions is accurate enough for radiative property predictions. In addition, this approach also improves the suggested solution in the previously published work by Stefanidis et al. (2007) in which a simplified non uniform division of four intervals and five transparent windows was used. It should be noticed that in their work, the effect of only five absorption bands of H_2O and CO_2 was taken into account, and they solved their case study using a fixed path length and gas composition. As shown in Figures 5.2 and 5.3, the ten non uniform intervals division shows good agreement with the exact solution of the benchmark. The four non uniform intervals division with five clear windows originally presented by Stefanidis et al. (2007) provides more variety between the results at the specified conditions, different from those which were presented in their work.

Theoretically, the uniform division of the entire radiative spectrum can be used, and it should provide a slightly lower level of accuracy compared to the non uniform division due to the coarse averaging of the radiative properties of the spectrum. However, the uniform division should provide more accurate results compared with the gray models. For example, when selecting a number of uniform wavenumber intervals which cover the entire radiative transfer spectrum, the effect of all the absorption lines in the desired ranges of effective parameters, that is Pr, T, and L, are safely taken into account. Because of certain errors of the DOM and opposite errors from uniform divisions provide results far from the exact solutions of two benchmarks. The errors of DOM and uniform divisions are "summed up" presenting higher discrepancy with the exact solution of radiative heat flux calculation. The results presented by four uniform intervals and ten uniform intervals are situated out of range of Figures 5.2 and 5.3; and not presented here.

Considering the results presented in the two benchmarks (see Figures 5.2 and 5.3), the ten non uniform wavenumber intervals which take into account all the eleven absorption bands have been selected to produce correlations for the spectral absorption coefficient. This division form with fixed limits provides an optimal solution for the spectral intervals meeting the theoretical issues and producing accurate enough calculations of non gray modeling. The results obtained by ten non uniform intervals support the changes of the absorption band spectral widths within the selected ranges of effective parameters because the selected limits have been obtained at the highest spectral widths of the absorption bands. Moreover, the analysis of the benchmarks shows that the using of the ten non uniform intervals in the presented banded approach results in a good level of agreement between the predicted radiative heat fluxes and the exact solution both in the air- and oxy-fired scenarios.

5.3 Analysis of angular discretization of DOM for being used with Banded Approach

Two non gray benchmarks presented by Liu (1999) and Porter et al. (2010) have been used to find the optimal angular discretization of DOM when it is used with the banded approach for non gray radiative heat transfer modeling. For the details of the two benchmark solutions of air-fired and oxy-fired combustion conditions, see Chapters 3.2.2 and 4.5.5 starting from pages 64 and 83, respectively.

The sensitivity of the predicted results to the different schemes of angular discretization is reported in Figure 5.4. The figure shows the radiative heat fluxes along the middle line of the side walls of the benchmark geometry obtained by using the DOM together with ten non uniform intervals division. The benchmark profiles are compared with the different solutions presented by the banded approach of ten non uniform intervals computed with the discretizations S_2, S_4, S_6, and S_8. These discretization schemes represent 4, 16, 36, and 64 directions per octant, respectively.

The figure confirms that the results for two benchmarks are in good agreement with the discretizations higher than or equal to S_4. The average relative errors in the radiative heat flux calculated by the S_4 discretization are 6% for the air-fired benchmark and 8.6% for the oxy-fired benchmark. For the S_6 and S_8 discretization schemes, the difference between both benchmark solutions and the obtained results reduced insignificantly. Thus, the solution presented by the discretization scheme S_4 is accurate enough in the calculation of the radiative heat transfer. This level of discretization can be considered as the optimal solution between the different schemes at the given gas compositions and effective parameters. Comparison of the WSGGM by Smith et al. (1982) in its non gray form shows that the WSGGM slightly underpredicts the radiative heat fluxes. The difference of the relative average errors between the results presented by the WSGGM in its non gray implementation and the suggested banded approach of ten non uniform intervals is not significant. However, Figure 5.4a shows that the non gray form of the WSGGM produces slightly higher inaccuracies compared to the presented banded approach of the modeling in high temperature regions. The data of the non gray WSGGM have been reproduced from Coelho (2002) for the discretization scheme S_4.

5.4 Band absorption coefficient database and curve fitting process

It is significantly necessary for the accurate and fast models of non gray modeling to include the effects of the spectral radiative features of gases in overall heat transfer calculations. Based on the results provided by the SNBM (Soufiani and Taine, 1997), by means of multivariate regression, some correlations can be obtained for band absorption coefficient of $\mathrm{H_2O}$–$\mathrm{CO_2}$ mixture in oxy-fired combustion condition.

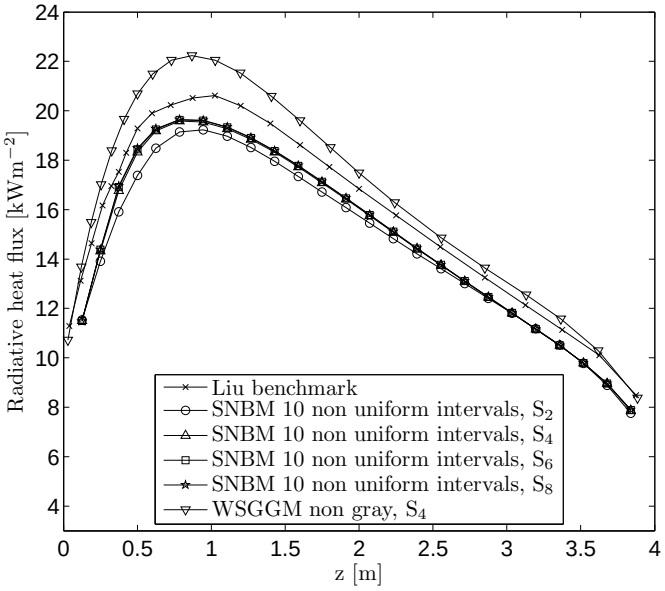

(a) H_2O–CO_2 mixture of $\mathrm{Pr} = 2$, at the temperature range of 300 K $\leq$ T $\leq$ 1800 K and pressure path length product $P_{w+c}L = 0.432$ bar m.

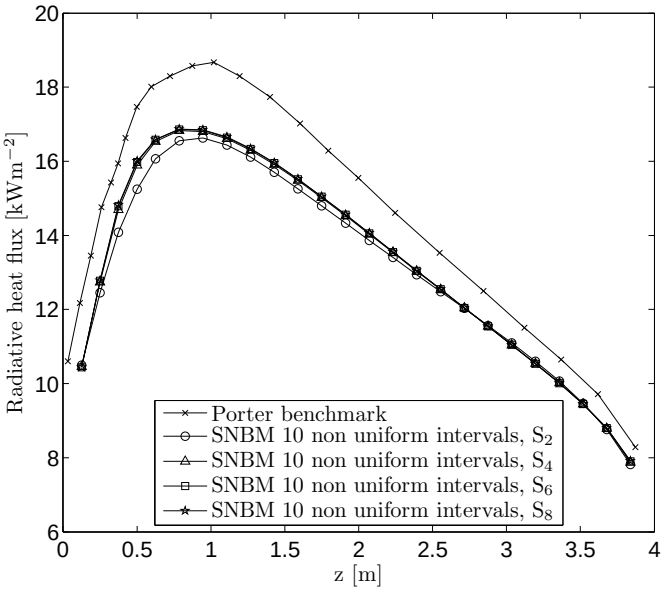

(b) H_2O–CO_2 mixture of $\mathrm{Pr} = 0.1176$, at the temperature range of 300 K $\leq$ T $\leq$ 1800 K and pressure path length product $P_{w+c}L = 1.368$ bar m.

Figure 5.4: A comparison of radiative heat fluxes calculated by DOM using the banded approach with ten non uniform wavenumber intervals and different angular discretization schemes of DOM with benchmark solutions by Liu (1999) and by Porter et al. (2010); the non gray solution presented by the WSGGM reproduced from Coelho (2002).

To obtain the SNBM based databases for band absorption coefficients, the ranges of gas composition, pressure, path length, and temperature are selected according to the industrial combustion requirements. New correlations which are based on the SNBM can be used to calculate the local absorption coefficient of the wavenumber intervals in a faster and simpler manner than using the original formulation of the SNBM with an adequate accuracy reduction. Moreover, the obtained correlations should provide competitive accuracy and computational performance compared to other non gray methods.

By using the SNBM (Soufiani and Taine, 1997), the database of the band absorption coefficient with the effective parameters corresponding to oxy-fired combustion conditions has been generated for each of the ten non uniform wavenumber intervals, and they shown in Figure 5.5. Three effective parameters – Pr, T, and $\mathrm{P_{w+c}L}$ – are used to calculate the band absorption coefficient, similarly to correlation of the total emissivity in Chapter 4.5.1 on page 78. In the same way as the total emissivity (see Chapter 4.5.2 on page 78), for the band absorption coefficient, the $\mathrm{P_{w+c}L}$ range has been regrouped into three smaller ranges. However, to extend capability of new correlations for non gray radiative heat transfer of the large scale industrial oxy-combustion systems, an additional fourth $\mathrm{P_{w+c}L}$ range has been considered, i.e., from 10 bar m to 60 bar m. The considered ranges for Pr, T, and $\mathrm{P_{w+c}L}$ with the related steps in each of the ranges have been done in the same way as with the total emissivity which was reported previously. By using SNBM, for the different values of three effective parameters, the transmissivity values have been calculated individually for each interval to estimate the band absorption coefficients and the obtained results were collected into a band database.

By analyzing Figure 5.5, the following correlations have been chosen for the band absorption coefficient as a function of three effective parameters supporting the range of oxy-fired combustion scenario

$$\epsilon = \mathrm{a_1} + \mathrm{a_2}\ln(\mathrm{T}) + \mathrm{a_3}\ln(\mathrm{P_{w+c}L}) + \mathrm{a_4}[\ln(\mathrm{T})]^2 + \mathrm{a_5}[\ln(\mathrm{P_{w+c}L})]^2 + \mathrm{a_6}\ln(\mathrm{T})\ln(\mathrm{P_{w+c}L}), \tag{5.3}$$

$$\mathrm{a}_i(\mathrm{Pr}) = \mathrm{b}_{1,i}(\mathrm{Pr})^4 + \mathrm{b}_{2,i}(\mathrm{Pr})^3 + \mathrm{b}_{3,i}(\mathrm{Pr})^2 + \mathrm{b}_{4,i}\mathrm{Pr} + \mathrm{b}_{5,i}, \tag{5.4}$$

where i is the number of a coefficients ($i = 1, 2, 3...6$).

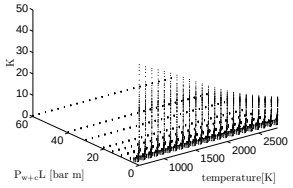

(a) Interval 1: 150–600 cm^{-1}

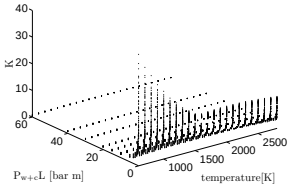

(b) Interval 2: 600–775 cm^{-1}

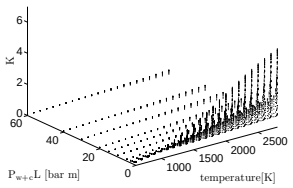

(c) Interval 3: 775–1125 cm^{-1}

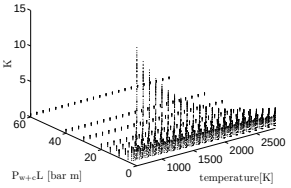

(d) Interval 4: 1275–1625 cm^{-1}

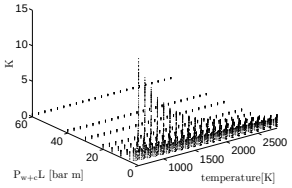

(e) Interval 5: 1675–1900 cm^{-1}

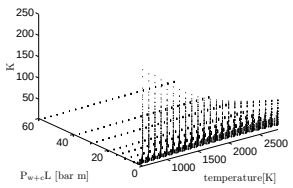

(f) Interval 6: 2125–2400 cm^{-1}

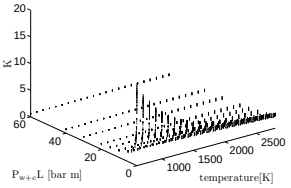

(g) Interval 7: 3475–3800 cm^{-1}

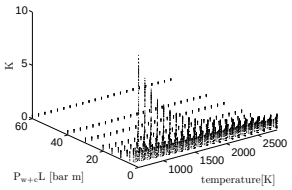

(h) Interval 8: 3800–4075 cm^{-1}

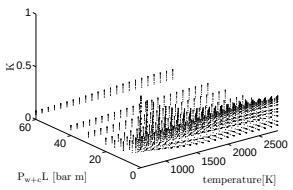

(i) Interval 9: 4780–5650 cm^{-1}

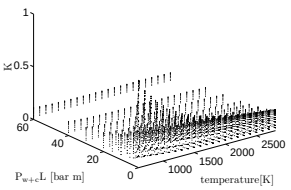

(j) Interval 10: 6825–7475 cm^{-1}

Figure 5.5: The profiles of the band absorption coefficient (K) obtained by the SNBM of the following ranges: $0.125 \leq \mathrm{Pr} \leq 4$, 600 K $\leq \mathrm{T} \leq 2800$ K, and 0.001 bar m $\leq \mathrm{P_{w+c}L} \leq 60$ bar m.

Again, the general logarithmic correlation (Eq. 5.3) has been used for correlating the unique database of the band absorption coefficient of oxy-fired combustion scenario. The curve fitting process has been obtained through the multivariate regression to obtain the coefficients of the logarithmic correlation. The two developing steps of the fitting process

to correlate the total emissivity (see Chapter 4.5.2 on page 78) have been repeated and applied to each of ten intervals. In the first step, the values of the coefficients (a_i) have been obtained by minimizing the deviation of the correlated band absorption coefficients of the original band absorption coefficient databases for each Pr. In the second step, the coefficients b_j have been obtained by minimizing the values of a_i, produced by Eq. 5.4, and those given in the first step by Eq. 5.3. Similarly to the total emissivity correlation in Chapter 4.5.2 on page 78, the effect of Pr has been considered in the overall calculation of the absorption coefficient by substituting Eq. 5.3 with Eq. 5.4. Therefore, the new correlations can easily support inhomogeneous media by the changes in the gas compositions of the $\mathrm{H_2O}$–$\mathrm{CO_2}$ mixtures.

5.5 New correlation for band absorption coefficient

Based on the benchmark analyses and spectral analysis of how the absorption bands of $\mathrm{H_2O}$ and $\mathrm{CO_2}$ are located in the wavenumber spectrum, the spectrum is divided into ten non uniform intervals as in Figure 5.1 with certain band width limits. For presenting useful scientific contribution which can be used for the non gray radiative heat transfer modeling of oxy-fired combustion scenario, the coefficients of Eq. 5.4 were obtained to calculate the band absorption coefficient in the ten non uniform wavenumber intervals.

By carrying out two developing steps of the fitting process for the new correlation (see Chapter 4.5.2 on page 78), the coefficients have been iteratively obtained for band absorption coefficient in ten non uniform wavenumber intervals. The $\mathrm{P_{w+c}L}$ range was divided into four ranges for better accuracy. The coefficients of Eq. 5.4 of the band absorption coefficient are given in Tables 5.1–5.4 for ten non uniform intervals.

The results obtained with the new correlation (Eq. 5.4) and those obtained with the SNBM agree reasonably well for band absorption coefficient calculations for all four ranges of path length: optically thin, moderate optical thickness, thick, and intensely thick optical thickness. Figure 5.6 shows that the deviation in the differences for ten intervals of band absorption coefficient calculation is less than $\pm 5\%$. The difference of the last two non uniform intervals ($4750 - 5650$ and $6825 - 7475\ \mathrm{cm^{-1}}$) does not affect the overall accuracy of radiation calculation very strongly because of the absence of the most important bands of $\mathrm{H_2O} - \mathrm{CO_2}$ mixture, as shown in Figure 5.1. Moreover, as it can be seen in Figure 5.1, the Planck function is quite small at the end of the wavenumber spectrum, and therefore, the effect of the last two intervals is not significant in the overall results.

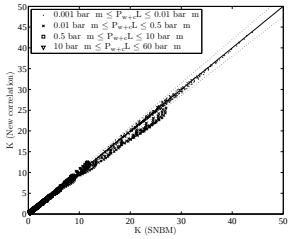

(a) Interval 1: 150–600 cm^{-1}

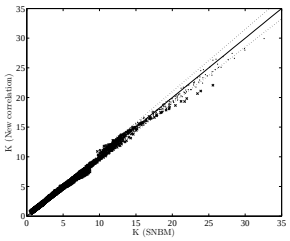

(b) Interval 2: 600–775 cm^{-1}

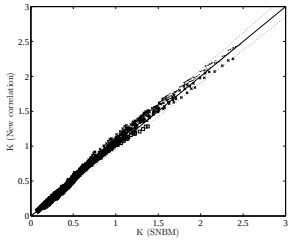

(c) Interval 3: 775–1125 cm^{-1}

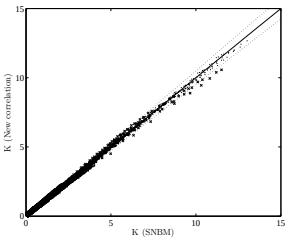

(d) Interval 4: 1275–1625 cm^{-1}

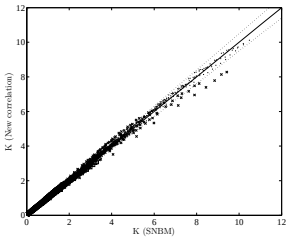

(e) Interval 5: 1675–1900 cm^{-1}

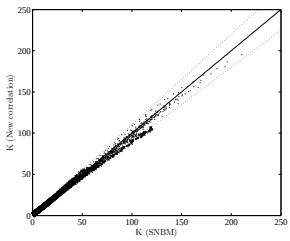

(f) Interval 6: 2125–2400 cm^{-1}

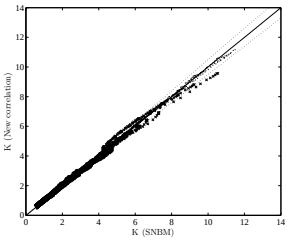

(g) Interval 7: 3475–3800 cm^{-1}

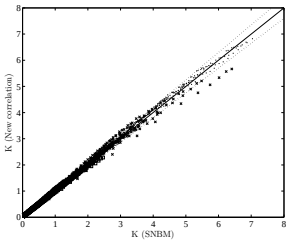

(h) Interval 8: 3800–4075 cm^{-1}

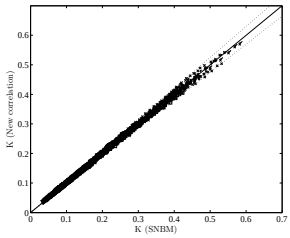

(i) Interval 9: 4780–5650 cm^{-1}

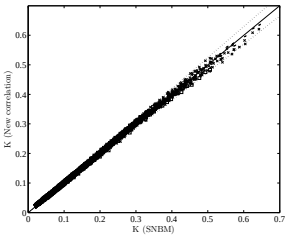

(j) Interval 10: 6825–7475 cm^{-1}

Figure 5.6: The deviation plot of comparing the band absorption coefficients for ten non uniform intervals predicted by the SNBM as a benchmark and the new correlation (Eq. 5.4) with coefficients listed in Tables 5.1–5.4. The range of the molar fractions ratio $0.125 \leq \mathrm{Pr} \leq 4$, temperature range $800\ \mathrm{K} \leq \mathrm{T_g} \leq 1800\ \mathrm{K}$, and $0.001\ \mathrm{bar\ m} \leq \mathrm{P_{w+c}L} \leq 60\ \mathrm{bar\ m}$.

5.6 Application of Banded Approach to oxy-/air-fired combustion benchmarks

The banded approach together with DOM has been applied to two previously described benchmarks. The benchmarks, one represented by the air-fired combustion and the second one by the oxy-fired combustion of H_2O–CO_2 mixture, have been used in the present chapter. The details of the two benchmarks are presented in Chapters 3.2.2 and 4.5.5 starting from pages 64 and 83, respectively. The comparison of the band property calculation is obtained using the banded approach based on the SNBM using the benchmark by Liu (1999) for the air-fired combustion and the new correlation (Eq. 5.4) with the coefficients listed in Tables 5.1–5.4 using the benchmark by Porter et al. (2010) for the oxy-fired combustion. The distribution of the radiative heat flux along the center line of the side wall for both benchmarks of H_2O–CO_2 mixtures are shown in Figure 5.7.

Figures 5.7a and 5.7b show the distribution of radiative heat fluxes along the center lines of the side walls. Comparison of the WSGGM by Smith et al. (1982) in its gray implementation shows that model significantly underpredicts the radiative heat fluxes with exact benchmark values. For the air-fired and oxy-fired benchmarks, the differences of radiative flux predictions by the WSGGM are equaled to 40% and 11.1%, respectively.

By analyzing the results, one can conclude that the proposed banded approach with the coefficients reported in Tables $5.1-5.4$ provides a good level of agreement with the exact benchmark solutions. The results obtained by the banded approach for the first and the new correlation for the second benchmarks include average relative errors of 5.7% and 5.5%, respectively.

5.7 Summary

The SNBM (Soufiani and Taine, 1997) has been used to present some useful results for the non gray radiative heat transfer modeling. The developments are presented by the calculation of the band absorption coefficient of the limited wavenumber intervals. The band absorption coefficient of each interval is obtained by the integration of absorption lines over specified intervals.

The new approach for non gray modeling is based on dividing the entire radiative spectrum into a certain number of wavenumber intervals with corresponding wavenumber limits. For the oxy-fired combustion systems, the values of the band absorption coefficient, calculated by the SNBM, have been correlated for each of the wavenumber intervals including the effect of three effective parameters. By comparing the obtained results of the new approach with previously published benchmark solutions by Liu (1999) and by Porter et al. (2010), the usage of a different number of non uniform spectral intervals in the proposed approach has been analyzed.

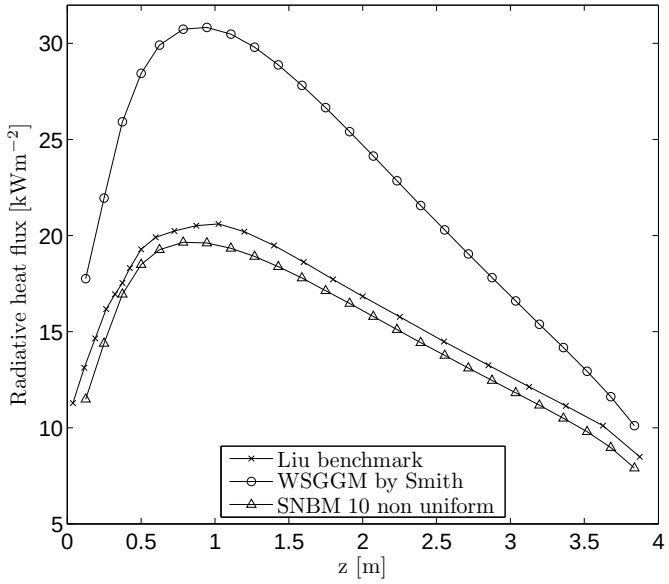

(a) H_2O–CO_2 mixture of $\mathrm{Pr} = 2$, at the temperature range of 300 K $\leq$ T $\leq$ 1800 K and pressure path length product $P_{w+c}L = 0.432$ bar m.

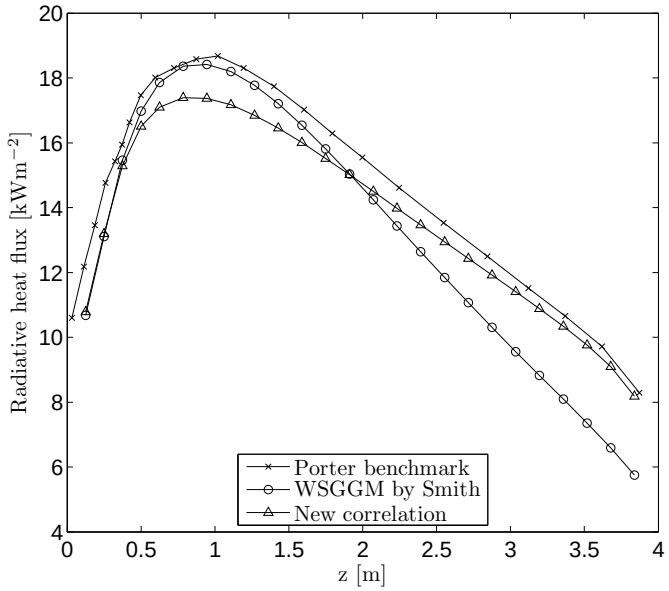

(b) H_2O–CO_2 mixture of $\mathrm{Pr} = 0.1176$, at the temperature range of 300 K $\leq$ T $\leq$ 1800 K and pressure path length product $P_{w+c}L = 1.368$ bar m.

Figure 5.7: Comparison of the radiative heat fluxes calculated by DOM using the banded approach and the new correlation with ten non uniform wavenumber intervals at S_4 discretization scheme of DOM with the benchmarks by Liu (1999) for air-fired and by Porter et al. (2010) for oxy-fired combustion; the new correlation (Eq. 5.4) with the coefficients of the banded approach (Tables 5.1–5.4).

Based on the analyses of two benchmarks for H_2O–CO_2 mixtures under air- and oxy-fired combustion and the previously published results by Stefanidis et al. (2007), the suitable form and number of spectrum division has been set as ten non uniform intervals. This form of the division of the entire radiative spectrum meets the theoretical aspects of the quantitative spectroscopy as well as the engineering requirements for accurate and fast CFD calculations.

Furthermore, the SNBM has been used to generate a database of band absorption coefficients of H_2O–CO_2 mixtures for a range of effective parameters of Pr, T, and $\mathrm{P_{w+c}L}$ in ten non uniform wavenumber intervals, supporting the oxy-fired combustion. Based on the absorption coefficient profiles as a function of T and $\mathrm{P_{w+c}L}$ at certain Pr, the general logarithmic form of Eq. 5.3 is used. By means of the least-squares method for multivariate regression, the coefficients of the new correlation (Eq. 5.4) have been derived for band properties, and listed in Tables 5.1–5.4.

The new correlation of the banded properties with the coefficients presented in Tables 5.1–5.4 provides accurate and simple calculations compared with other methods of non gray modeling. The new correlation decreases the CPU time with a tolerable reduction in the accuracy of the band absorption coefficient calculations compared with the original SNBM data.

After various comparisons it was shown that the new correlation with ten non uniform intervals is adjusted to the most suitable division of the radiative spectrum giving the best comparison with the results from more refined calculations. To improve the accuracy of the presented correlations, the representation is divided into four pressure path length ranges, each involving 300 optimized fitting parameters. With modern computers the number of parameters is not important; it is the computational time and accuracy that matters. However, the order of CPU times required for the non gray modeling using the obtained correlations is quite acceptable with the current available computational resources as reported in Chapter 5.2.1 in more details.

The new correlation (Eq. 5.4 with the coefficients reported in Tables 5.1–5.4) for oxy-fired combustion can be easily implemented in non gray radiative heat transfer modeling, producing more efficient, accurate, and simple calculations. The new correlations can be simply applied in any commercial CFD packages, for example Fluent or CFX. The ready feature in Fluent software for doing the non gray modeling by dividing the spectrum into wavelength intervals facilitates the use of the presented correlations of the band absorption coefficient.

Table 5.1: Coefficients of the new correlation for band absorption coefficient of ten non uniform wavenumber intervals in oxy-fired combustion scenario for 0.001 bar m $\leq P_{w+c}L < 0.01$ bar m.

	b_1	b_2	b_3	b_4	b_5
Interval $1: 150-600$ cm^{-1}					
a_1	$7.0348813447356768e+000$	$-7.5940433322900205e+001$	$3.0957317858897159e+002$	$-6.2447062009281137e+002$	$-8.3252902210049946e+000$
a_2	$-1.7959525464958668e+000$	$1.9252518644189355e+001$	$-7.7628712053511521e+001$	$1.5387330820253857e+002$	$5.6731152095653528e+000$
a_3	$4.8769631215431225e-001$	$-5.3845656152646413e+000$	$2.2742185696466169e+001$	$-4.8539024426988107e+001$	$7.5015930579733880e-001$
a_4	$1.1424074203892845e-001$	$-1.2176209309957042e+000$	$4.8647448376582112e+000$	$-9.4991780462020454e+000$	$-5.6116273231062508e-001$
a_5	$4.4036188715427423e-003$	$-4.9083226635006735e-002$	$2.1013840751437901e-001$	$-4.5688197338900421e-001$	$1.1825571556640262e-002$
a_6	$-5.5690518317491611e-002$	$6.1298026244106929e-001$	$-2.5769172864052927e+000$	$5.4614170937836741e+000$	$-7.1526668150402650e-002$
Interval $2: 600-775$ cm^{-1}					
a_1	$9.7274433494735622e+000$	$-1.0198208373381841e+002$	$3.9438560698907116e+002$	$-7.0831919696857994e+002$	$5.2738117540569556e+002$
a_2	$-2.4270788449105445e+000$	$2.5431644223475789e+001$	$-9.8226696519933128e+001$	$1.7557154526969623e+002$	$-1.2883937263417988e+002$
a_3	$5.3866009223459063e-002$	$-4.2758259005806609e-001$	$6.2209053670432624e-001$	$3.1691437250510082e+000$	$-1.1832753857501457e+001$
a_4	$1.5049753165929511e-001$	$-1.5772861387943584e+000$	$6.0917953986385793e+000$	$-1.0851424396462074e+001$	$7.9171954397759636e+000$
a_5	$1.5690895959871753e-003$	$-1.8499243578385366e-002$	$8.4150557963007216e-002$	$-1.7943129996217350e-001$	$-2.1593228047496582e-002$
a_6	$-5.0037990825318084e-003$	$3.1009963513166386e-002$	$3.7407036758500135e-002$	$-6.8659410244942209e-001$	$1.4839154941141497e+000$
Interval $3: 775-1125$ cm^{-1}					
a_1	$-1.1296734143011435e+000$	$1.2212116084614278e+001$	$-4.9860567143893114e+001$	$1.0055059792369386e+002$	$-1.1669033118545986e+001$
a_2	$3.4433693278127991e-001$	$-3.7220981166781280e+000$	$1.5197625717207567e+001$	$-3.0664860828616057e+001$	$3.3403337297859510e+000$
a_3	$-1.2538042779962021e-003$	$1.4552681475525776e-002$	$-6.5002696506930371e-002$	$1.4435847455756667e-001$	$-1.5153052208928482e-002$
a_4	$-2.6186359867214650e-002$	$2.8306135831271095e-001$	$-1.1559674678997029e+000$	$2.3341982276236553e+000$	$-2.3048272433464476e-001$
a_5	$3.7577667869242355e-005$	$-3.7038948572366669e-004$	$1.2815206559117396e-003$	$-1.8403550057357664e-003$	$-3.3816959209818513e-004$
a_6	$2.5347099795436850e-004$	$-2.8372176996050982e-003$	$1.2082392936660911e-002$	$-2.5259068736599569e-002$	$1.6631618111865411e-003$
Interval $4: 1275-1625$ cm^{-1}					
a_1	$-1.9707182057486985e+000$	$2.0981311625047521e+001$	$-8.3840032152176533e+001$	$1.6456109137461840e+002$	$1.1910863115487894e+001$
a_2	$4.5697939973699009e-001$	$-4.8718627919489359e+000$	$1.9513301058296719e+001$	$-3.8463704121801527e+001$	$-2.7330326542680279e+000$
a_3	$1.7612719072519434e-002$	$-2.1854626300982299e-001$	$1.0794332527633264e+000$	$-2.8169488883524618e+000$	$1.7510676468370956e-001$
a_4	$-2.6718626694623104e-002$	$2.8529002306496654e-001$	$-1.1456960676547725e+000$	$2.2689919693902842e+000$	$-1.5747807899965446e-001$
a_5	$1.1957167924625329e-004$	$-1.5502240125413907e-003$	$8.0566481904887945e-003$	$-2.2227807727419991e-002$	$1.4807824546220207e-003$
a_6	$-2.0839003280680832e-003$	$2.5728571474588059e-002$	$-1.2630024512107096e-001$	$3.2726477209792187e-001$	$-2.0149188885010924e-002$
Interval $5: 1675-1900$ cm^{-1}					
a_1	$-2.3482145681705719e+000$	$2.5223232301666116e+001$	$-1.0224136469664100e+002$	$2.0544425595361540e+002$	$1.1539574574550782e+001$
a_2	$5.7149332671914721e-001$	$-6.1447516172573708e+000$	$2.4948400179097845e+001$	$-5.0272338854260241e+001$	$-2.7688554972250978e+000$
a_3	$9.3486499811694362e-003$	$-1.1827266907637768e-001$	$5.9753913029981887e-001$	$-1.5981784384487407e+000$	$1.0385360137140841e-001$
a_4	$-3.5031711877728917e-002$	$3.7704987521510963e-001$	$-1.5334440834352672e+000$	$3.0987843367645405e+000$	$1.6707285314321316e-001$
a_5	$5.5457817142431337e-005$	$-7.3763141717492686e-004$	$3.9395974082513273e-003$	$-1.1166405155521864e-002$	$7.7370694388120365e-004$
a_6	$-1.1180323452893769e-003$	$1.4076653098295927e-002$	$-7.0717074122467166e-002$	$1.8795459287557137e-001$	$-1.2122823455425638e-002$
Interval $6: 2125-2400$ cm^{-1}					
a_1	$-3.6832033638363271e+001$	$4.0152489510919457e+002$	$-1.6468195217847594e+003$	$3.1955494330592746e+003$	$-2.4770711229545391e+003$
a_2	$8.3268808503488838e+000$	$-9.0952910032900533e+001$	$3.7421299371118403e+002$	$-7.2966100807517171e+002$	$5.6624916734424437e+002$
a_3	$-2.5444216599050558e+000$	$2.7989304108771158e+001$	$-1.1722237895633543e+002$	$2.4258224195081610e+002$	$-2.6700071549935188e+002$
a_4	$-4.6019393901260447e-001$	$5.0383861339975082e+000$	$-2.0803477763653049e+001$	$4.0742414176841400e+001$	$-3.1265864648345282e+001$
a_5	$-1.1434788946500034e-002$	$1.2949567222223801e-001$	$-5.6721642575336451e-001$	$1.2566687792972153e+000$	$-1.5139411916613101e+000$
a_6	$3.0394483848166953e-001$	$-3.3428328469287307e+000$	$1.3996484821192077e+001$	$-2.8955835632399648e+001$	$3.1864191709975156e+001$
Interval $7: 3475-3800$ cm^{-1}					
a_1	$-1.7240712819547803e+000$	$1.8185524249733316e+001$	$-7.1369546404384337e+001$	$1.3473144909368619e+002$	$9.7431040662191378e+001$
a_2	$4.3405723261828250e-001$	$-4.5907625909479490e+000$	$1.8099243433982426e+001$	$-3.4453313819001217e+001$	$-2.1853038107327993e+001$
a_3	$-4.4129809983877695e-003$	$2.3932664876569330e-002$	$5.9002661496413755e-002$	$-6.4691373883486636e-001$	$-6.2995051934228719e-001$
a_4	$-2.7285452866415479e-002$	$2.8926935394452657e-001$	$-1.1450493252545726e+000$	$2.1954539598647171e+000$	$1.2508773851010735e+000$
a_5	$-3.3203967345188666e-005$	$1.6836036297124230e-004$	$5.4387451819417384e-004$	$-5.1003903708415716e-003$	$-5.2128010580476149e-003$
a_6	$5.1913689290007355e-004$	$-2.8519133229590208e-003$	$-6.5753756747952670e-003$	$7.4775852306201027e-002$	$7.3594471848237877e-002$
Interval $8: 3800-4075$ cm^{-1}					
a_1	$-1.6880374492476415e+000$	$1.8172598925948520e+001$	$-7.3926811500817323e+001$	$1.4942088551805722e+002$	$7.9335151272281115e+000$
a_2	$4.1507053027234359e-001$	$-4.4723776257938743e+000$	$1.8220093705882668e+001$	$-3.6916407794047210e+001$	$-1.9236940548518462e+000$
a_3	$5.5580287767924988e-003$	$-7.0332011963078186e-002$	$3.5543425419639202e-001$	$-9.5096492060759796e-001$	$6.1815879460314707e-002$
a_4	$-2.5739526202051232e-002$	$2.7759246696513312e-001$	$-1.1325496826061026e+000$	$2.3003387001297257e+000$	$1.1747737311264511e-001$
a_5	$3.5325021320316794e-005$	$-4.6843767315197377e-004$	$2.4942110531973511e-003$	$-7.0491306852784059e-003$	$4.8667532980509437e-004$
a_6	$-6.6249031016840339e-004$	$8.3426436938226316e-003$	$-4.1920887847583466e-002$	$1.1144956741820755e-001$	$-7.1904299902074114e-003$
Interval $9: 4750-5650$ cm^{-1}					
a_1	$-4.1753853391647729e-002$	$4.5212261350403410e-001$	$-1.8562856991696834e+000$	$3.8076993465969959e+000$	$2.6745175630839171e+000$
a_2	$9.0327332019268756e-003$	$-9.7824856631063384e-002$	$4.0175711794875074e-001$	$-8.2455187339954461e-001$	$-6.5476919615379370e-001$
a_3	$5.7199541852586860e-005$	$-8.3689276376978992e-004$	$4.8790096678515303e-003$	$-1.4878568236059589e-002$	$1.0590887857378530e-003$
a_4	$-5.2793134676788560e-004$	$5.7210450582270041e-003$	$-2.3519520545166653e-002$	$4.8352403241933670e-002$	$4.0325030077580058e-002$
a_5	$3.8555402752352063e-007$	$-7.8317113450461403e-006$	$5.6675815917244448e-005$	$-2.0038245312027931e-004$	$1.7548399363857372e-005$
a_6	$-6.7851514787570300e-006$	$9.6020164738637844e-005$	$-5.4338973270152686e-004$	$1.6158637834420377e-003$	$-1.1036846986938378e-004$
Interval $10: 6825-7475$ cm^{-1}					
a_1	$-1.1900440686946299e-001$	$1.2959844210085782e+000$	$-5.3692936372330076e+000$	$1.1174316197902019e+001$	$4.1743027838865049e-001$
a_2	$2.8099987507661611e-002$	$-3.0604282548960943e-001$	$1.2681288457044215e+000$	$-2.6398086209617180e+000$	$-9.8419498192964985e-002$
a_3	$4.0503528678851377e-005$	$-5.3989763056657238e-004$	$2.8867701949725107e-003$	$-8.1743243009022703e-003$	$5.7290114858671824e-004$
a_4	$-1.6833942292014967e-003$	$1.8336091859519812e-002$	$-7.5990561634214401e-002$	$1.5822871239590294e-001$	$5.8849752335206548e-003$
a_5	$3.2513194539445574e-007$	$-4.6058665041842253e-006$	$2.6242466031908570e-005$	$-7.8985305705369537e-005$	$5.7565085478103838e-006$
a_6	$-4.7345407599861923e-006$	$6.2624697459123498e-005$	$-3.3198703236033349e-004$	$9.3181340676501867e-004$	$-6.4880075330307370e-005$

Table 5.2: Coefficients of the new correlation for band absorption coefficient of ten non uniform wavenumber intervals in oxy-fired combustion scenario for 0.01 bar m $\leq$ $\mathrm{P_{w+c}L} < 0.5$ bar m.

	b_1	b_2	b_3	b_4	b_5
Interval $1: 150-600$ cm^{-1}					
a_1	$1.2054155764358987e+000$	$-1.2250814872018259e+001$	$4.5280959274344006e+001$	$-7.7360711957259312e+001$	$5.5654651540594941e+001$
a_2	$-3.1357767600720421e-001$	$3.1911920455618095e+000$	$-1.1821959046477879e+001$	$2.0275159979735523e+001$	$-1.5685303531955899e+001$
a_3	$2.0693021112088733e-001$	$-2.1353423389019568e+000$	$8.1157809797223344e+000$	$-1.4683336310069576e+001$	$3.9263976873043545e+000$
a_4	$1.9543501002028577e-002$	$-1.9886700328072313e-001$	$7.3651020005039181e-001$	$-1.2617326506994635e+000$	$1.0814408246101093e+000$
a_5	$-1.8568508604359581e-003$	$2.2912843932529570e-002$	$-1.1162872843950271e-001$	$2.8309700817117378e-001$	$-5.9352292321191415e-002$
a_6	$-2.3817219488642287e-002$	$2.4583626967279285e-001$	$-9.3498178784162012e-001$	$1.6948599740495400e+000$	$4.6297634842174124e-001$
Interval $2: 600-775$ cm^{-1}					
a_1	$1.2664510338042356e-001$	$1.3738672425313334e-001$	$-1.1012972343400820e+001$	$6.1179090933568695e+001$	$-1.2581913439955370e+002$
a_2	$-7.6294230972434270e-004$	$-3.8837868782120438e-001$	$4.3818132374918930e+000$	$-1.9601831400181382e+001$	$3.8558948604884165e+001$
a_3	$-8.2248366196093547e-002$	$1.1016831386300550e+000$	$-6.0009810443992695e+000$	$1.7821439256597884e+001$	$-2.4406365524148196e+001$
a_4	$-2.3727027380683291e-003$	$5.1390754120644262e-002$	$-3.9409748665024130e-001$	$1.5254314567424363e+000$	$-2.8199564929023082e+000$
a_5	$1.5227655522183563e-003$	$-1.3553438379375523e-002$	$3.6642617573187077e-002$	$-1.3277812527396174e-002$	$-1.0691741607575979e-001$
a_6	$1.2688994918268913e-002$	$-1.6340085983121372e-001$	$8.5415900456475646e-001$	$-2.4439285453506048e+000$	$3.0191538800309763e+000$
Interval $3: 775-1125$ cm^{-1}					
a_1	$-9.3164809454228570e-001$	$9.852414213938757 8e+000$	$-3.8838835944074461e+001$	$7.3924884804048787e+001$	$-9.0166955918102012e+000$
a_2	$2.7877985359507801e-001$	$-2.9493913429558116e+000$	$1.1637075261627070e+001$	$-2.2197375334419476e+001$	$2.5312165020745114e+000$
a_3	$-1.9634132748466392e-002$	$2.0707935423410165e-001$	$-8.0711728284399809e-001$	$1.4755610376872521e+000$	$-8.2138136880577112e-002$
a_4	$-2.0824448329106245e-002$	$2.2040475359280839e-001$	$-8.7037745234281827e-001$	$1.6636288205742087e+000$	$-1.7010158288412061e-001$
a_5	$1.3167617244002442e-004$	$-1.2190373294367581e-003$	$3.7572520923963154e-003$	$-4.1295228181421765e-003$	$-6.1668723196361824e-003$
a_6	$3.0649000996959487e-003$	$-3.2245809846394261e-002$	$1.2526215239183974e-001$	$-2.2812018218273764e-001$	$6.1347881061744282e-003$
Interval $4: 1275-1625$ cm^{-1}					
a_1	$3.0408224182174920e-001$	$-3.0761284910291855e+000$	$1.1197116004506068e+001$	$-1.8168248721999383e+001$	$3.0481234820334864e+000$
a_2	$-9.5901267686263295e-002$	$9.7222168743055137e-001$	$-3.5577581441057773e+000$	$5.8633750839750221e+000$	$-4.6511452780439472e-001$
a_3	$1.2020980430321362e-001$	$-1.2984002883005634e+000$	$5.3041513821488842e+000$	$-1.0766586241221029e+001$	$-1.1110100880169657e-001$
a_4	$6.9059456936059549e-003$	$-6.9945410823766263e-002$	$2.5571931670843850e-001$	$-4.2156758202507422e-001$	$1.2433458761594667e-002$
a_5	$1.0996262811198314e-003$	$-1.1588136686212586e-002$	$4.5396209741712941e-002$	$-8.5447051455094278e-002$	$-2.1471054271737094e-003$
a_6	$-1.4446137794113835e-002$	$1.5594947542578486e-001$	$-6.3654690890806420e-001$	$1.2904678919886110e+000$	$1.4651511934308324e-002$
Interval $5: 1675-1900$ cm^{-1}					
a_1	$-1.1581372518515481e-001$	$1.3037834964805137e+000$	$-5.7307969668126750e+000$	$1.3243034280389141e+001$	$7.0551987301471071e+000$
a_2	$1.6376367243922139e-002$	$-1.9882966626358967e-001$	$9.6812140161466986e-001$	$-2.5373991443111166e+000$	$-1.5938072965612133e+000$
a_3	$8.7044090076072083e-002$	$-9.4812294700589750e-001$	$3.9237290051439628e+000$	$-8.1249329961833396e+000$	$1.4203552550165458e-002$
a_4	$-4.7906364119627436e-004$	$7.0586272431122452e-003$	$-4.1786942609724910e-002$	$1.3052295005974177e-001$	$9.0332515676882663e-002$
a_5	$7.3696601746968198e-004$	$-7.9058202243115459e-003$	$3.1886530608487833e-002$	$-6.3091167404622103e-002$	$-9.2542161579978532e-005$
a_6	$-1.0552988640503044e-002$	$1.1485847684804490e-001$	$-4.7477696238349126e-001$	$9.8139694136090816e-001$	$-7.3545851512122143e-004$
Interval $6: 2125-2400$ cm^{-1}					
a_1	$3.4156903349314764e+000$	$-3.5292627521590376e+001$	$1.2741066092594734e+002$	$-1.4539133557101511e+002$	$-3.6987796395247574e+002$
a_2	$-9.8201730540611565e-001$	$1.0275914240468017e+001$	$-3.8244849311999801e+001$	$5.0353460216942430e+001$	$8.2511681375436410e+001$
a_3	$4.8446338204218359e-001$	$-4.7214891396991803e+000$	$1.4792520710968441e+001$	$-6.4408680373236074e+000$	$-7.5141344272414500e+001$
a_4	$7.1671972453772728e-002$	$-7.6052352320828842e-001$	$2.9238296647212660e+000$	$-4.3912932208396160e+000$	$-3.8087644597303627e+000$
a_5	$2.0884915709531368e-002$	$-2.2245879208374567e-001$	$8.7677020408350026e-001$	$-1.5783128447014567e+000$	$1.0285505492206755e+000$
a_6	$-6.8465366229038566e-002$	$6.7568244646091680e-001$	$-2.1969188528204397e+000$	$1.4929368762918307e+000$	$8.6384190771312497e+000$
Interval $7: 3475-3800$ cm^{-1}					
a_1	$-1.0641735791888114e+000$	$1.1504293531538130e+001$	$-4.6653717515323400e+001$	$8.9854593880253901e+001$	$-3.6965744277253158e+001$
a_2	$2.6676223967041957e-001$	$-2.9038019094351486e+000$	$1.1914167591600451e+001$	$-2.3462760504864068e+001$	$1.1854586455982517e+001$
a_3	$1.0736228789894817e-002$	$-1.3057934224010681e-001$	$6.5144730092824987e-001$	$-1.8783400700676174e+000$	$-5.5652646359130227e+000$
a_4	$-1.6686165753155090e-002$	$1.8280073213231984e-001$	$-7.5803133507680698e-001$	$1.5222027080535285e+000$	$-8.6457547741732954e-001$
a_5	$-5.1320022687550890e-005$	$4.9491112620533970e-004$	$-1.3493682632542505e-003$	$-1.3874140383361507e-003$	$-5.3145116847360091e-002$
a_6	$-1.4254771734835429e-003$	$1.6986344588392883e-002$	$-8.2408969301877633e-002$	$2.2993717691413490e-001$	$6.7573172298881568e-001$
Interval $8: 3800-4075$ cm^{-1}					
a_1	$-2.0634419570422560e-001$	$2.2251154201952992e+000$	$-9.1212865968780985e+000$	$1.8873384437724980e+001$	$5.8463851450834481e+000$
a_2	$4.4553758423470195e-002$	$-4.8590695426277952e-001$	$2.0280095386213524e+000$	$-4.3162676762620572e+000$	$-1.3675340111882821e+000$
a_3	$5.4840078254284927e-002$	$-5.9990694608409612e-001$	$2.4990229177247087e+000$	$-5.2267224011762163e+000$	$3.2687186862594329e-002$
a_4	$-2.5464287158204978e-003$	$2.8121734445662537e-002$	$-1.1961588852055567e-001$	$2.6165195501186939e-001$	$8.0656596121203891e-002$
a_5	$4.9199447886789189e-004$	$-5.3465169856168598e-003$	$2.2018109461928639e-002$	$-4.5102007380021875e-002$	$3.8230575826930362e-004$
a_6	$-6.6450921384658872e-003$	$7.2600621658611406e-002$	$-3.0184657857164104e-001$	$6.2944120858104302e-001$	$-3.1704734540628997e-003$
Interval $9: 4750-5650$ cm^{-1}					
a_1	$-3.2643386490536848e-003$	$2.0938469775940390e-002$	$4.4024100568594796e-003$	$-2.9121486755029108e-001$	$2.6740708750139630e+000$
a_2	$-5.7795224378445222e-004$	$9.3744310006960378e-003$	$-5.7877962165436052e-002$	$1.7858903513516031e-001$	$-6.5127044709427684e-001$
a_3	$1.6754505721933413e-003$	$-1.9882680703509084e-002$	$9.2867248785871756e-002$	$-2.2695385070885790e-001$	$9.1529256908227229e-003$
a_4	$7.3141632501146358e-005$	$-9.5619500936056816e-004$	$4.9368075121750850e-003$	$-1.3201747116618066e-002$	$3.9906031501684640e-002$
a_5	$2.1065183430777036e-005$	$-2.6819380059957211e-004$	$1.3630064362039767e-003$	$-3.6608089373356134e-003$	$2.3837973477265341e-004$
a_6	$-2.0085761598684308e-004$	$2.3659988646678488e-003$	$-1.0943420489324939e-002$	$2.6417451948072851e-002$	$-9.9234602399568008e-004$
Interval $10: 6825-7475$ cm^{-1}					
a_1	$-8.6420321572541800e-002$	$9.1990199774678938e-001$	$-3.6772103134226088e+000$	$7.2343379455016930e+000$	$6.0049791830883070e-001$
a_2	$1.9870067364986269e-002$	$-2.1131140673458626e-001$	$8.4353428499347227e-001$	$-1.6562874787235817e+000$	$-1.4339655647810279e-001$
a_3	$1.1263284570492669e-003$	$-1.3501525785162158e-002$	$6.3911911399582799e-002$	$-1.5883383616064631e-001$	$8.7732339276740973e-003$
a_4	$-1.1632528917372013e-003$	$1.2364188850382324e-002$	$-4.9320343142496934e-002$	$9.6755969644656159e-002$	$8.6524160711565958e-003$
a_5	$1.0714135684725065e-005$	$-1.3332835484309549e-004$	$6.6142904051164628e-004$	$-1.7376909187593009e-003$	$1.0565780421595130e-004$
a_6	$-1.3742803082491783e-004$	$1.6415125001645909e-003$	$-7.7341536281742016e-003$	$1.9108727037533971e-002$	$-1.0437796222583021e-003$

Table 5.3: Coefficients of the new correlation for band absorption coefficient of ten non uniform wavenumber intervals in oxy-fired combustion scenario for 0.5 bar m $\leq P_{w+c}L <$ 10 bar m.

	b_1	b_2	b_3	b_4	b_5
Interval $1: 150-600$ cm^{-1}					
a_1	$9.20081784083940370e-002$	$-9.18205139125005340e-001$	$3.20705226228593880e+000$	$-4.25515406717052170e+000$	$-1.77721344260387080e+001$
a_2	$-3.21956419351795770e-002$	$3.29429823212905700e-001$	$-1.21063993862179920e+000$	$1.87015587484691450e+000$	$5.41917053326890660e+000$
a_3	$8.69770707149931590e-003$	$-1.01451335670027020e-001$	$4.59832257356539820e-001$	$-1.05600192466170300e+000$	$-9.23718443687907120e-001$
a_4	$1.80447097235442950e-003$	$-1.86478981395342860e-002$	$6.94533473188507360e-002$	$-1.07931615424680350e-001$	$-3.87096080803652580e-001$
a_5	$-3.39510160383592500e-003$	$3.57307115253789400e-002$	$-1.40261476369811950e-001$	$2.68238468612497890e-001$	$2.91713988785327300e-002$
a_6	$1.74207166247656490e-003$	$-1.69737652296811440e-002$	$5.80879855520829673e-002$	$-8.58968736630788270e-002$	$8.07674373917004470e-002$
Interval $2: 600-775$ cm^{-1}					
a_1	$-1.29344343054777960e-001$	$1.61835418560851600e+000$	$-8.48958522852392330e+000$	$2.69970712832266600e+001$	$-6.66229110640811940e+001$
a_2	$6.20138582942596630e-002$	$-7.35899355518009780e-001$	$3.58570670635802900e+000$	$-1.04080796660892220e+001$	$2.28515040302188090e+001$
a_3	$-6.39331555830100070e-002$	$6.98592773708987760e-001$	$-2.96744930134641690e+000$	$6.88127244257863780e+000$	$-9.23145438721595470e+000$
a_4	$-6.28445607059292810e-003$	$7.23571966576085910e-002$	$-3.36522618515134100e-001$	$9.14432664840503560e-001$	$-1.77906113256434840e+000$
a_5	$-2.07419590935270640e-003$	$2.08478423304615870e-002$	$-7.44016502048499560e-002$	$1.08698486457145760e-001$	$1.03707123790530210e-001$
a_6	$9.82425770298791900e-003$	$-1.05933671369838720e-001$	$4.39072798520547420e-001$	$-9.70895754717660540e-001$	$1.05386734827328700e+000$
Interval $3: 775-1125$ cm^{-1}					
a_1	$-3.68898892072424490e-001$	$3.87659526066273850e+000$	$-1.51744504792364340e+001$	$2.87985179643309410e+001$	$-5.42244607720478730e+000$
a_2	$1.17427707660845050e-001$	$-1.23281421128056620e+000$	$4.81653840015983280e+000$	$-9.10245996750502860e+000$	$1.49739077148916770e+000$
a_3	$-2.77793753473347880e-002$	$2.85550759230742800e-001$	$-1.06917353818669360e+000$	$1.82512102742398930e+000$	$5.22826294985742760e-002$
a_4	$-9.31888307589399420e-003$	$9.77410599933817300e-002$	$-3.81140612770153650e-001$	$7.17191030167664170e-001$	$-9.60503066060580110e-002$
a_5	$-1.50438299023982930e-004$	$1.51714430591889070e-003$	$-5.55813198915479890e-003$	$9.51586029278518940e-003$	$-4.16167537968972160e-003$
a_6	$4.22560447542925930e-003$	$-4.34423164841722730e-002$	$1.62728533659196650e-001$	$-2.78246526659748530e-001$	$1.40653825621808030e-002$
Interval $4: 1275-1625$ cm^{-1}					
a_1	$-1.02787731634592270e-002$	$1.59458118036162920e-001$	$-9.55534375304784360e-001$	$2.88707531600087240e+000$	$-9.08252894824319810e-001$
a_2	$-1.28408301197387690e-002$	$1.23516664030625720e-001$	$-4.11027159698418190e-001$	$5.51459975479378080e-001$	$4.96011841573783470e-001$
a_3	$3.38267139506187450e-002$	$-3.59223091206779640e-001$	$1.43269791254662590e+000$	$-2.81838035366638940e+000$	$-5.43760262904203650e-001$
a_4	$1.41672429257233510e-003$	$-1.42401314914752490e-002$	$5.17279765059149510e-002$	$-8.60235403654840410e-002$	$-4.57104026491139260e-002$
a_5	$-1.00997308241185310e-003$	$1.09751103435945240e-002$	$-4.52256069251647240e-002$	$9.28961110883275570e-002$	$-4.53867937579431270e-003$
a_6	$-3.26215863394979610e-003$	$3.45589981074975740e-002$	$-1.37435299881066540e-001$	$2.69768164601986830e-001$	$6.79923426776134210e-002$
Interval $5: 1675-1900$ cm^{-1}					
a_1	$-7.58710230985237820e-002$	$8.51545168842986810e-001$	$-3.68412829314673740e+000$	$8.13854146538340650e+000$	$4.68368540798492990e-001$
a_2	$5.76681991970198150e-003$	$-7.34657668516602580e-002$	$3.69988441531780010e-001$	$-9.67084338591314490e-001$	$9.34140135888271020e-002$
a_3	$3.32300924268692230e-002$	$-3.51488800747181200e-001$	$1.39236238209483740e+000$	$-2.70610854403334860e+000$	$-4.81788614556479760e-001$
a_4	$2.21304825507643790e-004$	$-1.54316913312259390e-003$	$1.09382122694168140e-003$	$1.34698728896868040e-002$	$-1.76854078278633221e-002$
a_5	$-6.44066376000605760e-004$	$7.08744003023710580e-003$	$-2.97481947947238550e-002$	$6.27337875451104420e-002$	$-4.78976019552157340e-003$
a_6	$-3.53126536552225530e-003$	$3.72239636480959510e-002$	$-1.46722526507280270e-001$	$2.83229282507018180e-001$	$6.15265501397285820e-002$
Interval $6: 2125-2400$ cm^{-1}					
a_1	$3.50121958666034790e-001$	$-4.06795407784930330e+000$	$1.89303025561676140e+001$	$-4.82203476682531760e+001$	$4.16921862001518800e+001$
a_2	$-1.37558250896600980e-001$	$1.60120253943980970e+000$	$-7.46898275252588120e+000$	$1.91260284865000970e+001$	$-1.98536819576147570e+001$
a_3	$1.04518314995967800e-001$	$-1.20971932991973290e+000$	$5.57142396834916290e+000$	$-1.38571000268490770e+001$	$1.62988379234892950e+001$
a_4	$1.34324649071477460e-002$	$-1.57111270919320870e-001$	$7.38634902042566770e-001$	$-1.92364075325904760e+000$	$2.46132208768416930e+000$
a_5	$5.27147909970852170e-003$	$-6.19974905429612480e-002$	$2.94117799904229370e-001$	$-7.84480079722572280e-001$	$1.42778519535356360e+000$
a_6	$-1.89162264309957260e-002$	$2.20431508779274590e-001$	$-1.02782427704077190e+000$	$2.63015892669718370e+000$	$-3.75723515375978190e+000$
Interval $7: 3475-3800$ cm^{-1}					
a_1	$-9.14750243095515950e-002$	$1.14775491691289270e+000$	$-5.98898173136774050e+000$	$1.81917287715363580e+001$	$-1.82552365504432110e+001$
a_2	$3.38398286863009650e-003$	$-8.99678766305477550e-002$	$7.99705798707681440e-001$	$-3.63172336212755780e+000$	$6.24697661655250690e+000$
a_3	$4.93545485108279200e-002$	$-4.99650131353355010e-001$	$1.78366527836746870e+000$	$-2.49350567460052730e+000$	$-3.62464207249256100e+000$
a_4	$1.10301535695851426e-003$	$-7.84175435016739970e-003$	$-9.57177421058259470e-004$	$1.56471386560201490e-001$	$-4.51618177989748350e-001$
a_5	$2.40483237972298170e-004$	$-1.99587982628956440e-003$	$3.55852812103392940e-003$	$1.22171384150536360e-002$	$4.69831639366589250e-003$
a_6	$-6.60229961005356480e-003$	$6.68718876689358700e-002$	$-2.38728841950193920e-001$	$3.32113095277830170e-001$	$4.04739878769329260e-001$
Interval $8: 3800-4075$ cm^{-1}					
a_1	$-8.43621272136741710e-002$	$9.27958882246783130e-001$	$-3.89872247972040500e+000$	$8.26223053467083270e+000$	$7.61808028097323510e-001$
a_2	$1.23890115944498370e-002$	$-1.40254015456493240e-001$	$6.13040968778711810e-001$	$-1.36731299470212810e+000$	$-5.20338429409557200e-002$
a_3	$2.43503666137213260e-002$	$-2.56836270637787470e-001$	$1.01274142832779800e+000$	$-1.95321623300448500e+000$	$-3.39394746484833370e-001$
a_4	$-4.28384554903240730e-004$	$5.13561207074001750e-003$	$-2.40845922001069360e-002$	$5.81077272424681200e-002$	$-4.39249053838142340e-003$
a_5	$-3.68029757658887480e-004$	$4.14938276384104860e-003$	$-1.80318912996131650e-002$	$3.99069281473043780e-002$	$-4.31740901077281530e-003$
a_6	$-2.61115225616750800e-003$	$2.73951461114763200e-002$	$-1.07139155820017120e-001$	$2.04079728509017400e-001$	$4.39395522540603140e-002$
Interval $9: 4750-5650$ cm^{-1}					
a_1	$1.71302533135644750e-002$	$-1.65763758003480810e-001$	$5.61268440235023310e-001$	$-8.16792339400648220e-001$	$1.43821125881263080e+000$
a_2	$-5.81523946149736970e-003$	$5.67052018021859050e-002$	$-1.94609620042748930e-001$	$2.89743132713048410e-001$	$-3.18622993161497023e-001$
a_3	$4.62540532818089040e-003$	$-4.72046330488170430e-002$	$1.75561757405167220e-001$	$-3.03302838937284600e-001$	$-7.26122074525641650e-002$
a_4	$4.09219972602006910e-004$	$-3.95293422227465260e-003$	$1.32970787552569770e-002$	$-1.87607207260638770e-002$	$1.75696644033569960e-002$
a_5	$1.01860408552277720e-004$	$-1.00225996575694440e-003$	$3.45242240005985910e-003$	$-4.87505140978895630e-003$	$-8.93257416672959430e-004$
a_6	$-5.81609440867962980e-004$	$5.86808950206726880e-003$	$-2.13607028985310300e-002$	$3.52478860026115560e-002$	$9.76397213086619210e-003$
Interval $10: 6825-7475$ cm^{-1}					
a_1	$-1.90156589552025540e-002$	$2.11294270994242920e-001$	$-9.04999701474314520e-001$	$1.99033026786178980e+000$	$3.16973665934879250e-001$
a_2	$2.02887497264873710e-003$	$-2.39683054937655450e-002$	$1.12003986656312280e-001$	$-2.76982463126077380e-001$	$-6.57576574997580380e-002$
a_3	$6.05128301623331090e-003$	$-6.47765169297214870e-002$	$2.60905750350061030e-001$	$-5.17796976759734460e-001$	$-1.22304000763638030e-002$
a_4	$1.56538331282401740e-005$	$-1.49702318212422340e-006$	$-1.12219713041429910e-003$	$6.15783035926191230e-003$	$3.35876629465648150e-003$
a_5	$6.58832874720941500e-005$	$-6.91908965121243420e-004$	$2.69447856298104600e-003$	$-5.01547494458470020e-003$	$-1.69797391051108770e-004$
a_6	$-7.75811129188312560e-004$	$8.27927908786525200e-003$	$-3.31782978798953260e-002$	$6.52748182734036590e-002$	$1.75167455998806320e-003$

Table 5.4: Coefficients of the new correlation for band absorption coefficient of ten non uniform wavenumber intervals in oxy-fired combustion scenario for 10 bar m $\leq \mathrm{P_{w+c}L} \leq$ 60 bar m.

	b_1	b_2	b_3	b_4	b_5
Interval $1: 150-600$ cm^{-1}					
a_1	$2.440016803955260e-002$	$-2.317108503201080e-001$	$7.175227126653289e-001$	$-4.909433210245859e-001$	$-6.385182153731849e+000$
a_2	$-1.327390928395061e-002$	$1.353200922561426e-001$	$-4.937362224532688e-001$	$7.413128407705139e-001$	$2.053554459515576e+000$
a_3	$7.310940993965830e-003$	$-8.043488150299738e-002$	$3.373415589788434e-001$	$-7.036895123209578e-001$	$-3.143575407837511e-001$
a_4	$6.538494065145270e-004$	$-6.766661058809082e-003$	$2.519675224102465e-002$	$-3.797985924161997e-002$	$-1.418350215196628e-001$
a_5	$-1.157829323635782e-003$	$1.215635609933627e-002$	$-4.745839400288777e-002$	$8.943112866056927e-002$	$2.606376926952416e-002$
a_6	$6.932656501160330e-004$	$-6.778531723852412e-003$	$2.326419159506902e-002$	$-3.426629157322976e-002$	$1.368609058979242e-003$
Interval $2: 600-775$ cm^{-1}					
a_1	$-1.219810123280532e-002$	$1.983593834350660e-001$	$-1.383785862853763e+000$	$5.941705516121732e+000$	$-2.314922561432063e+001$
a_2	$1.629392064206460e-002$	$-1.967834785775456e-001$	$9.915780788709337e-001$	$-3.092107517263696e+000$	$8.851821396518195e+000$
a_3	$-1.829547486958930e-002$	$1.996064995688244e-001$	$-8.453993208112284e-001$	$1.960233651954065e+000$	$-3.039819226299488e+000$
a_4	$-2.292198736103716e-003$	$2.595521719086512e-002$	$-1.179348373966679e-001$	$3.147083212005977e-001$	$-6.912389618321366e-001$
a_5	$-6.545022750992127e-004$	$6.294966972448242e-003$	$-2.004041781906979e-002$	$1.648574585808820e-002$	$1.124477933482968e-001$
a_6	$3.323268549072914e-003$	$-3.513646409406549e-002$	$1.399654176509406e-001$	$-2.840268674457521e-001$	$2.332175769431265e-001$
Interval $3: 775-1125$ cm^{-1}					
a_1	$-1.063456244124834e-001$	$1.126644168173557e+000$	$-4.494232363740867e+000$	$9.006088855883646e+000$	$-2.818914088539040e+001$
a_2	$3.813960477551613e-002$	$-4.022770154728248e-001$	$1.590408064941230e+000$	$-3.120101002726397e+000$	$7.476619236818954e-001$
a_3	$-1.125424840873954e-002$	$1.160863920898968e-001$	$-4.380349697158506e-001$	$7.613255652661700e-001$	$7.364440364400422e-002$
a_4	$-3.379107988597036e-003$	$3.548644385763555e-002$	$-1.390698669945851e-001$	$2.672175643755866e-001$	$-4.135037197706589e-002$
a_5	$-1.446307425654987e-004$	$1.407256829061622e-003$	$-4.733251551994727e-003$	$6.247356218390481e-003$	$5.658254271622576e-003$
a_6	$1.853630387976893e-003$	$-1.902587583198784e-002$	$7.112642673791606e-002$	$-1.211793239673352e-001$	$-2.325513165941935e-002$
Interval $4: 1275-1625$ cm^{-1}					
a_1	$-3.210220060513825e-002$	$3.545973008037722e-001$	$-1.500692721569775e+000$	$3.221900119792740e+000$	$2.555990154198270e-002$
a_2	$3.294486651428782e-004$	$-5.639805287711092e-003$	$3.597983671387684e-002$	$-1.126095677157580e-001$	$1.139937825733327e-001$
a_3	$1.047175794530845e-002$	$-1.133478787411273e-001$	$4.656981564018968e-001$	$-9.592261985573437e-001$	$-1.534743690917008e-001$
a_4	$8.142105214129611e-005$	$-8.549737667828950e-004$	$3.393897667207347e-003$	$-6.863486504858858e-003$	$-1.072958073619865e-002$
a_5	$-7.366648322461893e-004$	$7.771156554107911e-003$	$-3.059618719025810e-002$	$5.859339624943407e-002$	$5.985312921482872e-003$
a_6	$-3.237168814303768e-004$	$3.800723489265011e-003$	$-1.756388370601533e-002$	$4.263815560776926e-002$	$1.031899461563995e-002$
Interval $5: 1675-1900$ cm^{-1}					
a_1	$-5.375231357783935e-002$	$5.826156995919830e-001$	$-2.396520932684118e+000$	$4.933713361436943e+000$	$4.246779916604552e-001$
a_2	$6.756222507709498e-003$	$-7.380728179508969e-002$	$3.070085038171821e-001$	$-6.415148048581358e-001$	$-7.080977206395720e-004$
a_3	$1.006628745500384e-002$	$-1.084158098973731e-001$	$4.418987166871726e-001$	$-8.986183754023728e-001$	$-1.496251481378076e-001$
a_4	$-2.856556664221281e-004$	$3.073082638067730e-003$	$-1.245522073787792e-002$	$2.485884809072461e-002$	$-3.799274592459104e-003$
a_5	$-5.647004562426084e-004$	$5.952964910051130e-003$	$-2.341004107374149e-002$	$4.473617256432524e-002$	$4.246011653285855e-003$
a_6	$-5.203262746878997e-004$	$5.790194983741053e-003$	$-2.483150050101229e-002$	$5.462080034677516e-002$	$1.254878694748015e-002$
Interval $6: 2125-2400$ cm^{-1}					
a_1	$5.355625910217369e-002$	$-6.270886552262463e-001$	$2.983525464448610e+000$	$-8.353215208985606e+000$	$1.538080986664327e+001$
a_2	$-2.585977546203537e-002$	$3.088632379101748e-001$	$-1.513035956496625e+000$	$4.393733089504174e+000$	$-9.159499084776729e+000$
a_3	$1.625940610792501e-002$	$-1.991066550436836e-001$	$1.009357185290303e+000$	$-3.042977728914460e+000$	$6.977222078948233e+000$
a_4	$3.233121644480383e-003$	$-3.929497685864791e-002$	$1.974276284298565e-001$	$-5.925895115181893e-001$	$1.400139420697438e+000$
a_5	$1.118546194516066e-003$	$-1.385220246845052e-002$	$7.143947126981164e-002$	$-2.214278842973769e-001$	$6.007336023702832e-001$
a_6	$-3.929207475508849e-003$	$4.848870779163662e-002$	$-2.486833016022169e-001$	$7.634629074806669e-001$	$-1.928306520743365e+000$
Interval $7: 3475-3800$ cm^{-1}					
a_1	$-5.736030423408506e-002$	$5.938510079561991e-001$	$-2.263875003571440e+000$	$4.288011562810027e+000$	$1.975000274563157e+000$
a_2	$3.480180227411653e-003$	$-2.919568536379361e-002$	$6.658461839736852e-002$	$-5.268473259228867e-002$	$-4.835675945692555e-001$
a_3	$1.713034960506233e-002$	$-1.866536803928578e-001$	$7.709663653057146e-001$	$-1.537186904271056e+000$	$-1.371356877904229e-001$
a_4	$4.465297020631330e-004$	$-5.804380579922051e-003$	$3.018009430586880e-002$	$-7.597168249367566e-002$	$9.371080500837308e-002$
a_5	$-1.562645810537562e-004$	$1.162989039841962e-003$	$-1.150449292617783e-003$	$-9.425225674459265e-003$	$7.388570964683631e-002$
a_6	$-2.063633340533754e-003$	$2.326957503774492e-002$	$-1.015682087238513e-001$	$2.217017857271964e-001$	$-1.113067227878343e-001$
Interval $8: 3800-4075$ cm^{-1}					
a_1	$-5.180271597446056e-002$	$5.569772113703213e-001$	$-2.261813072975050e+000$	$4.560808098360070e+000$	$4.901337509083975e-001$
a_2	$8.712530563491159e-003$	$-9.344420297024030e-002$	$3.776918866586110e-001$	$-7.544849300913508e-001$	$-5.151077895085087e-002$
a_3	$6.910924634985221e-003$	$-7.460759415989072e-002$	$3.052860459675646e-001$	$-6.249462011198867e-001$	$-1.076805188514446e-001$
a_4	$-5.151741436125507e-004$	$5.452588102493390e-003$	$-2.154888728519291e-002$	$4.135190898106341e-002$	$8.976652220512570e-004$
a_5	$-4.446574535545974e-004$	$4.693753851501135e-003$	$-1.849744373317313e-002$	$3.547157366734847e-002$	$2.786096059087600e-003$
a_6	$-2.660145889606759e-004$	$3.031141337300178e-003$	$-1.345979135177278e-002$	$3.110806712565983e-002$	$9.116113996541797e-003$
Interval $9: 4750-5650$ cm^{-1}					
a_1	$-3.478335705501447e-003$	$3.991195323234351e-002$	$-1.737474022430557e-001$	$3.553130095237876e-001$	$6.439617758866215e-001$
a_2	$1.237658689525568e-003$	$-1.420505652176873e-002$	$6.230282175887919e-002$	$-1.322587169843386e-001$	$-9.779965416408746e-002$
a_3	$-2.298560731056450e-003$	$2.906589300418842e-003$	$-1.451505627182218e-002$	$3.750883018146113e-002$	$-9.093665926196346e-002$
a_4	$-1.796604879245586e-004$	$1.999665528664427e-003$	$-8.480899749748393e-003$	$1.773759571843598e-002$	$2.307318134745478e-003$
a_5	$-7.028090516969487e-005$	$7.728903312814604e-004$	$-3.247040352663804e-003$	$6.910661396494372e-003$	$-9.669371240899674e-004$
a_6	$1.703677045905978e-004$	$-1.896497357141885e-003$	$8.101992802034427e-003$	$-1.756953710685439e-002$	$1.216382019384701e-002$
Interval $10: 6825-7475$ cm^{-1}					
a_1	$-1.534081828488046e-002$	$1.680512316466669e-001$	$-7.018004593595176e-001$	$1.474525229862597e+000$	$7.066945324388154e-002$
a_2	$2.169565981574187e-003$	$-2.445350192154570e-002$	$1.062281808098820e-001$	$-2.349590031149189e-001$	$7.143487422031279e-003$
a_3	$2.707198359622190e-003$	$-2.860238954570581e-002$	$1.130973466084614e-001$	$-2.191753433713141e-001$	$-3.346502889561815e-002$
a_4	$-7.907526733554081e-005$	$9.455320572673913e-004$	$-4.418826253905142e-003$	$1.061071821041864e-002$	$-1.987642830190194e-003$
a_5	$-3.315528880793119e-005$	$3.883611746534702e-004$	$-1.775851844590823e-003$	$4.191307683750949e-003$	$-6.230541344007966e-004$
a_6	$-2.647735031555351e-004$	$2.753766662346065e-003$	$-1.061822782349143e-002$	$1.975786990337313e-002$	$4.782200058167724e-003$

6 Application of the new Banded Approach in gray and non gray modeling of a real industrial combustion system

The correlations obtained in the previous chapters for the mean absorption coefficient and the band absorption coefficient of the H_2O–CO_2 mixtures can be used for gray and non gray radiative heat transfer modeling in real industrial combustion systems. In the present chapter, the CFD simulations were obtained by using Fluent commercial software package, and the new correlations were integrated into the CFD software by means of the user defined function (UDF). The simulation of the backpass channel on industrial scale is presented in this chapter. By using different gray and non gray models, the effect of gas spectral features on the overall radiation heat transfer predictions in such a large scale backpass channel has been addressed. Both the oxy- and air-fired combustion scenarios have been simulated in the same geometry with similar thermal conditions. Then it is addressed how the radiative heat transfer is changed by different types of combustion in both the air and oxygen fired systems.

6.1 Geometry of backpass channel

Gray and non gray radiative heat transfer modeling have been performed for a backpass channel as a constituent part of an industrial large scale boiler. Both the oxy- and air-fired combustion conditions have been studied. The comparison between the predictions of different radiative models was carried out in order to address the importance of the spectral radiative features of the gas mixture in oxy-fired combustion conditions. Moreover, an analysis done to address how the combustion type may affect the radiative heat transfer, and in turn, the overall performance of a large scale backpass channel.

A schematic of the backpass channel is shown in Figure 6.1. The backpass channel is a rectangular shape channel with heat transfer surfaces in which the flue gas comes through four inlet sections and exits from the end part (right side wall) of the geometry.

The flow of hot flue gases from the furnace enters the backpass channel through four identical squared inlets, positioned in a row in the middle line of one of the walls. The species concentration remains constant in the simulated domain for each of the combustion conditions. About 600 thousands cubical cells are used for the entire domain as shown in Figure 6.2.

6.2 Boundary conditions

In the presented simulations, the internal surfaces are assumed to be black in radiation, and their temperatures are equal to 750K for both the oxy- and air-fired combustion condi-

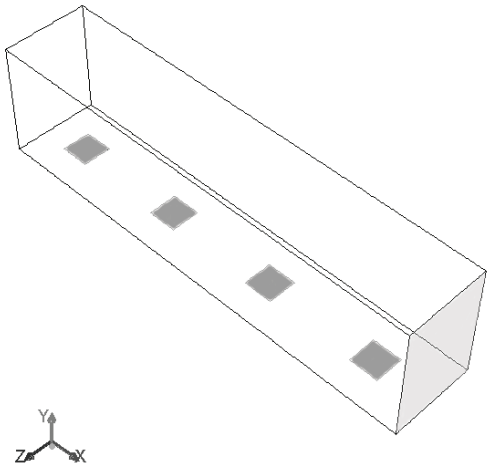

Figure 6.1: The geometry of the simulated industrial large scale backpass channel.

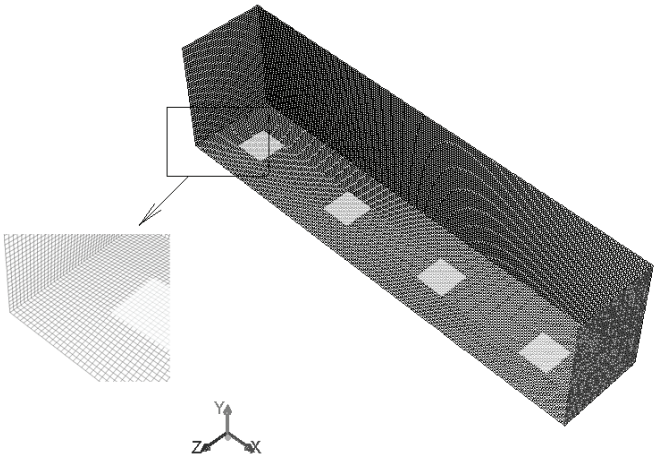

Figure 6.2: The mesh structure of the simulated backpass channel.

tions. The molar fractions of the different species in the flue gases are presented by 21% H_2O, 70% CO_2 for the oxy-fired scenario and 9.7% H_2O, 14.3% CO_2 for the air-fired scenario. The rest of the mixture for both oxy- and air-fired conditions is assumed to contain N_2. The temperature of the inlet flue gases in the present simulations is $T = 1220$K. The mass flow rate of the flue gases at the inlet section of the geometry is equal and fixed

for both the oxy- and air-fired combustion conditions. The temperature profile along the middle planes for the oxy-fired scenario calculated by using the DOM with the WSGGM (domain based) is shown in Figure 6.3. The optical path length L used in the WSGGM calculations is taken as domain based and it is equal to $\mathrm{L} = 5$ m.

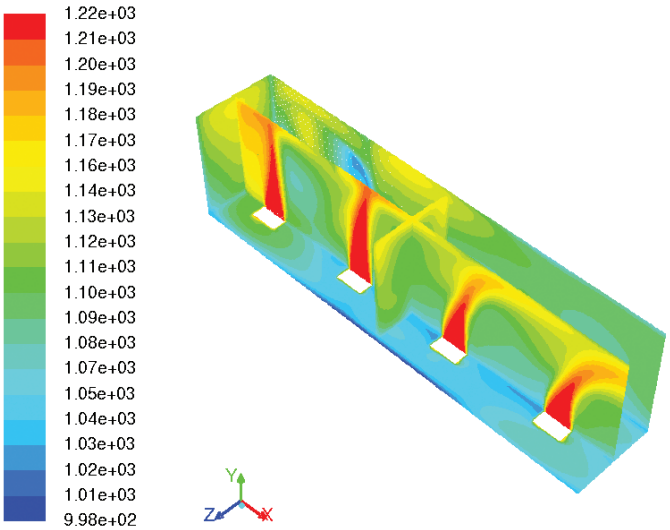

Figure 6.3: Results of the modeling of the temperature distribution of the simulated back-pass channel for the oxy-fired scenario.

6.3 Models for radiative properties of gas mixture

The gray gas radiative heat transfer modeling has been carried out by using the standard WSGGM proposed by Smith et al. (1982). The non gray modeling is done by using the new correlation (Eq. 5.4) with the coefficients reported in Tables 5.1–5.4 for oxy-fired combustion. For the air-fired combustion scenario, the results of the SNBM (Soufiani and Taine, 1997) for each of the ten non uniform intervals have been correlated with the fifth order polynomial and values of the band absorption coefficients were integrated to the DOM Fluent solver through the UDF presenting non gray modeling solution. The gray gas radiative heat transfer modeling for the case of air-fired combustion is done by using the results of the SNBM in the form of mean absorption coefficient. In this case, the eighth order polynomial has been implemented to interpret the mean absorption coefficient into Fluent solver through the UDF. The mean absorption coefficient is calculated by means of the Beer's law from the transmissivity data provided by the SNBM.

Figures 6.4 and 6.5 show the radiative heat fluxes along the center line of the top wall of

the backpass channel geometry, shown in Figure 6.1, by using different radiative methods of gray/non gray modeling. Figure 6.4 shows results for the air-fired combustion and Figure 6.5 presents results for oxy-fired combustion scenarios, respectively.

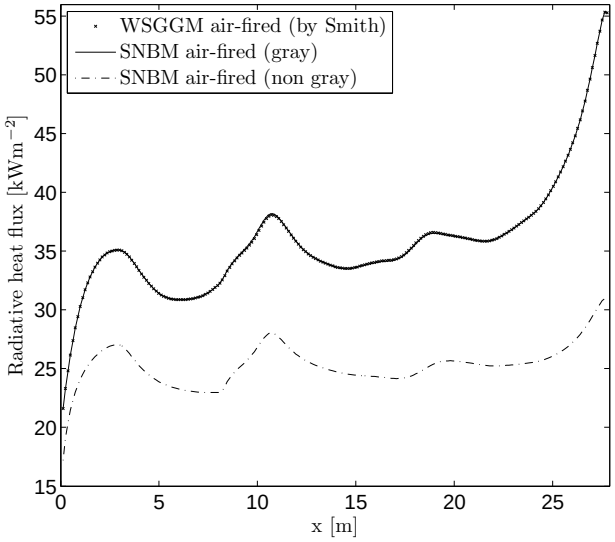

Figure 6.4: A comparison of the radiative heat fluxes at the center line of the top wall for the different methods under the air-fired combustion conditions.

The non gray radiative heat transfer is modeled in air-fired backpass channel by using the SNBM for calculating band absorption coefficient of the ten non uniform intervals and band absorption coefficient of each of the intervals is correlated by fitting the ten correlations as a function of temperature in a constant gas composition and a fixed path length. As mentioned earlier, these ten correlations are integrated into the DOM Fluent solver through the UDF. The non gray modeling is assumed to present the most accurate results because of considering the gas spectral features in its calculations. The radiative heat flux profile obtained by using the SNBM, proposed by Soufiani and Taine (1997) for calculating the band absorption coefficient of the ten non uniform intervals, is taken as the reference solution for the air-fired combustion scenario. Figure 6.4 shows that for the air-fired combustion scenario the average of differences between the WSGGM, and the SNBM in the gray form with the non gray results of the SNBM equal to about 41% for both solutions. The results by the WSGGM and the SNBM in their gray implementations are almost identical to each other.

For the oxy-fired combustion scenario, the radiative heat flux profile produced by Eq. 5.4 with the coefficients reported in Tables 5.1–5.4 for the ten non uniform intervals is taken as the reference solution to evaluate the other models for the oxy-fired combustion scenario. Figure 6.5 shows that for the oxy-fired combustion scenario the average of differences

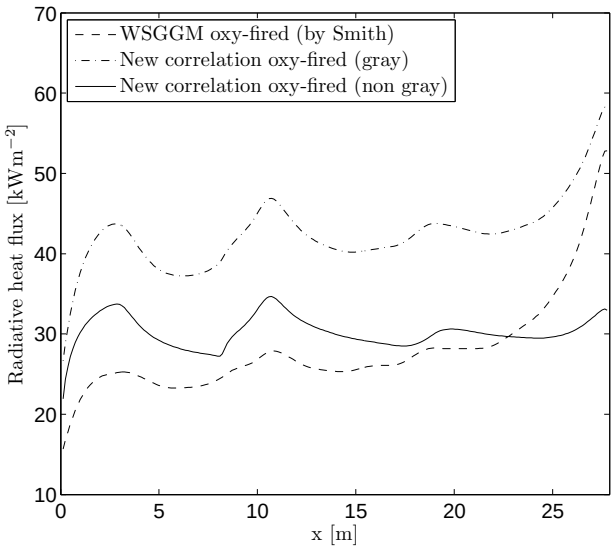

Figure 6.5: A comparison of the radiative heat fluxes at the center line of the top wall for the different methods under the oxy-fired combustion conditions.

between the WSGGM, and the new correlation in the gray form with the non gray results equal to 16.6% and 40.4%, respectively.

Figure 6.5 shows that in most part of the profile line the WSGGM underpredicts heat flux for the oxy-fired combustion case. It is partly because of the weakness of the gray models in proper modeling of spectral features, and partly because of the fact that the standard WSGGM by Smith et al. (1982) was basically proposed to support the air-fired combustion.

Figure 6.6 shows the radiative heat fluxes along the center line of the top wall of the backpass channel geometry predicted by the non gray radiative modeling using the developed banded approach with the ten non uniform intervals for the oxy-fired combustion condition, and air-fired combustion.

Figure 6.6 shows how the combustion type affects the radiative heat flux predictions, and overall performance of the backpass channel. The results of air-fired combustion show low radiative heat flux values compared to the oxy-fired combustion scenario. The average of differences between the non gray modeling of air-fired combustion with the non gray results of the oxy-fired combustion equal to about 16%.

Figures 6.7 and 6.8 show how gray and non gray radiative modeling affect on the prediction of the total heat flux in the walls of the backpass channel in the case of the oxy-fired combustion. Figure 6.7 shows the predicted total heat flux in the walls of the geometry

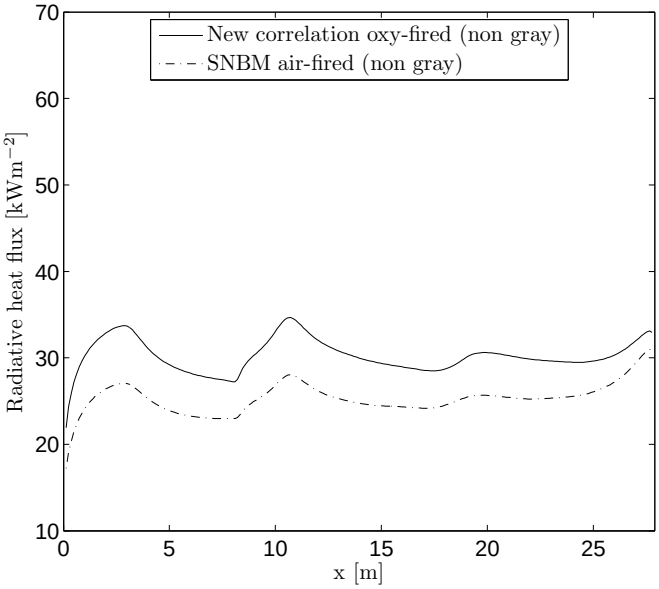

Figure 6.6: Comparison of the radiative heat flux at the center line of the top wall for the new correlation of non gray modeling under the oxy- and air-fired combustion conditions.

in the case of using non gray banded approach with the ten non uniform intervals while Figure 6.8 shows the same quantity when the standard WSGGM is used for the gray modeling of the radiative heat transfer.

Figures 6.7 and 6.8 show how important is using the proper radiation model in overall modeling of this backpass channel. Implementing the gray models (WSGGM) leads to clear underprediction values for the total radiative heat flux. It is because of the fact that the coefficients reported by Smith et al. (1982) of the WSGGM and implemented by Fluent were originally obtained based on the emissivity charts of the air-fired combustion products in specified rates of molar fractions. Thus, using the standard WSGGM for modeling oxy-fired combustion systems may not be trustful.

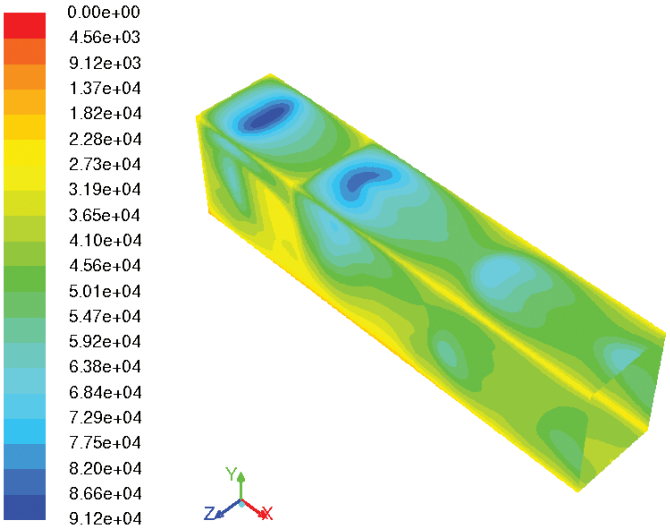

Figure 6.7: The total radiative heat flux contours obtained by the new correlation with the ten non uniform intervals (non gray) for the oxy-fired combustion.

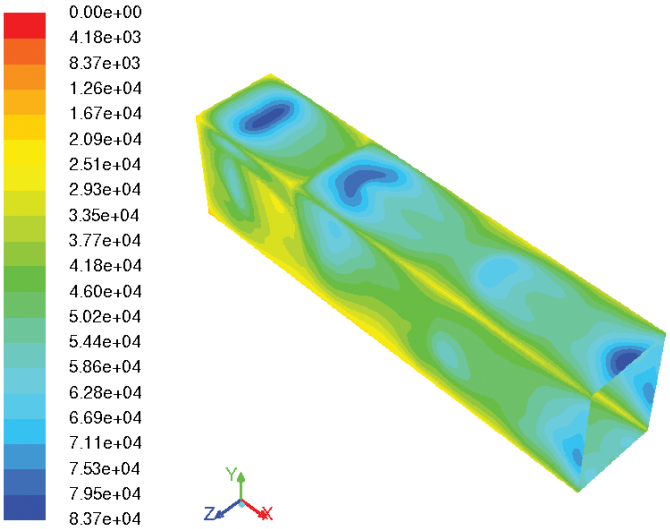

Figure 6.8: The total radiative heat flux contours obtained by the WSGGM (gray) for the oxy-fired combustion.

7 Conclusions

In this thesis, two formulations of the EWBM have been carefully analyzed, that is the EWBM-4RE and the EWBM-IM. The comparison of two formulations of EWBM with some experimental data and benchmarks showed that the original EWBM-4RE with its originally developed parameters is a more accurate method for total property calculation. The spectral analysis provides important information about the accuracy of the spectral predictions for different absorption bands of H_2O and CO_2. In order to improve the accuracy, the listed absorption bands should be modified for different formulations of the EWBM (Edwards and Balakrishnan, 1973) as a further step of research. Furthermore, by avoiding the usage of the originally developed parameters for the EWBM-4RE and obtaining new model parameters, the accuracy of the EWBM-IM of the total radiative property calculations can be improved.

One of the main focuses of the presented research is proposing new methods for the calculation of the total emissivity and band absorption coefficient in H_2O–CO_2 mixtures. The SNBM (Soufiani and Taine, 1997) version presented by (Ronney, 2012) is modified to develop new methods for the gray and non gray radiative heat transfer modeling in homogeneous and inhomogeneous media of the oxy-fired combustion scenario. The suggested method of gray gas assumption presents a total value of the emissivity averaged over the entire radiative spectrum. The developed approach of non gray modeling is presented using the SNBM to calculate the band absorption coefficient inside the limited wavenumber intervals. Implementing the presented methods to any commercial CFD software packages for gray and non gray modeling results into computationally more efficient, more accurate, and more simple calculations of radiative heat transfer.

The SNBM has been used to produce databases of the total emissivity for obtaining new correlations. The SNBM is often used as a benchmark method (Soufiani and Djavdan, 1994; Parthasarathy et al., 1996; Bedir et al., 1997; Liu, 1999; Chu et al., 2011) when the LBLM data are not available. Moreover, Chu et al. (2011) have reported that the results estimated by the SNBM can be almost as accurate as the results presented by the LBLM. One of the most significant problems of the radiative methods is the validation in industrial scale modeling. The high scale dimensions of the modern commercial boilers and furnaces creates difficulties in producing accurate experimental data which can be used later for validating different radiative models. Furthermore, the deficiency of the available experimental data of the industrial systems in addition to some commercial proprietary information creates certain barriers for radiative heat transfer modeling and further research.

The general logarithmic correlation for the total emissivity of air-fired combustion is presented as a function of two effective parameters, that is P_tL, and T, for four different gas compositions; the coefficients are listed in Table 4.1. In Addition, a single correlation with the included effect of gas composition of H_2O–CO_2 mixtures of air-fired combustion is proposed by linear interpolations/extrapolations; the coefficients are presented in Table 4.2. These correlations decrease the CPU time with an insignificant accuracy re-

duction for the calculations of the total emissivity compared with the original results by the SNBM.

In order to improve the previously obtained correlations of this thesis for a wider range of adaptability, the total emissivity of H_2O–CO_2 mixtures has been interpreted as a function of three effective parameters, that is Pr, T, and $P_{w+c}L$, corresponding to the oxy-fired combustion scenario. Using the SNBM data of the total emissivity as a function of the three effective parameters, the coefficients of the new correlation have been obtained. The new correlation of the oxy-fired combustion calculates the total emissivity in homogeneous and inhomogeneous H_2O–CO_2 mixtures; the coefficients are listed in Tables 4.6–4.8. The new correlation provides accurate, simple, and fast calculations compared with other methods of total properties. The obtained correlations of the total properties can be used in the modeling of gray radiative heat transfer of oxy-fired conditions.

The other scientific contribution of this thesis is related to the proposal of a new approach towards the non gray modeling providing support for the oxy-fired combustion condition. The new approach is based on dividing the entire radiative spectrum into limited wavenumber intervals. The suitable form and number of spectrum division has been set as ten non uniform intervals based on the analyses of two benchmarks by Liu (1999) and by Porter et al. (2010) and the previously published results by Stefanidis et al. (2007). The coefficients of the new correlation (Eq. 5.4) have been obtained for band properties in each wavenumber interval as a function of three effective parameters; the coefficients are listed in Tables 5.1–5.4.

The proposed banded approach in the form of a new correlation accompanied with the coefficients presented in Tables 5.1–5.4 results into accurate and simple calculations compared with other methods of non gray modeling. With the low CPU time and high accuracy of the band absorption coefficient calculations, the new correlation has shown its benefits compared to the WSGGM in its gray and non gray form which is widely used by engineers in radiative calculations. Extra benefits of using the new correlation (Eq. 5.4) are listed as high accuracy, effectiveness and simplicity of calculations, and its easiness to be implemented in non gray radiative heat transfer modeling.

The new approach for gray and non gray modeling of radiative properties calculates the total emissivity and band absorption coefficient of oxy-fired combustion systems as a function of Pr, T, and $P_{w+c}L$. By applying the presented methods to any commercial CFD packages, the operational conditions can be quickly and easily analyzed for using different fuel options for bio-fuels, moist fuels, or difficult fuels of the oxy-fired scenario producing improved and more efficient systems. The main possibility for further development of the new correlations is to include the effect of the presence of the particles on the overall calculations of radiative heat transfer in H_2O–CO_2 mixtures.

The key component lacking of the existing spectral models is the radiative heat transfer in gas mixtures with the presence of the particles. The radiative heat transfer properties

can be approximated thoroughly if the presence of the particles in the gas mixture is eliminated. Thus, there is a need for obtaining methods which can consider the presence of the particles and provide fast and accurate algorithm for the calculations. As the further developing steps of research, the proposed correlations of oxy-fired combustion can be modified to include the presence of soot particles in H_2O–CO_2 mixtures.

References

Ansys (2009). *Theory Guide Fluent 12.0*. ANSYS, Inc.

Bedir, H., T'ien, J., and Lee, H. (1997). Comparison of different radiation treatments for a one-dimensional diffusion flame. *Combust. Theory Modelling*, 1, pp. 395–404.

Bordbar, M. and Hyppänen, T. (2007). Modeling of Radiation Heat Transfer in a Boiler Furnace. *Advanced Studies in Theoretical Physics*, 1(12), pp. 571–584.

Bordbar, M. and Hyppänen, T. (2013). Multiscale Numerical Simulation of Radiation Heat Transfer in Participating Media. *Heat Transfer Engineering*, 31(1), pp. 54–69.

Briggs, L., Miller, W., and Lewis, E. (1975). Ray-effect mitigation in discrete ordinate-like angular finite element approximations in neutron transport. *Nuclear Science and Engineering*, 57, pp. 205–217.

Carlson, B. and Lathrop, K. (1968). *Transport theory - the method of discrete ordinates, in Computing Methods in Reactor Physics, eds. H. Greenspan, C.N. Kelber and D. Okrent*. Gordon & Breach.

Chai, J., Lee, H., and Patankar, S. (1994). Finite volume method for radiation heat transfer. *Journal of Thermophysics and Heat Transfer*, 8(3), pp. 419–425.

Chandrasekhar, S. (1960). *Radiative Transfer*. Dover Publications.

Chu, C. and Churchill, S. (1960). Numerical solution of problems in multiple scattering of electromagnetic radiation. *Journal of Physical Chemistry*, 59, pp. 855–863.

Chu, H., Liu, F., and Zhou, H. (2011). Calculations of gas thermal radiation transfer in one-dimensional planar enclosure using LBL and SNB models. *Int. J. of Heat and Mass Transfer*, 54, pp. 4736–4745.

Chui, E. and Raithby, G. (1993). Computation of Radiant Heat Transfer on a Non-Orthogonal Mesh Using the Finite-Volume Method. *Numerical Heat Transfer*, 23(Part B), pp. 269–288.

Coelho, P. (2002). Numerical simulation of radiative heat transfer from non-gray gases in three-dimensional enclosures. *J. Quant. Spectrosc. Radiat. Transfer*, 74, pp. 307–328.

Cumber, P. and Fairweather, M. (2005). Evaluation of flame emission models combined with the discrete transfer method for combustion system simulation. *Int. J. of Heat Mass Transfer*, 48, pp. 5221–5239.

Cumber, P., Fairweather, M., and Ledin, H. (1998). Application of wide band radiation models to non-homogeneous combustion systems. *Int. J. of Heat Mass Transfer*, 41(11), pp. 1573–1584.

Denison, M. and Webb, B. (1993). A spectral line-based weighted-sum-of-gray-gases model for arbitrary RTE solvers. *Transactions of the ASME*, 115, pp. 1004–1012.

Denison, M. and Webb, B. (1995). The spectral-line weighted-sum-of-gray-gases model for H_2O/CO_2 mixtures. *ASME J. Heat Transfer*, 117, pp. 788–792.

Edwards, D. (1963). *Studies of infrared radiation in gases*. Technical report.

Edwards, D. (1976). Molecular gas band radiation. *Adv. Heat. Transfer*, 12, pp. 115–193.

Edwards, D. and Balakrishnan, A. (1973). Thermal radiation by combustion gases. *Int. J. Heat Mass Transfer*, 16, pp. 25–40.

Edwards, D. and Menard, W. (1964). Comparison of models for correlation of total band absorption. *Appl. Optics*, 3, pp. 621–625.

Felske, J. and Tien, C. (1974). Infrared radiation from non-homogeneous gas mixtures having overlapping bands. *J. Quant. Spectrosc. Radiat. Transfer*, 14, pp. 35–48.

Ferriso, C. and Ludwig, C. (1964a). High-temperature spectral emissivities of H_2O-CO_2 mixtures in the 2.7-μ region. *Applied Optics*, 3(12), pp. 1435–1444.

Ferriso, C. and Ludwig, C. (1964b). Spectral emissivities and integrated intensities of the 2.7 μm H_2O band between 530 and 2200 K. *J. Quant. Spectrosc. Radiat. Transfer*, 4, pp. 215–227.

Fiveland, W. (1984). Discrete ordinates solutions of the radiative transport equation for rectangular enclosures. *ASME Journal of Heat Transfer*, 106, pp. 699–706.

Fiveland, W. (1987). Discrete ordinate methods for radiative heat transfer in isotropically and anisotropically scattering media. *ASME J. of Heat Transfer*, 109, pp. 809–812.

Goody, R. (1964). *Atmospheric Radiation*. Oxford University Press.

Goutiere, V., Liu, F., and Charette, A. (2000). An assessment of real-gas modelling in 2D enclosures. *J. Quant. Spectrosc. Radiat. Transfer*, 64, pp. 299–326.

Green, D. and Perry, R. (2008). *Perry's Chemical Engineers' Handbook, eight edition*. New York: McGraw-Hill. ISBN 0-07-142294-3.

Grosshandler, W. (1993). *RADCAL: A Narrow-Band Model for Radiation Calculations in a Combustion Environment*. Technical report.

Hammersley, J. and Handscomb, D. (1964). *Monte Carlo Methods*. New York: John Wiley & Sons.

Hostikka, S. (2008). *Development of fire simulation models for radiative heat transfer and probabilistic risk assessment*. Ph.D. thesis. Helsinki University of Technology, VTT Technical Research Center of Finland.

Hottel, H. and Mangelsdorf, H. (1935). Heat transmission by radiation from non-luminous gases II. Experimental study of carbon dioxide and water vapor. *Transactions of AIChE*, 31, pp. 517–549.

Hottel, H. and Sarofim, A. (1967). *Radiative Transfer*. New York: McGraw-Hill Education - Europe. ISBN 0-07-030450-5.

Hottel, H., Sarofim, A., Evans, L., and Vasalos, I. (1968). Radiative transfer in anistropically scattering media: Allowance for Fresnel reflection at the boundaries. *ASME Journal of Heat Transfer*, 90, pp. 56–62.

Isachenko, V., Osipova, V., and Sukomel, A. (1975). *Heat Transfer*. Energy.

Jensen, K., Ripoll, J., Wray, A., Joseph, D., and Hafi, M. (2007). On various modeling approaches to radiative heat transfer in pool fires. *Combust. Flame*, 148, pp. 263–279.

Johansson, R. (2008). *Modelling elements in conversion of solid fuels - fixed bed combustion and gaseous radiation*. Ph.D. thesis. Chalmers University of Technology, Department of Energy and Environment, Göteborg, Sweden.

Johansson, R., Andersson, K., Leckner, B., and Thunman, H. (2010). Models for gaseous radiative heat transfer applied to oxy-fuel conditions in boilers. *Int. J. Heat and Mass Transfer*, 53, pp. 220–230.

Johansson, R., Leckner, B., Andersson, K., and Johnsson, F. (2011). Account for variations in the H_2O to CO_2 molar ratio when modelling gaseous radiative heat transfer with the weight-sum-of-grey-gases model. *Combustion and Flame*, 158, pp. 893–901.

Kayakol, N., Selçuk, N., Campbell, I., and Gülder, Ö. (2000). Performance of discrete ordinates method in a gas turbine combustor simulator. *Experimental Thermal and Fluid Science*, 21, pp. 134–141.

Krishnamoorthy, G. (2010). A comparison of gray and non-gray modeling approaches to radiative transfer in pool fire simulations. *J. Hazardous Materials*, 182, pp. 570–580.

Lallemant, N., Sayret, A., and Weber, R. (1996). Evaluation of emissivity correlations for H_2O–CO_2-N_2/air mixtures and coupling with solution methods of the radiative transfer equation. *Prog. Energy Combust. Sci.*, 22, pp. 543–574.

Lallemant, N. and Weber, R. (1996). A computationally efficient procedure for calculating gas radiative properties using the exponential wide band model. *Int. J. Heat Mass Transfer*, 39(15), pp. 3273–3286.

Lathrop, K. and Carlson, B. (1965). *Discrete-ordinates angular quadrature of the neutron transport equation*. Technical report.

Leckner, B. (1972). Spectral and total emissivity of water vapor and carbon dioxide. *Combustion and flame*, 19, pp. 33–48.

Lee, C. (1962). *The discrete S_n approximation to transport theory*. Technical report.

Liu, F. (1999). Numerical solutions of Three-dimensional non-gray gas radiative transfer using the statistical narrow-band model. *Journal of Heat Transfer*, 121, pp. 200–203.

Liu, F., Gülder, Ö., Smallwood, G., and Ju, Y. (1998). Non-grey gas radiative transfer analyses using the statistical narrow-band model. *Int. J. of Heat Mass Transfer*, 41, pp. 2227–2236.

Liu, F. and Smallwood, G. (2004). An efficient approach for the implementation of the SNB based correlated - k method and its evaluation. *J. Quant. Spectrosc. Radiat. Transfer*, 84, pp. 465–475.

Ludwig, C., Malkmus, W., Reardon, J., and Thompson, J. (1973). *Handbook of infrared radiation from combustion gases*. Technical report. Washington.

MathWorks (2010). *R2010b Documentation @ONLINE, MATLAB ® Product Family*. url: `http://www.mathworks.se/help/pdf_doc/allpdf.html`.

Maximov, A., Bordbar, M., and Hyppänen, T. (2012). Spectral analysis of the various implementations of the exponential wide band model (EWBM) for H_2O–CO_2 mixtures. *International Review of Mechanical Engineering*, 6(3), pp. 411–419.

Modest, M. (1989). The modified differential approximation for radiative transfer in general three-dimensional media. *Journal of Thermophysics and Heat Transfer*, 3(3), pp. 283–288.

Modest, M. (1991). The new weighted-sum-of-gray-gases model for arbitrary solution methods in radiative transfer. *Transactions of the ASME*, 113, pp. 650–656.

Modest, M. (1993). *Radiative Heat Transfer*. Series in Mechanical Engineering. McGraw-Hill.

Modest, M. (2003a). Narrow-band and full-spectrum k - distributions for radiative heat transfer - correlated - k vs. scaling approximation. *J. Quant. Spectrosc. Radiat. Transfer*, 76, pp. 69–83.

Modest, M. (2003b). *Radiative Heat Transfer, second edition*. New York: Academic Pr. ISBN 0-12-503163-7.

Modest, M. and Bharadwaj, S. (2002). High-resolution, high-temperature transmissivity measurements and correlations for carbon dioxide-nitrogen mixtures. *J. Quant. Spectrosc. Radiat. Transfer*, 73(2-5), pp. 329–338.

Modest, M. and Zhang, H. (2002). The full-spectrum correlated-k distribution for thermal radiation from molecular gas-particulate mixtures. *Journal of Heat Transfer*, 124, pp. 30–38.

Murthy, J. and Mathur, S. (1998). *A Finite Volume Method For Radiative Heat Transfer Using Unstructured Meshes*. AIAA-98-0860.

Myöhänen, K., Hyppänen, T., Pikkarainen, T., Eriksson, T., and Hotta, A. (2009). Near Zero CO_2 emissions in coal firing with oxy-fuel circulating fluidized bed boiler. *Chem. Eng. Technol.*, 32(3), pp. 355–363.

Nadezin, D. (1986). *Space Physics*. Soviet Encyclopedia.

Nilsson, T. and Sundén, B. (2003). Modelling of thermal radiation properties of gases: the exponential wide band model (EWBM). *J. Heat and Technology*, 21(2), pp. 1–10.

Park, S. and Kim, S. (1993). Thermophoretic deposition of absorbing, emitting and isotropically scattering particles in laminar tube flow with high particle mass loading. *International Journal of Heat and Mass Transfer*, 14, pp. 3477–3485.

Park, W.H. and Kim, T.K. (2002). Narrow band radiative solutions within a cubical enclosure filled with real gas mixtures. *KSME Int. J.*, 16(6), pp. 861–869.

Parthasarathy, G., Chai, J., and Patankar, S. (1996). A simple approach to non-gray gas modeling. *Numerical Heat Transfer, Part B*, 29, pp. 113–123.

Penner, S. (1959). *Quantitative molecular spectroscopy and gas emissivities*. Addison Wesley, Reading.

Pierrot, L., Soufiani, A., and Taine, J. (1999). Accuracy of narrow-band and global models for radiative transfer in H_2O,CO_2 and H_2O-CO_2 mixtures at high temperature. *J. Quant. Spectrosc. Radiat. Transfer*, 62, pp. 523–548.

Porter, R., Liu, F., Pourkashanian, M., Williams, A., and Smith, D. (2010). Evaluation of solution methods for radiative heat transfer in gaseous oxy-fuel combustion environments. *J. Quant. Spectrosc. Radiat. Transfer*, 111, pp. 2084–2094.

Pröell, T., Kolbitsch, P., Bolhòr-Nordenkampf, J., and Hofbauer, H. (2009). A novel dual circulating fluidized bed system for chemical looping processes. *AIChE Journal*, 55(12), pp. 3255–3266.

Raithby, G. and Chui, E. (1990). A Finite-Volume Method for Predicting a Radiant Heat Transfer in Enclosures with Participating Media. *J. Heat Transfer*, 112, pp. 415–423.

Riviére, P., Scutaru, D., Soufiani, A., and Taine, J. (1994). A New CK data basis suitable from 300 to 2500 K for spectrally correlated radiative transfer in CO_2-H_2O transparent gas mixtures. In: *in Tenth International Heat Transfer Conference*.

Ronney, P. (2010). *Excel spreadsheet models for thermal/fluid problems @ONLINE, University of Southern California, Los Angeles*. url: `http://ronney.usc.edu/spreadsheets/`.

Ronney, P. (2012). *Excel spreadsheet models for thermal/fluid problems @ONLINE, University of Southern California, Los Angeles*. url: `http://ronney.usc.edu/spreadsheets/`.

Rothman, L., et al. (2005). The HITRAN 2004 molecular spectroscopic database. *J. Quant. Spectrosc. Radiat. Transfer*, 96, pp. 139–204.

Rothman, L., et al. (2009). The HITRAN 2008 molecular spectroscopic database. *J. Quant. Spectrosc. Radiat. Transfer*, 110, pp. 533–572.

Rothman, L., Gordon, I., Barber, R., Dothe, H., Gamache, R., Goldman, A., Perevalov, V., Tashkun, S., and J.Tennyson (2010). HITEMP, the high-temperature molecular spectroscopic database. *J. Quant. Spectrosc. Radiat. Transfer*, 111, pp. 2139–2150.

Runstedtler, A. and Hollands, K. (2008). Modeling of band overlap in gas mixtures with the smoothed (re-ordered) band model. *J. Quant. Spectrosc. Radiat. Transfer*, 73, pp. 375–384.

Shih, T. and Chen, Y. (1983). A discretized-intensity method proposed for two-dimensional systems enclosing radiative and conductive media. *Numerical Heat Transfer*, 6, pp. 117–134.

Siegel, R. and Howell, J. (1981). *Thermal Radiation Heat Transfer, 2nd edition*. Washington: Hemisphere Publishing Corporation.

Siegel, R. and Howell, J. (1992). *Thermal Radiation Heat Transfer, 3rd edition*. Washington: Hemisphere Publishing Corporation. ISBN 0-89-116271-2.

Smith, T., Shen, Z., and Friedman, J. (1982). Evaluation of coefficients for the weighted sum of grey gases model. *J. of Heat Transfer*, 104, pp. 602–608.

Solovjov, V. and Webb, B. (2000). SLW modeling of radiative transfer in multicomponent gas mixtures. *J. Quant. Spectrosc. Radiat. Transfer*, 65, pp. 655–672.

Soufiani, A. and Djavdan, E. (1994). A comparison between weighted sum of gray gases and statistical narrow-band radiation models for combustion applications. *Combustion and Flame*, 97, pp. 240–250.

Soufiani, A., Hartmann, J., and Taine, J. (1985). Validity of band-model calculations for CO_2 and H_2O applied to radiative properties and conductive-radiative transfer. *J. Quant. Spectrosc. Radiat. Transfer*, 3, pp. 243–257.

Soufiani, A. and Taine, J. (1997). High temperature gas radiative property parameters of statistical narrow-band model for H_2O, CO_2 and CO correlated-K model for H_2O and CO_2. *Int. J. of Heat Mass Transfer*, 40, pp. 987–991.

Stefanidis, G., Merci, B., Heynderickx, G., and Marin, G. (2007). Gray/nongray gas radiation modeling in steam cracker CFD calculations. *AIChE Journal*, 53(7), pp. 1658–1669.

Ströhle, J. (2008). Assessment of the re-ordered wide band model for non-grey radiative transfer calculations in 3D enclosures. *J. Quant. Spectrosc. Radiat. Transfer*, 109, pp. 1622–1640.

Ströhle, J. and Coelho, P. (2002). On the application of the exponential wide band model to the calculation of radiative heat transfer in one- and two-dimensional enclosures. *Int. J. of Heat and Mass Transfer*, 45, pp. 2129–2139.

Tien, C. and Giedt, W. (1965). Experimental determination of infrared absorption of high-temperature gases. *in Advances in Thermophysical Properties at Extreme Temperatures and Pressures, ASME*.

Truelove, J. (1987). Discrete-ordinate solutions of the radiation transport equation. *ASME J. of Heat Transfer*, 109(4), pp. 1048–1051.

Truelove, J. (1988). Threedimensional readiation in absorbing-emitting-scattering media using the discrete-ordinates approximation. *J. Quant. Spectrosc. Radiat. Transfer*, 39(1), pp. 27–31.

Wang, A. and Modest, M. (2005). High-accuracy, compact database of narrow-band k - distributions for water vapor and carbon dioxide. *J. Quant. Spectrosc. Radiat. Transfer*, 93, pp. 245–261.

Wang, W. and Shi, G. (1988). Total band absorptance and k-distribution function for atmospheric gases. *J. Quant. Spectrosc. Radiat. Transfer*, 39, pp. 387–398.

Węcel, G., Ostrowski, Z., and Białecki, R. (2010). A novel approach of evaluating absorption line black body distribution function employing proper orthogonal decomposition. *J. Quant. Spectrosc. Radiat. Transfer*, 111(2), pp. 309–317.

Weiner, M. and Edwards, D. (1968). Theoretical expression of water vapor spectral emissivity with allowance for line structure. *Int. J. Heat Mass Transfer*, 11, pp. 55–65.

Yin, C., Johansen, L., Rosendahl, L., and Kær, S. (2010). New weighted sum of gray gases model applicable to computational fluid dynamics (CFD) modeling of oxy-fuel combustion: derivation, validation and implementation. *Energy & Fuel*, 24, pp. 6275–6282.

ACTA UNIVERSITATIS LAPPEENRANTAENSIS

459. WINTER, SUSANNA. Network effects: scale development and implications for new product performance. 2011. Diss.

460. JÄÄSKELÄINEN, ANSSI. Integrating user experience into early phases of software development. 2011. Diss.

461. KÄÄRIÄINEN, TOMMI. Polymer surface modification by atomic layer deposition. 2011. Diss.

462. KOCHURA, ALEKSEY. Growth, magnetic and transport properties of InSb and II-IV-As2 semiconductors doped with manganese. 2011. Diss.

463. PUTKIRANTA, ANTERO. Possibilities and challenges of longitudinal studies in operations management. 2011. Diss.

464. HAPPONEN, ARI. Muuttuvaan kysyntään sopeutuva varastonohjausmalli. 2011. Diss.

465. VASAVA, PARITOSH. Application of computational fluid dynamics in modelling blood flow in human thoracic aorta. 2011. Diss.

466. PURO, LIISA. Identification of extractives and polysaccharides as foulants in membrane filtration of pulp and paper mill effluents. 2011. Diss.

467. LAPPALAINEN, PIA. Socially Competent Leadership – predictors, impacts and skilling in engineering. 2012. Diss.

468. PLAMTHOTTATHIL, ANSHY OONNITTAN. Application of electrokinetic Fenton process for the remediation of soil contaminated with HCB. 2012. Diss.

469. EBRAHIMI, FATEMEH. Synthesis of percarboxylic acids in microreactor. 2012. Diss.

470. JANTUNEN, SAMI. Making sense of software product requirements. 2012. Diss.

471. VILKO, JYRI. Approaches to supply chain risk management: identification, analysis and control. 2012. Diss.

472. TANSKANEN, VESA. CFD modelling of direct contact condensation in suppression pools by applying condensation models of separated flow. 2012. Diss.

473. HUHTANEN MIKKO. Software for design of experiments and response modelling of cake filtration applications. 2012. Diss.

474. PARJANEN, SATU. Creating possibilities for collective creativity
Brokerage functions in practice-based innovation. 2012. Diss.

475. KUKKONEN, SAKU. Generalized differential evolution for global multi-objective optimization with constraints. 2012. Diss.

476. LAAKSONEN, JONNA. Tactile-proprioceptive robotic grasping. 2012. Diss.

477. KALLIO, ANNE. Enhancing absorptive capacity in a non-research and development context
An action research approach to converting individual observations into organizational awareness. 2012. Diss.

478. LÄTTILÄ, LAURI. Improving transportation and warehousing efficiency with simulation based decision support systems. 2012. Diss.

479. OYOMNO, WERE. Usable privacy preservation in mobile electronic personality. 2012. Diss.

480. LINNALA, MIKKO. Simulation and optimization tools in paper machine concept design. 2012. Diss.

481. KORPIJÄRVI, JUHA. Aging based maintenance and reinvestment scheduling of electric distribution network. 2012. Diss.

482. KORHONEN, JUHAMATTI. Active inverter output filtering methods. 2012. Diss.

483. KLODOWSKI, ADAM. Flexible multibody approach in bone strain estimation during physical activity: quantifying osteogenic potential. 2012. Diss.

484. VUORENMAA, MARKKU. Osaamisen johtaminen pk-yrityksen kansainvälisen kasvun elinkaarella. 2012. Diss.

485. RAUTIAINEN, MARITA. Dynamic ownership in family business systems – a portfolio business approach. 2012. Diss.

486. LILIUS, REIJO. THE FINNISH IT INDUSTRIES IN TRANSITION Defining and measuring the Finnish software product and IT services industries by applying theoretical frameworks . 2012. Diss.

487. TUOMINEN, PASI. The purpose of consumer co-operation: implications for the management and governance of co-operatives. 2012. Diss.

488. SAARI, ESA. Suurnopeus-turbokoneroottoreiden termodynaaminen ja mekaaninen mallinnus sekä rakenneanalyysi. 2012. Diss.

489. PAANANEN, MIKKO. On innovative search: the use of internal and external sources of innovation among Finnish innovators. 2012. Diss.

490. BELOVA, POLINA. Quasiclassical approach to the vortex state in iron-based superconductors. 2012. Diss.

491. HIETANEN, IIRO. Design and characterization of large area position sensitive radiation detectors. 2012. Diss.

492. PÄSSILÄ, ANNE. A reflexive model of research-based theatre Processing innovation of the cross-road of theatre, reflection and practice-based innovation activities. 2012. Diss.

493. RIIPINEN, TOMI. Modeling and control of the power conversion unit in a solid oxide fuel cell environment. 2012. Diss.

494. RANTALAINEN, TUOMAS. Simulation of structural stress history based on dynamic analysis. 2012. Diss.

495. SALMIMIES, RIINA. Acidic dissolution of iron oxides and regeneration of a ceramic filter medium. 2012. Diss.

496. VAUTERIN, JOHANNA JULIA. The demand for global student talent: Capitalizing on the value of university-industry collaboration. 2012. Diss.

497. RILLA, MARKO. Design of salient pole PM synchronous machines for a vehicle traction application. 2012. Diss.

498. FEDOROVA, ELENA. Interdependence of emerging Eastern European stock markets. 2012. Diss.

499. SHAH, SRUJAL. Analysis and validation of space averaged drag model for numerical simulations of gas-solid flows in fluidized beds. 2012. Diss.

500. WANG, YONGBO. Novel methods for error modeling and parameter identification of redundant hybrid serial-parallel robot. 2012. Diss.